

**A STUDY OF RAIN ATTENUATION ON TERRESTRIAL
PATHS AT MILLIMETRIC WAVELENGTHS IN SOUTH
AFRICA**

By

Fashuyi Modupe Olubunmi

**A Dissertation Submitted in Partial Fulfillment of the Requirement for
the Degree of**

**Masters in Electrical Engineering in Telecommunications and
Information Technology**



UNIVERSITY OF KWAZULU-NATAL
School of Engineering
Centre of Excellence in Radio Access and Rural Technologies

February 2006

Supervised by

Professor T.J.O Afullo

DISSERTATION TITLE

**A Study of Rain Attenuation on Terrestrial Paths at
Millimetric Wavelengths in South Africa**

SUBMITTED BY

Fashuyi Modupe Olubunmi

IN PARTIAL FULLFILMENT OF THE DEGREE

Masters in Electrical Engineering in Telecommunications and Information
Technology from the University of KwaZulu-Natal

DATE OF SUBMISSION

February 2006

SUPERVISED BY

Professor T.J.O Afullo

As the candidate's supervisor, I have approved this dissertation for submission.

Signed:

Name: Date:

Declaration

I, Fashuyi Modupe Olubunmi, Student Number 204002150, hereby declare that the dissertation entitled **A Study of Rain Attenuation on Terrestrial Paths at Millimetric Wavelengths in South Africa** is a result of my own investigation, and presents my work unless specifically referenced in the text. This work has not been submitted in part or in full for any degree to any university.

Signed:

Name: Date:

Acknowledgement

I give God the glory for strength and enablement bestowed on me to complete this work.

The unrelenting effort of my supervisor Prof. T.J.O. Afullo is highly appreciated. His patience, words of direction and constructive criticisms is worth mention.

My profound gratitude to Prof S.H. Mneney and Mr. Kumaran Naicker for assisting with the 1-minute integration time rain rate data and attenuation measurements data used in this dissertation.

Also appreciated is the support of Ms Tracey Gill of the South Africa Weather Service for facilitating access to the 5-year rainfall data used in this work,

My sincere gratitude to all the academic staffs in the school such as Mr. Rathi Sewsunker, Prof A.M. Chol, Prof. B. Nleya, for their moral support and professional advice throughout the research period.

I also appreciate the effort and assistance of the administrator, Mrs René Truter, for her moral support and words of encouragement during the research period.

I give thank to my husband Mr. Peter Kemi Odedina for his love, care and understanding during the research period. Finally, I appreciate the support of my friend and colleague Mr. Pius Adewale Owolawi.

ABSTRACT

Rain affects the design of any communication system that relies on the propagation of electromagnetic waves. Above a certain threshold of frequency, the attenuation due to rain becomes one of the most important limits to the performance of terrestrial line-of-sight (LOS) microwave links. Rain attenuation which is the dominant fading mechanism at these frequencies is based on nature which can vary from location-to-location and from year-to year.

In this dissertation, the ITU-R global prediction techniques for predicting the cumulative distribution of rain attenuation on terrestrial links are studied using a five-year rain rate data for twelve different geographical locations in the Republic of South Africa. The specific attenuation γ_R (dB/km) for both horizontal and vertical polarization is determined. The path attenuation (dB) exceeded for 0.01% of the time is estimated using the available existing models for the twelve different geographical locations on a 1-minute integration time rain rate at 0.01% exceedance of the time averaged over a period of 5 years.

A comparison study is done on these available rain attenuation models; The ITU-R model, Crane Global model, and the Moupfouma models at different frequencies and propagation path lengths based on the actual 1-minute integration time rain rate exceeded at 0.01% of the time averaged over a period of 5 years for each geographical locations.

Finally, from the actual signal attenuation measurements recorded in Durban over a period of 1-year at 19.5 GHz and a propagation path length of 6.73 km, a logarithmic attenuation model and power attenuation model is proposed for Durban, South Africa.

Recommendation for future work is given in the concluding chapter for future improvement on this study. Radio communication designers will find the results obtain in the report useful.

Table of Contents

<i>Title Page</i>	i
<i>Declaration</i>	ii
<i>Acknowledgement</i>	iii
<i>Abstract</i>	iv
<i>Table of Contents</i>	v
<i>List of Figures</i>	viii
<i>List of Tables</i>	x

Chapter One	1
Introduction	1
1.1 Introduction.....	1
1.2 The Atmosphere.....	2
1.2.1 The Troposphere.....	2
1.2.2 Effect of the Troposphere on Terrestrial Radio Paths.....	3
1.3 Nature of Precipitation.....	4
1.3.1 Effects of Hydrometeors on Microwave Propagation.....	4
1.3 Types of Rain.....	5
1.4 South Africa Climate and Physical Features.....	5
1.6 Seasonal Variability of South Africa Rainfall.....	7
1.7 Justification for the Dissertation.....	8
1.8 Aims and Objectives of the Study.....	9
1.9 Chapter Summary.....	10

Chapter Two	11
Propagation Phenomena	11
2.1 Propagation Fundamentals.....	11
2.1.1 Propagation in a Lossless Dielectric Medium.....	14
2.1.2 Propagation in a Low-loss Dielectric medium.....	14
2.2 Free Space Loss.....	15
2.3 Tropospheric Loss.....	16
2.4 Propagation Loss Factors.....	18
2.4.1 Atmospheric Gaseous Losses.....	18
2.4.2 Rain Losses.....	20
2.4.2 Clouds and Fog Losses.....	21
2.4.3 Obstacle Losses.....	21
2.4.5 Building Material Losses.....	23
2.4.6 Foliage Losses.....	23
2.5 Absorption and Scattering Effects.....	24
2.6 Excess Attenuation Due to Rainfall.....	24
2.7 Specific Attenuation.....	25
2.8 Rain Attenuation Prediction Methods.....	27
2.8.1 Prediction of Long-term Rainfall Attenuation Statistics.....	29
2.8.2 Moupfouma Model.....	31

Table of Contents

2.8.3	The Crane Attenuation Models	32
2.8.3.1	Global (Crane) Attenuation Model.....	33
2.9	Chapter Summary.....	34
Chapter Three		35
Previous Work Done.....		35
3.1	ITU-R View	35
3.2	Global Studies on Radioclimatological Modeling.....	37
3.3	African Scenario.....	39
3.4	Asian Scenario.....	42
3.5	European Scenario.....	43
3.6	South America Scenario	46
3.7	North America Scenario	47
3.8	Chapter Summary.....	49
Chapter Four.....		50
Prediction of Rainfall-rate Statistics.....		50
4.1	Rain Rate Statistics Measurement in South Africa.....	50
4.2	Effect of Integration Time on Rain Rate Statistics.....	50
4.2	Comparison of Rain Rate Statistics for Different Geographical Locations	54
4.3	Cumulative Distribution of Rain Intensities for Different Geographical Locations.....	59
4.5	Determination of South Africa Rain Climatic Zones	61
4.6	Chapter Summary.....	62
Chapter Five.....		64
Rain Attenuation Prediction and Modeling.....		64
5.1	Computation of Specific Rain Attenuation on Terrestrial Line-of-Sight Links	64
5.1.1	Results and Discussion from the Various Locations	65
5.2	Estimation of Path Attenuation Using Different Existing Models on the Available Local Rain Data	72
5.2.1	Results and Discussion of the Existing Models on the Available Local Data	73
5.3.1	Signal Attenuation Measurements in Durban for the Various Months	81
5.3.2	Rain Attenuation Modeling in Durban at 19.5 GHz from Measurements	82
5.3.3	Discussion for Rain Attenuation Measurements	83
5.3.3.1	The Behaviour of Point Rain rate along Radio propagation Path Lengths	89
5.4	Statistical Analysis of the Rain Attenuation Models Predicted from the Measurements in Durban	90
5.5	Application of Rain Attenuation Predictions	93
5.6	Chapter Summary.....	94
Chapter Six.....		95
Conclusion		95
6.1	Conclusion	95
6.2	Recommendation for Future Work.....	96
References		97

Table of Contents

<i>APPENDICES</i>	103
Appendix A: Computation of Specific Rain Attenuation.....	103
Appendix B: Estimation of Path Attenuation Using Different Existing Models on the Available Local Rain Data	111
Appendix C: The Threshold values of the Chi-Square Test.....	121

List of Figures

	Page
Chapter One	1
1.1 Generalized Vertical Distribution of Temperature and Pressure up to 110 km	3
1.2 Map of South Africa and Neighbouring Countries.....	6
 Chapter Two	 11
2.1 Tropospheric Effects of cloud and Precipitation on Radiowave Propagation.....	17
2.2 Specific Attenuation caused by Oxygen and Water Vapour at Sea Level.....	19
2.3 Variation of Specific Attenuation with Frequency caused by Rain.....	20
2.4 Comparison of Specific Attenuation due to Gaseous constituents, Fog and Precipitation Near the Earth Surface.....	22
2.5 The Fresnel Zone.....	22
 Chapter Three	 35
3.1 ITU-R Rain Climatic Zone Boundaries in America.....	36
3.2 ITU-R Rain Climatic Zone Boundaries in Europe and Africa.....	36
3.3 ITU-R Rain Climatic Zone Boundaries in Asia.....	37
 Chapter Four	 50
4.1 Determination of Coefficient a and b for Durban, South Africa.....	52
4.2 Cumulative Distribution of Rain-Rate for Durban for 1-minute and 60-minute Integration Time.....	54
4.3 Variation in the Annual Intensity (mm/h) Exceeded for 0.01% of the Time for South Africa (Coastal and Inland Regions).....	55
4.4 Variation in the Annual Intensity (mm/h) Exceeded for 0.01% of the Time for South Africa (Temperate and inland Temperate).....	55
4.5 Variation in the Annual Intensity (mm/h) Exceeded for 0.01% of the Time for South Africa (Mediterranean, Steppe, Savannah and Desert Regions).....	56
4.6 Comparison of the 5-year Rain Intensity (mm/h) for 12 locations in South Africa Exceeded for 0.01% of the Time.....	58
4.7 Cumulative Distribution of Rain Intensities for South Africa for an Average of 5-years...	59
 Chapter Five	 64
5.1 Specific Rain Attenuation for Horizontal and Vertical Polarization in Richards Bay; Taking Rain Rate Exceeded for 0.01% of the Time.....	66
5.2 Specific Rain Attenuation for Horizontal and Vertical Polarization in Cape Town; Taking Rain Rate Exceeded for 0.01% of the Time.....	67
5.3 Specific Rain Attenuation for Horizontal and Vertical Polarization in Pretoria; Taking Rain Rate Exceeded for 0.01% of the Time.....	68
5.4 Specific Rain Attenuation for Horizontal and Vertical Polarization in Brandvlei; Taking Rain Rate Exceeded for 0.01% of the Time.....	69

5.5	Specific Rain Attenuation for Horizontal and Vertical Polarization in Durban; Taking Rain Rate Exceeded for 0.01% of the Time.....	70
5.6	Rain Attenuation Prediction Models for Terrestrial Line-of-Sight Links for Richards Bay at Frequencies 10GHz (A) and 40GHz (B).....	73
5.7	Rain Attenuation Prediction Models for Terrestrial Line-of-Sight Links for Cape Town at Frequencies 10GHz (A) and 40GHz (B).....	74
5.8	Rain Attenuation Prediction Models for Terrestrial Line-of-Sight Links for Pretoria at frequencies 10GHz (A) and 40GHz (B).....	75
5.9	Rain Attenuation Prediction Models for Terrestrial Line-of-Sight Links for Brandvlei at Frequencies 10GHz (A) and 40GHz (B).....	76
5.10	Rain Attenuation Prediction Models for Terrestrial Line-of-Sight Links for Durban at frequencies 10GHz (A) and 40GHz (B).....	77
5.11	The Path Profile for 6.73 km Terrestrial Line-of-Sight Link from Howard College Campus to Westville Campus.....	79
5.12	An Aerial Photograph of the 6.73km Line-of-Sight Terrestrial Link.....	79
5.13	Non-Rain Faded Average Signal values for 10 months in 2004.....	81
5.14	Rain Attenuation in Durban for February: Measurement and Model at 19.5GHz.....	84
5.15	Rain Attenuation in Durban for March: Measurement and Model at 19.5GHz.....	84
5.16	Rain Attenuation in Durban for April: Measurement and Model at 19.5GHz.....	85
5.17	Rain Attenuation in Durban for September: Measurement and Model at 19.5GHz.....	85
5.18	Rain Attenuation in Durban for October: Measurement and Model at 19.5GHz.....	86
5.19	Rain Attenuation in Durban for November: Measurement and Model at 19.5GHz.....	86
5.20	Rain Attenuation in Durban for December: Measurement and Model at 19.5GHz.....	87
5.21	Extension of Rain Exceeding a given Intensity, from 0.5mm/h to 40mm/h.....	89

LIST OF TABLES

	<i>Page</i>
Chapter Two	11
2.1 Frequency Dependent Coefficient for Estimating Specific Attenuation	28
2.2 ITU-R Rain Climatic Zones: Rainfall Intensity Exceeded (mm/h).....	30
 Chapter Three	 35
3.1 Coefficients for $R\tau = aR_{\tau}^b$, for $\tau = 1$ minute.....	42
3.2 Rainfall Rate Integration Time for Conversion Parameters in China.....	43
3.3 Regression Coefficients for Locations in Brazil	47
 Chapter Four	 50
4.1 The 12 Geographical Locations and their Corresponding Rain Climatic Zones (Source: South Africa Weather Service).....	51
4.2 Comparison of Coefficients a and b for Durban, South Africa with the Measurements in Ile-Ife, Nigeria ($\tau = 1$ minute).....	53
4.3 Rain Intensity Exceeded (mm/h) for the 12 Selected Geographical Locations in South Africa.....	61
4.4 Proposed Rain Climatic Zone for 12 Geographical Locations in South Africa.....	62
 Chapter Five	 64
5.1 Annual Rain Rate Statistics for each Location at 0.01% Exceedance value.....	65
5.2 Values by which the ITU-R under-estimate the Specific Rain attenuation for Richards Bay.....	66
5.3 Values by which the ITU-R under-estimate the Specific Rain attenuation for Cape Town	67
5.4 Values by which the ITU-R under-estimate the Specific Rain attenuation for Pretoria.....	68
5.5 Values by which the ITU-R under-estimate the Specific Rain attenuation for Brandvlei.....	69
5.6 Values by which the ITU-R under-estimate the Specific Rain attenuation for Durban.....	71
5.7 Terrestrial Link Parameters.....	80
5.8 The Highest Rain Attenuation values and their corresponding Rain Rates recorded in Durban for year 2004 (6.73km at 19.5GHz).....	88
5.9 Equations Predicted by the Logarithmic and Power Models	91
5.10 Rain Attenuation Predicted for the year 2004 in Durban, South Africa in a typical Path of 6.73km	94

Chapter One

Introduction

1.1 Introduction

The study of precipitation effects on terrestrial paths in the millimetric frequency bands has increased in recent years. This is as a result of the congestion in the lower microwave bands and the need for high capacity communication channels. The use of this millimeter wave spectrum is inevitable to service providers and systems designers today due to the better spectrum availability and the inherent ability to provide higher data rates in supporting applications such as high speed data/voice transmission and video distributions [1]. However, communication systems may experience an extreme loss of signal due to attenuation caused by rain on radio link and be temporarily unavailable for use [2].

Precipitation and clouds which are formed by the airborne atmospheric water particles can be entirely in liquid state, composed of ice, or mixtures of ice and air, and water and air. Cloud particles are defined by a size small enough to move very slowly relative to air surrounding them. Fog particles are considered to be the same as cloud particles, the difference being that fogs are clouds in contact with the ground. Precipitation particles are larger and have a significant fall velocity relative to the surrounding air. Liquid precipitation is identified as rain. Taken together, the cloud and precipitation particles are identified as hydrometeors [2]. It has been a common practice to express rainfall loss as a function of precipitation rate. Such a rate depends on the liquid water content and the fall velocity of the drops [3].

Rain affects the design of any communication system that relies on the propagation of electromagnetic waves through the lowest 10 km of the Earth's atmosphere at frequencies above 1 GHz [2]. Above a certain threshold of frequency, the excess attenuation due to rainfall becomes one of the most important limits of the performance of line-of-sight (LOS) microwave links [4]. In the temperate climates this frequency threshold is about 10 GHz, while in the tropical climates and in equatorial climate particularly, the incidence of rainfall on radio links becomes important for frequencies as low as about 7 GHz, since raindrops are larger than in the temperate climate [4], [5]. Therefore, in the planning of terrestrial line-of sight systems at millimeter wavelengths,

an accurate and a fairly precise rainfall-rate statistics data are essential for the proper prediction of rain induced attenuation on propagation paths [6].

For the purpose of this study, a five-year rainfall rate statistics (2000-2004) for twelve different geographical locations in South Africa (see locations on Fig 1.2) have been supplied by the South Africa Weather Services (SAWS). These rainfall rate data are then processed with the 1- minute rain rate data measured in Durban to predict the rain rate and rain induced attenuation on terrestrial line-of-sight links for South Africa.

1.2 The Atmosphere

Our environment consists of the land (lithosphere), the water (hydrosphere), the air (atmosphere) and the living being (biosphere) around us [7]. The gaseous layer surrounding the Earth is commonly known as the atmosphere [8]. The atmosphere is a mixture of gases and vapours which are most dense at sea level. The atmosphere is divided into different layers according to the variability of the temperature gradient with altitude. These layers are the troposphere, stratosphere, mesosphere and ionosphere. The variation of these layers with altitude is shown in Fig 1.1. The boundaries of the layers are referred to as pauses with an identifying prefix [9].

Upon examination, the atmosphere is found to be a complex system not a simple chemical nor even a compound, but a relatively stable mixture of a number of gases [10]. First, there are several chemical elements, which remain permanently in gaseous form under all natural conditions. Secondly gaseous water known as water vapour is a variable part of this mixture. Under certain conditions liquid and solid forms of water also occur in the air but these are not included in the definition of air.

1.2.1 The Troposphere

The troposphere is the lowest region of the atmosphere, where all weather takes place. It is often thought of as the zone of weather. It is the region of rising and falling of air. The air pressure at the top of the troposphere is only 10% of that at sea level [11]. Temperature decreases with height in this layer. Its upper limit (the base of the tropopause) in which temperature ceases to decrease

with height is about 7 km at the equator and 9 km at the poles. The height of the tropopause varies with atmospheric conditions [12]. This temperature decrease is known as the environmental lapse rate and averages at $6.5^{\circ}\text{C}/\text{km}$. The troposphere extends from the surface up to an average altitude of 11 km. This altitude can range as high 16 km in tropics to less than 9 km over the poles. This range is due to the temperature differences between the tropics and poles [11], [12].

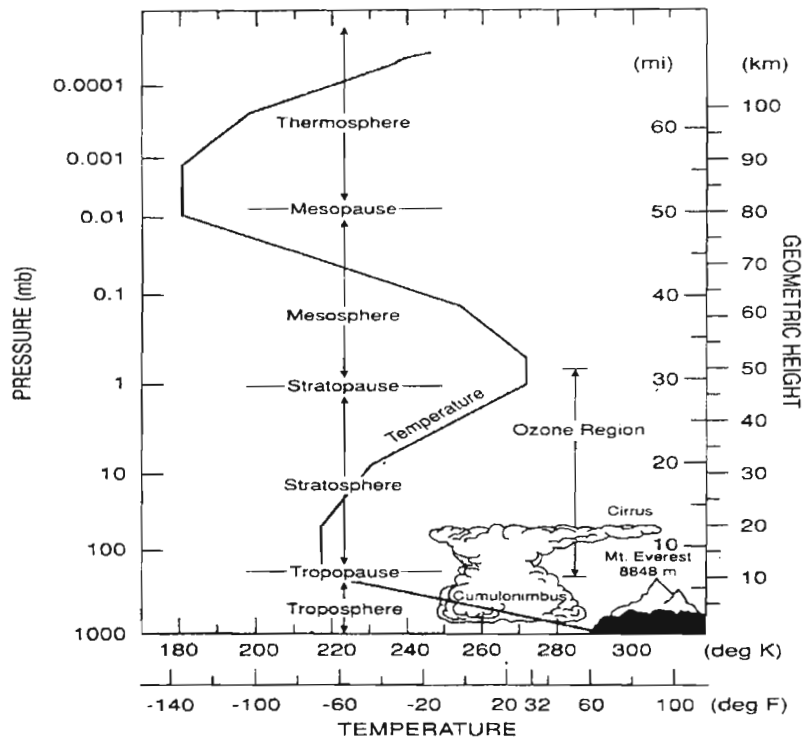


Fig. 1.1 Generalized vertical distribution of temperature and Pressure up to 110 km [8]

1.2.2 Effect of the Troposphere on Terrestrial Radio Paths

The presence of the troposphere in the link model for any Line-of-sight links will introduce five main effects [8]:

1. Excess attenuation, depending on link length and slope, due to atmospheric gases (mainly oxygen and water vapour) and hydrometeors (rain, fog, hail, snow);

2. Modification in the ray path shape which ceases to be straight line and becomes curved, in response to the changes in the refraction index along the path;
3. Creation of privileged directions for wave propagation (ducts) which enable signals to reach distances much larger away than would possible without atmosphere;
4. Considerable fluctuations in the amplitude of the received signal due to the existence of various signal paths, each with its own time delay, which interfere with each other. This phenomenon is known as multipath fading in microwave radio links and scintillation in satellite links;
5. Scattering due to irregularities in the higher layers of the troposphere which enable signals to reach very large distances (a few kilometers) and may be used to provide troposcatter links.

1.3 Nature of Precipitation

Water appears in the atmosphere in variety of forms, usually referred to by the term hydrometeor, which includes particles as diverse as cloud or fog, raindrops, snowflakes, ice crystals, and hail [12]. These hydrometeors attenuate radio waves above 5 GHz and also cause other impairments at communication systems [13]. Of these, rain, cloud or fog, hail, and snow are generally recognized as precipitation. The effects that hydrometeors have on communications systems are dependent both on system frequency and the type of particle present [12].

1.3.1 Effects of Hydrometeors on Microwave Propagation

The most important effects of hydrometeors on microwave propagation are [13]:

- (a) Attenuation caused by dissipation of radio wave energy as heat.
- (b) Scatter resulting in loss in the desired direction and consequently causing interference to other systems.
- (c) Depolarization due to non-spherical nature of raindrops.
- (d) Rapid amplitude and phase scintillations caused by equivalent multipath propagation.
- (e) Antenna gain degradation due to phase dispersion of ray paths reaching the antenna.
- (f) Bandwidth coherence reduction especially in digital systems involving carriers spanning over large channel bandwidths.

1.3 Types of Rain

Rain is a local phenomenon; its effect depends not only on the rain characteristics but also on spatial distribution [14]. Rain can be classified into five types:

1. **Stratified Rain:** Widespread areas with low rain rates up to 25 mm/h and small embedded showers, with horizontal extent of hundreds of kilometers and duration exceeding one hour [13], [14].
2. **Convective Rain:** Localized areas with relatively high rain rates, with strong ascending and descending wind currents that extend deeply in the troposphere. These areas have columnar shapes and sometimes extend up to the tropopause. Very high rain rates with horizontal regions of few kilometers are possible, but they do not last very long (tens of minutes at most). The more intense downpours in temperate climates are usually of this type [14].
3. **Orographic Rain:** Caused entirely or mostly by the forced uplift of moist air over high ground [13].
4. **Monsoon Rain:** A sequence of intense convection rain bands followed by periods of stratified rain. The rain bands have typical widths of 50 km and are hundreds of kilometers in length and produce heavy precipitation lasting for several hours daily [13]-[14].
5. **Tropical Storms Rain:** Large organized regions of rain which may extend over hundreds of kilometers. The tropical storms exhibit a number of spiral bands that terminate in regions of intense precipitation surrounding the central region (the eye) of the storm. Spiral bands also have regions with intense convective rain [13]-[14].

1.4 South Africa Climate and Physical Features

South Africa is situated at the southern tip of the continent of Africa; it is rich in climate and has unique physical features such as the coastal belts, plateaus, rich loamy soil, etc. It has a total area of 1,219,912 sq km. South Africa borders other countries like Botswana and Zimbabwe in the central north, Mozambique in north-east, Namibia in north-west. Swaziland and Lesotho are

embedded in the country (see Fig. 1.2). The Southern parts of the country are bordered by the Indian Ocean and the Atlantic Ocean. South Africa has a coastline of 2,798 km [16].

One of the greenest and best loamy areas of the country is KwaZulu-Natal, which is only 7.6% of the country and the second most populous province. Lying in a broad strip with the Indian Ocean as its western border, it borders Swaziland and Mozambique to the north. Its western border is marked by the dramatic Drakensberg mountain ranges, which has several peaks, well over 3 000m, and its topography combines mountainous areas, rugged green hills and deep-cut valleys [16].

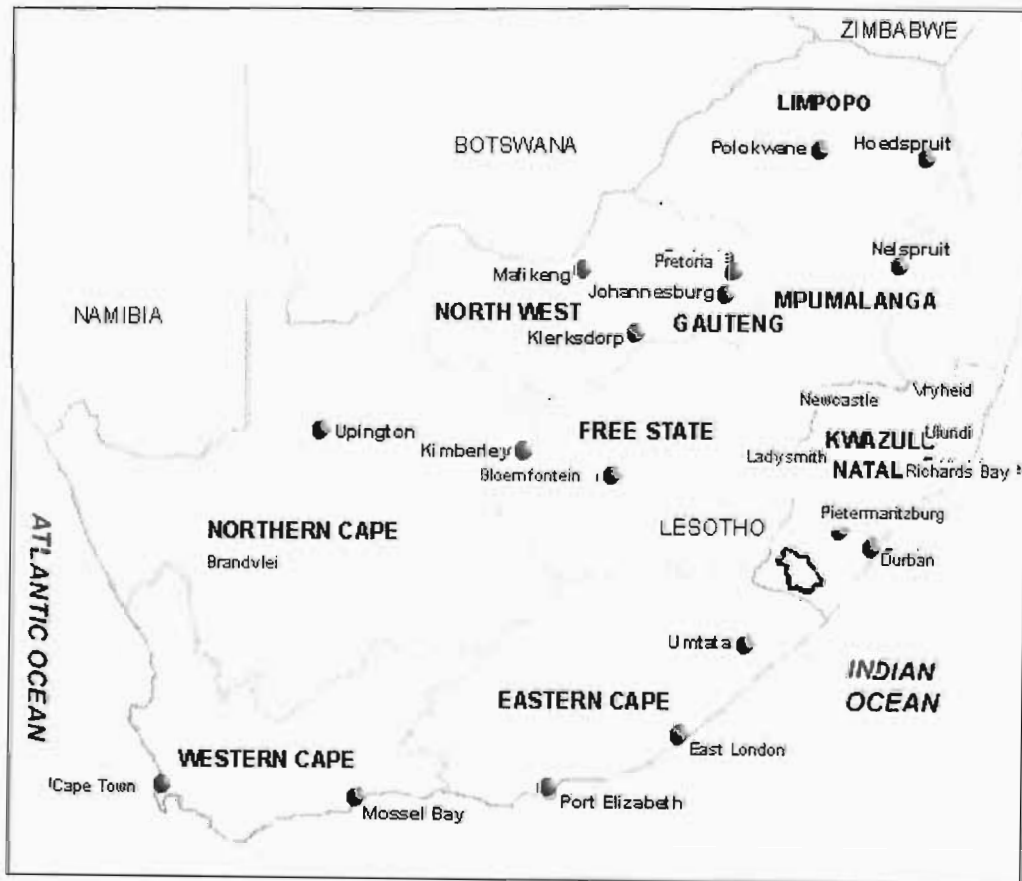


Fig 1.2 Map of South Africa and neighbouring countries [15]

Between the mountains and the humid subtropical coastline is savannah grassland, but there are also areas of indigenous forest here and along the coast. The largest of its many rivers is the Tugela. It is a summer rainfall area, with a climate that ranges from extremely hot along the coast in summer to heavy snow on the mountains in winter. The Midlands are drier than the coast and

can be very cold in winter. KwaZulu-Natal has two capitals: Pietermaritzburg (the province's second-largest city) and Ulundi (the traditional capital) in the north; these two capitals are both inland. The largest city in KwaZulu-Natal is Durban.

South Africa's two biggest harbours are situated in Durban and Richards Bay - the latter is a comparatively small town, its harbour specialises in bulk exports, especially coal which is mined in the interior. Durban's is the busiest port in sub-Saharan Africa.

The fertility of the soil and comparatively good rainfall (more than 1000 mm a year) make agriculture central to the economy. Sugar-cane and tropical fruits are major products of the coastal belt. Dairy, stock and vegetable farming are important land usage. Other land uses include forestry and tea plantations [16].

Temperatures in Durban are mild in winter and warm to hot in summer. The mean annual temperature is 20.4°C and the annual range is 8.0°C. Highest mean temperatures are experienced in February and lowest mean temperatures in July. The maximum temperatures occur in October in association with Berg wind conditions. Temperature is highly variable in any particular area of Durban as a result of topography, type of surface cover and artificial heat production due to combustion activities in industries and motor vehicles.

1.6 Seasonal Variability of South Africa Rainfall

Rainfall is highly seasonal over most of southern Africa. Precipitation over the interior northern regions of South Africa follows an annual cycle and is almost entirely a summer phenomenon [17]. South Africa has an average annual precipitation of 502 mm, as against a world mean of 857 mm. Twenty-one per cent of the country receives less than 200 mm annually, 48 per cent between 200 and 600 mm, while 31 per cent records a total above 600 mm [18]. The 400 mm rainfall line divides the country into a wet and a dry western half.

The moist Indian Ocean air masses, which are the chief source of rain over most of the country, gradually lose their moisture as they move towards the western interior. The second main feature of rainfall distribution pattern is the strong orographic influence. The highest rainfall occurs on the windward slopes of the cape ranges, the Drakensberg and the eastern Transvaal (now Mpumalanga) escarpment [18].

The coastal plain has abundant low stratus cloud and fog, particularly during the summer. The fog is produced when warm, moist tropical air drifts over the cold offshore of Benguela current. The air is cooled below dew point and condensation occurs. At night fog tends to advance on to the coastal plain to a depth of 30 to 50 km, receding again as the land heats up during the day [18]

The winter rainfall region is a relatively small area along the Cape west and South West Coast and has a rainfall regime of the Mediterranean type with a conspicuous winter maxima. The rain is often long lasting and not very intense, except along the mountains, where the orographic effect may induce heavy showers. Snow occurs on the mountains four to six times during winter, but it usually melts within a few days. Hail and thunderstorm are both rare [18].

In the summer rainfall region which covers most of the rest of the country, light orographic rains are common along the windward slopes of the eastern escarpment. Over most of the summer rainfall region, violent convection storms accompanied by thunder, lightning, sudden squalls and often hail are the source of most of the rainfall.

Between the winter and summer rainfall regions lies a transitional area, where rain comes in all seasons-i.e. neither in winter nor in summer is more than 60 per cent of the annual total recorded. There is in fact a clear double maximum, in autumn and spring respectively. This transitional area can be divided into two sub-regions: a southern coastal strip with annual total of 375 to 875 mm, and a drier inland corridor behind the coastal ranges with an annual total of 50 to 250 mm.

It can be seen that South Africa rainfall is unreliable and unpredictable throughout the country. Large fluctuations around the mean annual figure are the rule rather than exception. Like other countries in similar latitudes, South Africa, is periodically afflicted by severe and prolonged droughts. However, the droughts often end with in severe floods especially during summer [18]. Tyson et al. observed that over the period of 1910-1972, much of the summer rainfall area of South Africa experienced a quasi 20-year oscillation rainfall [19]. This rainfall spectrum shows a clear peak at about twenty years as well as peaks in 2-3 and 3-4 years bands [20].

1.7 Justification for the Dissertation

Because of the often severe tropospheric propagation conditions existing in regions of the world at low and mid-latitudes and the resulting constraints on the terrestrial communications systems operating in the microwave and the millimeter-wave bands, there is a particular need for accurate

propagation prediction. Over prediction of propagation effect can result in costly over design of systems. On the other hand, under prediction can result in a system that is unreliable [21].

Rain being a natural phenomenon, which can vary from location-to-location and from year-to-year, causes a rain induced attenuation which is a dominant fading mechanism for millimeter wave paths [22]. This means a solid database of propagation measurements should be made as nearly as possible in the intended geographical area of operations. Attempts have been made to use classification into climate zones on the worldwide basis to extend existing data to a wider range of situations. However, most of the measurements in the databases have been made in the Northern Hemisphere temperate zones [23]. Much evidence suggests that in the tropical and equatorial zones, the factors that make important contributions to propagation impairment are different [23].

This dissertation aims at acquiring enough propagation measurements for different geographical locations in the Republic of South Africa (as represented in Fig 1.2) for several years which can then be used to classify the country into various climatic rain zones. This is achieved by the five years rain rate measurements for twelve different geographical locations in South Africa supplied by the South Africa Weather Service to predict the rain rate and rain attenuation on terrestrial paths in South Africa.

With this, a better estimation of fade margin can be determined which is a major component of link margin. This gives a better performance and reduces the possibility of rain attenuation affecting service, and confines the effect to very heavy and very infrequent rain periods. This margin gives each customer more power than is needed at any given time, so that when rain attenuation occurs, it's rarely affects services. Through this a better system performance can be obtained [23].

1.8 Aims and Objectives of the Study

The objectives of this study are as follows:

1. To obtain an accurate rainfall rate data for different geographical locations in South Africa for several years at 1-minute integration time.

2. To determine the cumulative distributions of the rainfall rate for different geographical locations in South Africa.
3. To determine the rain rate exceeded for 0.01% of the time for each of the location.
4. To classify South Africa into different climatic rain zones based on the available data and measurements.
5. To compute the specific rain attenuation for the different locations based on the available rain data.
6. To estimate the rain path attenuation exceeded for 0.01% of the time for different climatic zones in South Africa using different existing models.
7. To formulate and propose a suitable rain attenuation model for South Africa.

1.9 Chapter Summary

This chapter has given the introduction and the general ideas needed for this research work. “Rain” being the key word in the context of this work has been studied. The South Africa seasonal variability of rainfall, its climate and physical features were reviewed. This chapter also shows the justification for this dissertation and the basic objectives for this work were discussed.

The next chapter gives the theoretical background on electromagnetic waves and radiowave propagation as it affects propagation paths.

Chapter Two

Propagation Phenomena

This chapter gives the necessary guiding background for electromagnetic waves propagation. It also focuses on building the theoretical aspect of radiowave propagation and its propagation losses on radio systems in general. Also reviewed to a reasonable in-depth is the effect of rain on terrestrial radio paths and existing rain attenuation models as it applied to this research focus.

2.1 Propagation Fundamentals

Maxwell's equations provide the starting point for studies of the propagation of electromagnetic waves through the propagation medium [24]. Maxwell's field equations can be expressed as follows [25]:

$$\vec{\nabla}_x \vec{E} = -\frac{\partial \vec{B}}{\partial t} \quad (2.1)$$

$$\vec{\nabla}_x \vec{H} = \vec{J} + \frac{\partial \vec{D}}{\partial t} \quad (2.2)$$

$$\vec{\nabla} \cdot \vec{D} = \rho \quad (2.3)$$

$$\vec{\nabla} \cdot \vec{B} = 0 \quad (2.4)$$

where,

\vec{E} = electric field intensity, in V/m.

\vec{H} = magnetic field intensity, in A/m.

\vec{D} = electric flux density, in coul/m².

\vec{B} = magnetic flux density, in Wb/m².

\vec{J} = electric current density, in A/m².

ρ = electric charge density, in coul/m³

The constitutive standard relationships between field intensity and flux density are given by:

$$\vec{D} = \epsilon \vec{E} \quad (2.5)$$

$$\vec{B} = \mu \vec{H} \quad (2.6)$$

$$\vec{J} = \sigma \vec{E} \quad (2.7)$$

in an isotropic medium.

Here,

ϵ = permittivity tensor in farad/m

μ = permeability tensor in henry/m

σ = conductivity tensor in mhos/m

In free-space, the following simple relations hold between the electric and magnetic field intensities flux densities [25]:

$$\vec{B} = \mu_0 \vec{H} \quad (2.8)$$

$$\vec{D} = \epsilon_0 \vec{E} \quad (2.9)$$

where,

$\mu_0 = 4\pi \times 10^{-7}$ henry/m is the permeability of free-space

$\epsilon_0 = 8.854 \times 10^{-12}$ farad/m is the permittivity of free-space.

$$\text{Let } \frac{\partial}{\partial t} = j\omega \quad (2.10)$$

Using equations (2.6) and (2.10), equation (2.1) becomes:

$$\vec{\nabla} \times \vec{E} = -j\omega \mu \vec{H} \quad (2.11)$$

Using equations (2.5) and (2.7), equation (2.2) becomes:

$$\vec{\nabla}_x \vec{H} = (\sigma + j\omega\varepsilon)\vec{E} \quad (2.12)$$

Then, Maxwell's equation becomes:

$$\begin{aligned} \vec{\nabla}_x \vec{E} &= -j\omega\mu\vec{H} \\ \vec{\nabla}_x \vec{H} &= (\sigma + j\omega\varepsilon)\vec{E} \\ \vec{\nabla} \cdot \vec{D} &= \rho \\ \vec{\nabla} \cdot \vec{B} &= 0 \end{aligned}$$

Taking the curl of equation (2.11):

$$\vec{\nabla}_x \vec{\nabla}_x \vec{E} = -j\omega\mu\vec{\nabla}_x \vec{H} \quad (2.13)$$

Using equation (2.11), equation (2.12) becomes

$$\vec{\nabla}_x \vec{\nabla}_x \vec{E} = -j\omega\mu\vec{\nabla}_x \vec{H} = -j\omega\mu(\sigma + j\omega\varepsilon)\vec{E} \quad (2.14)$$

Using the vector identity:

$$\vec{\nabla}_x \vec{\nabla}_x \vec{E} = -\vec{\nabla}^2 \vec{E} + \vec{\nabla}(\vec{\nabla} \cdot \vec{E})$$

Therefore, equation (2.14) becomes:

$$\vec{\nabla}_x \vec{\nabla}_x \vec{E} = -\vec{\nabla}^2 \vec{E} = -j\omega\mu(\sigma + j\omega\varepsilon)\vec{E}$$

So that,

$$\vec{\nabla}^2 \vec{E} = \gamma^2 \vec{E}$$

Where

$$\gamma = \sqrt{j\omega\mu(\sigma + j\omega\varepsilon)} = \alpha + j\beta \quad (2.15)$$

and γ is the propagation constant, α is the attenuation constant, and β is the phase constant [26].

2.1.1 Propagation in a Lossless Dielectric Medium

For propagation in a lossless dielectric medium, the conductivity, $\sigma = 0$. Therefore, the propagation constant γ becomes:

$$\gamma = \sqrt{j\omega\mu(j\omega\varepsilon)} = j\omega\sqrt{\mu\varepsilon} = \alpha + j\beta \quad (2.16)$$

where

$$\alpha = 0; \quad \gamma = j\omega\sqrt{\mu\varepsilon} = j\beta; \quad \beta = \omega\sqrt{\mu\varepsilon}.$$

2.1.2 Propagation in a Low-loss Dielectric medium

For a low-loss dielectric medium, the conductivity, $\sigma \neq 0$. Therefore, the propagation constant γ is given by:

$$\gamma = \sqrt{j\omega\mu(\sigma + j\omega\varepsilon)} = \sqrt{(j\omega\mu)(j\omega\varepsilon)\left(1 + \frac{\sigma}{j\omega\varepsilon}\right)} \quad (2.17)$$

$$= j\omega\sqrt{\mu\varepsilon}\left(1 - j\frac{\sigma}{\omega\varepsilon}\right)^{1/2} \quad (2.18)$$

where $\frac{\sigma}{\omega\varepsilon}$ is the loss tangent

Using binomial expansion to solve for equation (2.18), it then becomes:

$$\gamma = j\omega\sqrt{\mu\varepsilon}\left[1 + \frac{1}{8}\left(\frac{\sigma}{\omega\varepsilon}\right)^2\right] + \frac{\sigma}{2\omega\varepsilon}\omega\sqrt{\mu\varepsilon} \quad (2.19)$$

Therefore,

$$\alpha \cong \frac{\sigma}{2} \sqrt{\frac{\mu}{\varepsilon}} \quad ; \quad \beta \cong \omega \sqrt{\mu \varepsilon} \left[1 + \frac{1}{8} \left(\frac{\sigma}{\omega \varepsilon} \right)^2 \right]$$

2.2 Free Space Loss

In order to define the loss between the transmitting and receiving antenna separated by a particular distance we assume that the transmission medium between the transmitter and receiver is a vacuum, meaning transmission with no absorption or reflection of energy by nearby objects. The antenna at each end of the link is assumed to be an isotropic, so that we can say point source is an isotropic source¹.

Let the total power in watts radiated by the source be P_T . The envelope containing the radiation around the source can be considered to be an expanding sphere of radius r . The net power flow through the surface of a sphere at its center point is also P_T , hence, it follows that the power flow per unit area through any portion of the sphere's surface is given by [3]:

$$P_{av} = \frac{P_T}{4\pi r^2} \quad (2.20)$$

An isotropic antenna may serve either as a transmitting antenna or a receiving antenna. In the receive function, it absorbs power from the radiation field in which it is situated. Its effective aperture² determines the amount of power that the receiving antenna absorbs in relation to the RF power density of the field [3].

For an isotropic antenna, the effective area A_R , located on the surface of the sphere is $\lambda^2/4\pi$, where λ is the wavelength of the incident radiation field. From equation (2.20) it then follows that an isotropic antenna situated in a radiation field with a power density of P_{av} will deliver into its load, a power P_r given by:

¹ An isotropic source radiates uniformly in all directions (i.e. has a gain of 1 or 0 dB).

² Defined as the area of the incident wave front that has a power flux equal to the power dissipated in the load connected to the receive antenna output terminals.

$$P_R = P_T \left(\frac{\lambda}{4\pi r} \right)^2 \quad (2.21)$$

where r is the radius of the sphere. The transmission loss between transmit and receive antennas is defined as:

$$L_{dB} = 10 \log_{10} \frac{P_T}{P_R} \quad (2.22)$$

Combining equations (2.21) and (2.22), the transmission loss becomes:

$$L_{dB} = 21.98 + 20 \log_{10} \left(\frac{r}{\lambda} \right) \quad (2.23)$$

Equation (2.23) can be restated in a more useful form:

$$L_{dB} = 32.4 + 20 \log(r_{km}) + 20 \log(F_{MHz}) \quad (2.24)$$

where r_{km} is the distance, in kilometers, between transmit and receive antennas, and F_{MHz} is the frequency of the emitted radio field in megahertz.

2.3 Tropospheric Loss

Most of the radio signals passing through the terrestrial transmission paths are very susceptible to rain induced attenuation due to the fact that the radio signals may pass through the entire rain cells [27].

In clear-air, the radio refractive-index³ of the troposphere is slightly greater than unity (typically about 1.0003). The way in which the refractive-index changes with height has immense consequences for radio wave propagation at frequencies greater than 30 MHz and at frequencies

³ A measure of the ability of a medium to bend electromagnetic waves

greater than about 10 GHz in the troposphere. The absorption and scatter due to clouds, rain, snow, etc. which occur at this region also have much effect [12]. Fig 2.1 illustrates some of the effects of cloud and precipitation on radio wave propagation.

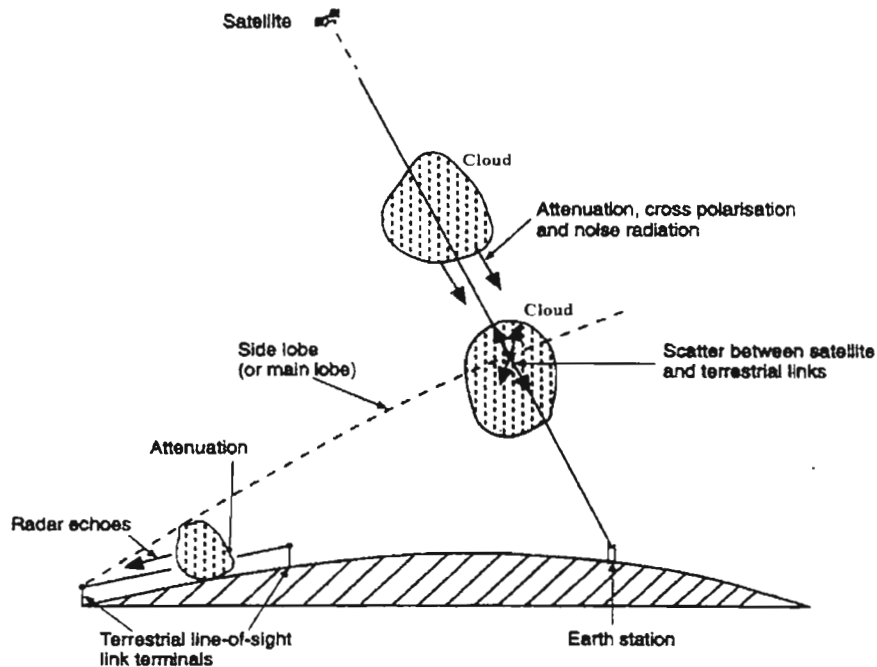


Fig 2.1 Tropospheric effects of cloud and precipitation on radiowave propagation [12]

Above 30 MHz the wavelength is comparable with distance over which variations of atmospheric refractive index occur in the troposphere. These variations are due to changes of temperature, pressure and humidity. The refractive index of the troposphere generally decreases with height. This leads to slight downward refraction of radio rays, which can be very important for communication at VHF, UHF and SHF. If the rate of refractive index decrease with height is sufficiently large and extends over a sufficient height interval and horizontal extent, it may give rise to atmospheric ducts which guide radio energy beyond the normal horizon.

Over a large horizontal area, the refractive index decreases with height abruptly, this may lead to partial reflection of radio energy. Both ducting and partial reflection mechanisms may cause multipath interference on line-of-sight or path interference on beyond-horizon links. Randomly distributed small-scale partial fluctuations of refractive index about the local mean value cause weak signal levels always to be present at large distances beyond the horizon. This is due to

tropospheric scattering from the irregularities, and such scattering may be used to provide radio communication over several hundred kilometers. On line-of-sight paths, these refractive index fluctuations may cause significant scintillation (rapid fading), which is larger in magnitude for longer or higher frequency [12].

For two terrestrial radio terminals within line-of-sight, there may often be a ground reflected ray in addition to the direct ray. There may be also reflected rays (or more than one) from layers of abrupt change of refractive index with height. According to their relative phase, the multipath contributions may give rise to signal enhancement or fading⁴.

At frequencies greater than 3 GHz, rain or cloud may give rise to significant absorption and scattering of radio energy. Scattering from cloud or precipitation (hydrometeors) may cause considerable interference between systems, but even in clear air, the absorption by atmospheric gases alone and the associated noise radiation are important for frequencies greater than 20 GHz [12].

2.4 Propagation Loss Factors

Different propagation mechanisms are important at different frequencies. For microwave systems, transmission loss is accounted for principally by the free-space loss. However, in the millimeter-wave bands additional loss factors come into play. For frequencies below 3 GHz, path attenuation due to atmospheric gases, clouds and rain is small and often neglected, whereas for terrestrial paths at frequencies above 30 GHz, path attenuation due to rain will be important [1], [24].

Electromagnetic wave propagation through the ground, building material, buildings, vegetation, water, atmospheric gases, fog, clouds, wet snow, rain and hail produces attenuation. Depending on the frequency and application, some of these sources of path attenuation may be very important in system design [24].

2.4.1 Atmospheric Gaseous Losses

Transmission losses occur when millimeter wave traveling through the atmosphere are absorbed by molecules of oxygen, water vapour, and other atmospheric constituents. These losses are

⁴ Signal fluctuations above and below its long time median value [14]

greater at certain frequencies, coinciding with the mechanical resonant frequencies of gas molecules [1]. Other gases display resonant lines as well, such as N_2O , SO_2 , O_3 , NO_2 and NH_3 , but because of their low density in the atmosphere, they have negligible effect on propagation [3].

Fig 2.2 gives the specific attenuation⁵ due to absorption of oxygen and water vapour near the surface of the earth as a function of frequency. It shows several peaks that occur due to absorption⁶ of the radio signal by water vapour (H_2O) and oxygen (O_2) [1], [2]. At these frequencies absorption results in high attenuation of the radio signals and, therefore, short propagation distance. For current technology, the important absorption peaks occur at 24 and 60 GHz. The spectral regions between the absorption peaks provide windows where propagation can more readily occur [1].

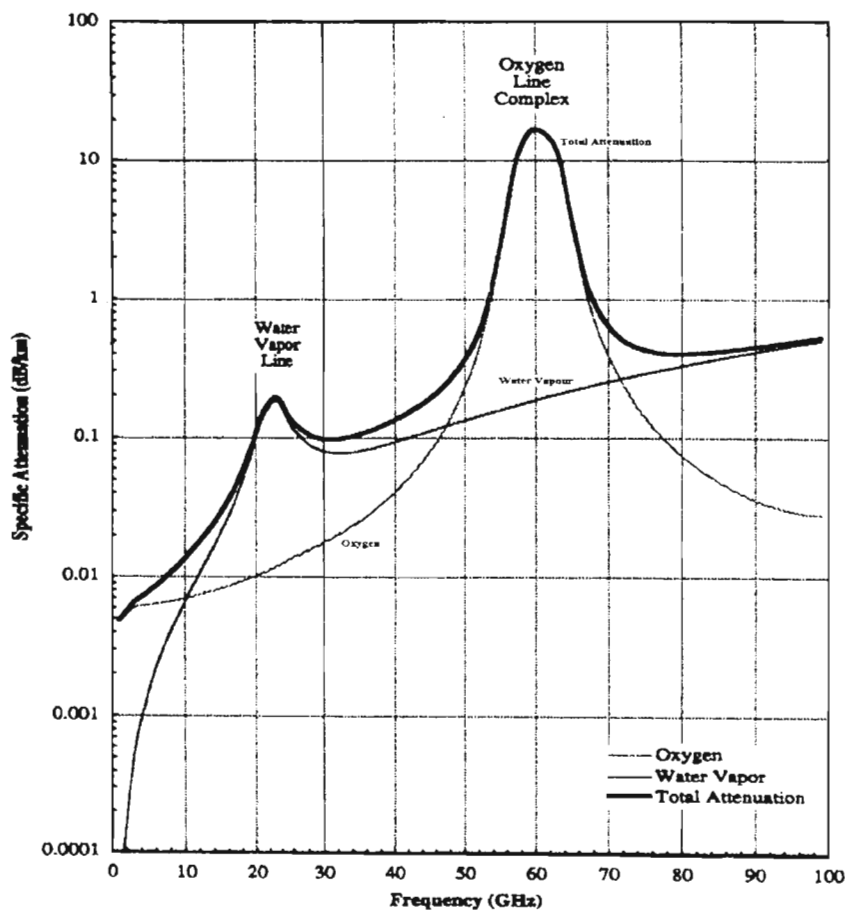


Fig. 2.2 Specific attenuation caused by oxygen and water vapour at sea level [2].

⁵ Reduction per unit length on propagation path [2]

⁶ A reduction in the amplitude (field strength) of a radio wave caused by an irreversible conversion of energy from the radio wave to matter in the propagation path

2.4.2 Rain Losses

Rain has long been recognized as one of the principal causes of unwanted signal loss on centimeter or millimeter wave propagation paths through the lower atmosphere [28]. Raindrops are roughly the same size as the radio wavelengths and, therefore, cause scattering⁷ of radio signals. Fig. 2.3 depicts the variation of specific attenuation with frequency for rain rates of 1, 10, and 100 mm/h. In contrast to absorption by atmospheric gases, the attenuation produced by rain increases nearly monotonically with frequency throughout the 1-100 GHz range. The specific attenuation values reach a maximum and then slowly decrease as frequency continues to increase. At 100 mm/h, the maximum attenuation occurs at about 40 GHz. In the range 1-100 GHz, no frequency window regions occur [2].

The lower the frequency, the better the system designs. An increase in the rain factor reduces the communication signal availability.

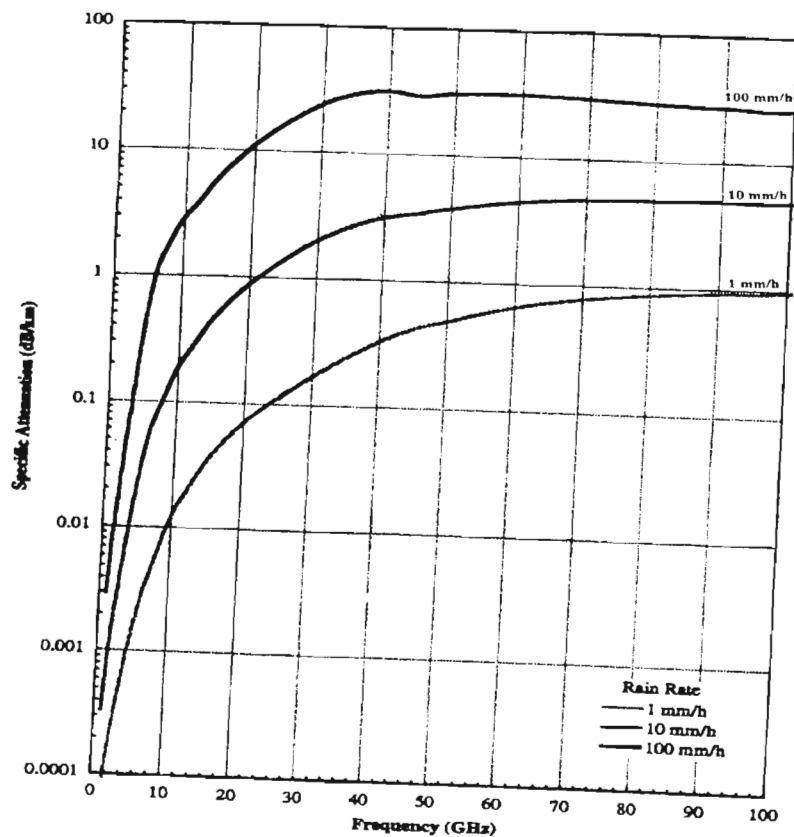


Fig. 2.3 Variation of specific attenuation with frequency caused by rain [2]

⁷ A process in which the energy of a radio wave is dispersed in direction due to interaction with inhomogeneities in the propagation medium

2.4.2 Clouds and Fog Losses

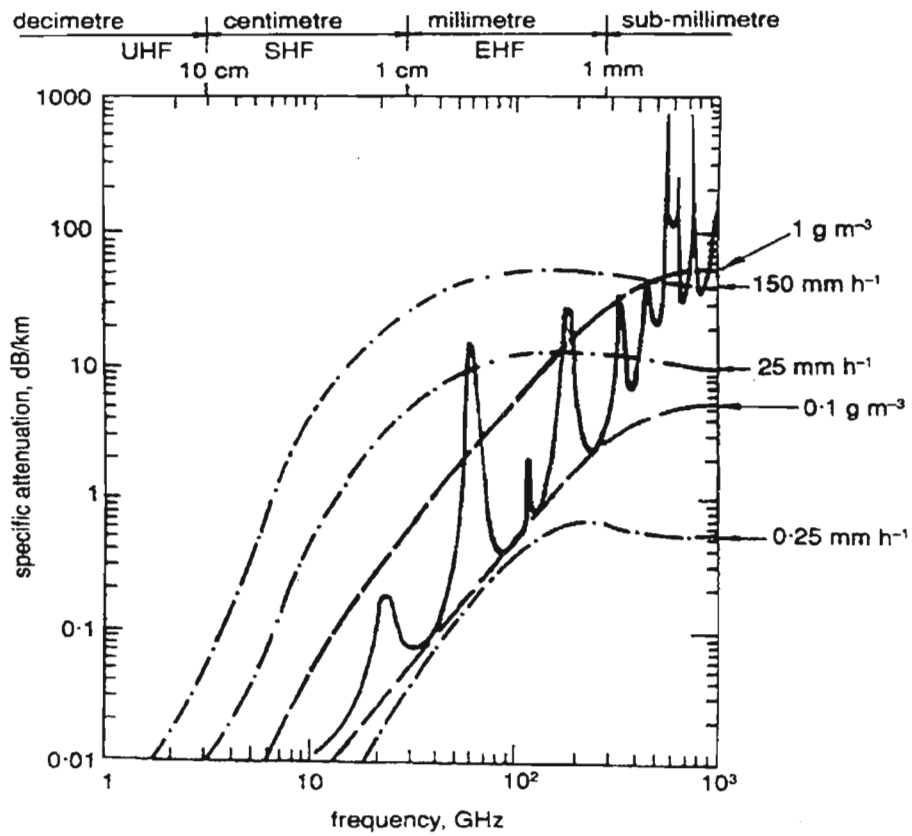
Cloud particles are defined by a size small enough to move very slowly relative to the air surrounding them. Fog particles are considered to be the same as cloud particles, the difference being that fogs are clouds in contact with the ground [2].

Scattering by the very small liquid water droplets that make up liquid water fogs near the earth's surface and liquid water clouds higher in the atmosphere can produce significant attenuation at the higher frequencies. Clouds in the most active parts of mid-latitude thunderstorms may have liquid water content in excess of 5 g/m^3 . The liquid water heights in the atmosphere can range 0 km above ground (a fog) to 6 km above ground in the strong updrafts in convective clouds. For a 1-g/m^3 cloud at a water temperature of 10°C , the specific attenuation increases monotonically with frequency through the UHF, SHF, and EHF frequency bands [24] as shown in Fig 2.4. For frequencies lower than 10 GHz, cloud (fog) attenuation can be ignored. At a frequency of 30 GHz, cloud (fog) attenuations may approach 3 to 4 dB. At a frequency of 120 GHz, this result translates to 30 to 40 dB [24].

2.4.3 Obstacle Losses

Obstacles such as buildings, trees, Earth mounds and hills may attenuate the electromagnetic waves depending on the wavelength considered. If the attenuation through the obstacles is high enough, the obstacle will diffract the wave over or around the obstruction [24]. Such obstacles can also cause reflection (and multipath), scattering and absorption. In a built-up area this results in a wide variation in field strength. The losses caused by absorption and scattering increase with frequency, until at frequencies above UHF, walls or masonry more than 20 cm thick may be regarded as opaque, together with buildings (except those of very light construction) and woods which are visually opaque [12].

A single propagation path between a transmitting antenna and a receiving antenna is a clear line-of-sight path if no obstruction occurs within the few Fresnel zones about the path. Fresnel zones are enclosed within equiphase ellipsoids enclosing path as seen in Fig 2.5 [24].



Key:

- Gaseous attenuation calculated assuming 1013 mb, 20°C, 7.5 g/m³
- · - Rain attenuation for rates shown
- - - Fog attenuation for water content shown, at 20°C

Fig 2.4 Comparison of specific attenuation due to gaseous constituents, fog, and precipitation near the Earth surface [12]

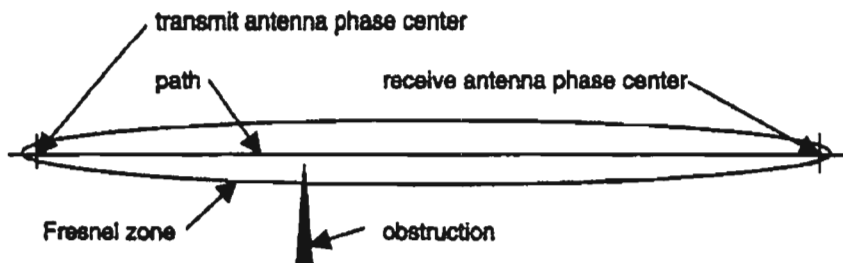


Fig 2.5 The Fresnel zone [24]

2.4.5 Building Material Losses

The elements of building structures- the walls, floors and roofs- are generally constructed from several different materials, each with its own dielectric and conductivity properties. Electromagnetic waves are scattered by, reflected from and transmitted through buildings. Buildings have openings such as windows and doors that have transmission properties different from surrounding walls. The calculation of the scattered fields is complex. Measurements have been made to characterize the scattering properties of “typical” building [24], [29].

Within a building, the received power levels may vary widely with location. Multiple propagation paths between the transmitter and receiver cause these variations [24].

2.4.6 Foliage Losses

Foliage losses at millimeter-wave frequencies are significant. In fact, foliage loss may be a limiting propagation impairment in some cases [1]. Leaves and branches of individual trees scatter electromagnetic waves. Measurements show differences in the path loss through a tree with season and, at higher frequencies, with the amount of water in and on the leaves. Path loss also depends on the number and species of trees along the path and the height and orientation of the propagation path through the leaves [24].

An empirical relationship has been developed (CCIR Rpt 236-2), which can predict the loss. For the case where the foliage depth is less than 400 m, the loss is given by [1]:

$$L = 0.2 f^{0.3} R^{0.6} R^{0.6} \text{ dB.} \quad (2.29)$$

where f is the frequency in megahertz, and R is the depth of foliage transversed in meters and applies for $R < 400m$. This relationship is applicable for frequencies in the range 200-95,000 MHz [1].

2.5 Absorption and Scattering Effects

As indicated before, a major problem in radio propagation is attenuation due to precipitation, which exceeds that of all other sources of excess attenuation above 18 GHz [3]. Rainfall and its effect on propagation are the major focus here. To better understand these loss mechanisms due to rainfall, absorption and scattering are reviewed.

When an incident electromagnetic waves passes over on object that has dielectric properties different from the surrounding medium, some energy is absorbed and some is scattered. That which is absorbed heats the absorbing material; that which is scattered is quasi-isotropic and relates to the wavelength of the incident wave. The smaller the scatterer, the more isotropic it is in direction with respect to the wavelength of the incident energy [3].

We can develop a formula derived from equation (2.24) to calculate total transmission loss for a given link [1], [3]:

$$\text{Attenuation}_{\text{dB}} = 92.45 + 20 \log F_{\text{GHz}} + 20 \log r_{\text{km}} + a + b + c + d + e \quad (2.25)$$

Where

F = Operating frequency in GHz

r = Link length in kilometers

a = Excess attenuation⁸ (dB) due to water vapour

b = Excess attenuation (dB) due to mist and fog

c = Excess attenuation (dB) due to oxygen (O₂)

d = Sum of absorption losses (dB) due to other gases

e = Excess attenuation (dB) due to rainfall

2.6 Excess Attenuation Due to Rainfall

Of the factors a through e in equation (2.25), factor e , excess attenuation due to rainfall is the principal one affecting path loss. For instance, even at 22 GHz for a 10 km path only 1.6 dB must be added to free space loss to compensate for water vapour loss. This is negligible when compared to free space loss itself, such as 19.3 dB for the first kilometer at 22 GHz,

⁸ "Excess" in this context means excess in free-space loss

accumulating thence approximately 6 dB each time the path length is doubled. On the other hand, in certain regions of the world, excess attenuation due to rainfall can exceed 150 dB depending on the availability desired for a particular path [3].

Rain attenuation can be obtained directly through measurement or predicted from knowledge of rain rate and rain drop size distributions. The spectrum of the rain drop sizes determines the rainfall rate. It is thus possible to estimate the attenuation by means of indirect measurements performed with rain gauges, radiometers and radars [30].

Considering the horizontal and the vertical non-uniformity of rain structure, the radar is undoubtedly, the best tool for observing the spatial variation of rain intensity, thus allowing the estimation of the attenuation along propagation path. However, due to its high initial investment, high operation and maintenance cost and difficult calibration for direction measurement of the attenuation, this method has not been widely applied [30]. Rainfall rate measurements, on the hand, require very little hardware and can be set-up in considerably less time at a low cost [31]. Therefore, the most common attenuation prediction methods are those based on point rainfall rate distributions [30], [31].

The procedure for predicting the attenuation is based on the relationship between specific attenuation and rain rate, established through the modelling of rain microstructure. For example: shape, size, temperature and terminal speed of the raindrops. The rain induced attenuation is computed by integrating the specific attenuation along propagation path. The non-uniform character of the rain along the path is taken into account by means of statistical model for rain intensity. The statistical distribution of rain attenuation is, thus, obtained from the rain rate distribution for the region considered [30].

2.7 Specific Attenuation

The term specific attenuation⁹ is a fundamental quantity in calculating rain attenuation [32]. The hydrometeors that constitute the rain behave like dissipative dielectric particles causing significant absorption and scattering effects on radio waves at frequencies above 10 GHz. The relative contribution of these two effects in terms of the wave attenuation depends on the relation

⁹ Attenuation per unit distance

between drop size and the wavelength of the transmitted energy. The attenuation experienced by a wave crossing a rainy medium is given by the sum of individual contributions of the drops that constitute the medium. Considering the various raindrops of different dimensions, the specific attenuation is calculated by integrating each raindrop contribution [30].

The specific attenuation, γ in (dB/km) due to precipitation is evaluated from the classical Mie scattering theory. The evaluation depends on the knowledge of the complex refractive index of water at the raindrop temperature as well as the terminal velocity and the size distribution of the raindrops. The specific attenuation γ is given as [30]:

$$\gamma = 4.343 \int_0^{\infty} Q_t(D)N(D)dD \quad (2.26)$$

where,

$Q_t(D)$ = extinction cross section

$N(D)dD$ = the number density of raindrops with diameter D in dD

$Q_t(D)$ is determined theoretically from classical scattering theory developed by Mie for frequencies above 3 GHz. $Q_t(D)$ is a function of drop size diameter, wavelength, and complex refractive index n of the water drops and is given as:

$$Q_t(D) = Q_s(D) + Q_A(D) \quad (2.27)$$

where $Q_s(D)$ and $Q_A(D)$ are scattering and absorption cross sections respectively.

Olsen et al have determined the specific attenuation to be related to the rainfall rate through the relation [32]:

$$\gamma = KR^\alpha \quad (2.28)$$

This is known as the power-law form of rain specific attenuation [33]. Here R is the rain rate in mm/h, k and α are power law parameters, which depend on frequency, raindrop size distribution, rain temperature and polarization.

Values for k and α for the frequency range 1-400 GHz were calculated for raindrops with the assumed shape of oblate spheroids, at the temperature of 20°, using the drop size distribution proposed by Laws and Parsons [34], terminal velocity following Gunn and Kinzer [35], and refractive index values according to the model of Ray. These values were adopted by the ITU-R recommendation 838-2 [36]. The values are shown in Table 2.1 and these have been tested and found to be sufficiently accurate for attenuation prediction up to frequencies of 55 GHz [36].

For intermediate values of k_H , k_V , α_H , and α_V for an operating frequency f , one must use logarithmic interpolations for f and k , and linear interpolation for α . If k_1 , k_2 , α_1 , and α_2 are the values at frequencies f_1 and f_2 to be interpolated in order to have the values at frequency f , then:

$$k(f) = \log^{-1} \left\{ \log \frac{k_2}{k_1} x \left[\frac{\log(f / f_1)}{\log(f_2 / f_1)} \right] + \log k_1 \right\} \quad (2.29)$$

$$\alpha(f) = \left\{ [\alpha_1 - \alpha_2] x \left[\frac{\log(f / f_1)}{\log(f_2 / f_1)} \right] + \alpha_1 \right\}$$

To find the total attenuation path due to rain, it is necessary to know the specific attenuation or the rain rate exceeded for the percentage of time of interest, the raindrop size distribution on which the coefficient k and α depend [30].

2.8 Rain Attenuation Prediction Methods

Rainfall is a natural, time-varying phenomenon [30]. Estimate of rain attenuation are usually derived from the available information on rain rate observed in the geographical area considered. Most of the many methods proposed for predicting rain induced attenuation make use of the rainfall cumulative distribution measured at a point.

Certain authors have used the concept of equivalent path average rain rate which is obtained by multiplying the point rain rate for the time percentage of interest by a reduction factor [4], while other authors use an effective path length¹⁰, the value of which is obtained by multiplying the actual path length by a reduction coefficient [4].

¹⁰ Effective path length is the hypothetical length of a path along which the attenuation for a given time percentage result from a point rainfall rate that occurs for the same time percentage[4]

Table 2.1 Frequency dependent coefficients for estimating specific attenuation [36]

Frequency (GHz)	k_H	k_V	α_H	α_V
1	0.0000387	0.0000352	0.9122	0.8801
1.5	0.0000868	0.0000784	0.9341	0.8905
2	0.0001543	0.0001388	0.9629	0.9230
2.5	0.0002416	0.0002169	0.9873	0.9594
3	0.0003504	0.0003145	1.0185	0.9927
4	0.0006479	0.0005807	1.1212	1.0749
5	0.001103	0.0009829	1.2338	1.1805
6	0.001813	0.001603	1.3068	1.2662
7	0.002915	0.002560	1.3334	1.3086
8	0.004567	0.003996	1.3275	1.3129
9	0.006916	0.006056	1.3044	1.2937
10	0.01006	0.008853	1.2747	1.2636
12	0.01882	0.01680	1.2168	1.1994
15	0.03689	0.03362	1.1549	1.1275
20	0.07504	0.06898	1.0995	1.0663
25	0.1237	0.1125	1.0604	1.0308
30	0.1864	0.1673	1.0202	0.9974
35	0.2632	0.2341	0.9789	0.9630
40	0.3504	0.3104	0.9394	0.9293
45	0.4426	0.3922	0.9040	0.8981
50	0.5346	0.4755	0.8735	0.8705
60	0.7039	0.6347	0.8266	0.8263

Many of the propagation predictions models employed in the design of terrestrial line-of-sight systems make use of long-term cumulative Distribution of point rainfall intensity. Then a number of years of observations are required to establish an accurate estimate of true long-term mean rainfall-rate distribution.

2.8.1 Prediction of Long-term Rainfall Attenuation Statistics

For the prediction of long-term statistics of rain attenuation, ITU-R P.530-10 [37] has given following simple technique that may be used for estimating the long-term statistics of rain attenuation:

Step 1: Obtain the rain rate $R_{0.01}$ exceeded for 0.01% of the time (with an integration time of 1 minute). If this information is not available from local sources of long-term measurements, an estimate can be obtained from the information given in Recommendation ITU-R P.837 [38]. The ITU-R P. 837-1 provides global distributions of rainfall rate for various time percentages according to specified zones as shown in Table 2.2.

Step 2: Compute the specific attenuation, γ_R (dB/km) for the rainfall rate at the frequency, polarization of the transmission. ITU-R P.838 [36] provides a method for achieving this using the power-law relationship stated in equation (2.28).

Having obtained the specific attenuation corresponding to the reference rainfall rate, the total path attenuation needs to be estimated. At this point, it is necessary to recognize that, because of the spatial inhomogeneity present in rain, it is unlikely that the reference rainfall rate will extend uniformly over the length of the transmission path, unless this is very short [12]. The longer the path, the less likely it is that rain will extend the full length of the path, and so an effective path length d_{eff} is introduced [12]. This leads to the next step.

Step 3: Compute the effective path length, d_{eff} of the link by multiplying the actual path length d by a distance factor r .

$$d_{eff} = rd \quad (2.30)$$

Table 2.2 ITU-R Rain climatic zones: Rainfall intensity exceeded (mm/h) [38]

Percentage of time (%)	A	B	C	D	E	F	G	H
1.0	<0.1	0.5	0.7	2.1	0.6	1.7	3	2
0.3	0.8	2	2.8	4.5	2.4	4.5	7	4
0.1	2	3	5	8	6	8	12	10
0.03	5	6	9	13	12	15	20	11
0.01	8	12	15	19	22	28	30	32
0.003	14	21	26	29	41	54	45	55
0.001	22	32	42	42	70	71	65	53
Percentage of time (%)	J	K	L	M	N	P	Q	
1.0	8	1.5	2	4	5	12	24	
0.3	13	4.2	7	11	15	34	49	
0.1	20	12	15	22	35	65	72	
0.03	21	23	33	40	65	105	96	
0.01	35	42	60	63	95	145	115	
0.003	45	70	105	95	140	200	142	
0.001	55	100	150	120	180	250	170	

where d is the actual path length, and r is a factor which reduces in magnitude as d increases. It is given by:

$$r = \frac{1}{1 + d/d_0} \quad (2.31)$$

The quantity d_0 is a rainfall-rate-dependent factor introduced, to reflect the fact that the greater the intensity of rainfall in a storm, the smaller the physical dimensions of the storm are. It is given by [12], [37]:

$$d_0 = 35e^{-0.015 R_{0.01}} \quad (2.32)$$

where, for $R_{0.01} \leq 100$ mm/h:

For $R_{0.01} > 100$ mm/h, use the value 100 mm/h in place of $R_{0.01}$.

Then, finally, the path attenuation exceeded for 0.01% of time is obtained from:

$$A_{0.01} = \gamma_R d_{eff} = \gamma_R dr \quad dB \quad (2.33)$$

If attenuation statistics are required for other time percentages, they can be obtained from

$$A_p = A_{0.01} \times 0.12 p^{-(0.546+0.0431 \log_{10} p)} \quad (2.34)$$

where p is the required time percentage, in the range $0.001\% \leq p \leq 1\%$. [12], [37]

The prediction procedure outlined above is considered to be valid in all parts of the world at least for frequencies up to 40 GHz and path lengths up to 60 km.

2.8.2 Moupfouma Model

Moupfouma [4] proposed an empirical model for predicting rain-induced attenuation on terrestrial paths from the knowledge of 1-minute rain intensities recorded in the considered geographical area and the corresponding percentages of time P during which these rain rate was exceeded. He used experimental data obtained in 30 terrestrial radio links in the 7-38 GHz band range with path length ranging from 1.3 to 58 km located in Africa, Japan, United States and Europe and well-known fitting procedures.

His work was found to be in agreement with prediction method proposed by the International Radio Consultative Committee (CCIR) now ITU-R. The rain induced attenuation on a line-of-sight path can be expressed as:

$$A(dB) = kR^\alpha L_{eff} \quad (2.35)$$

with

$$L_{eff} = rl$$

where l (km) is the actual path length, L_{eff} the effective path length and r a reduction factor coefficient having the well-known form:

$$r = \frac{1}{1 + Cl^m} \quad (2.36)$$

The attenuation $A(dB)$ and the 1 min rain rate R (mm/h) are calculated for the same time percentage, k and α are the regression coefficients depending on frequency and polarization. To derive C and m experimental data obtained were used. It was found that C depends on probability level P (percent) of interest for which data are available, and m depends on the radio link path length and its frequency. The resultant formula for the path length reduction factor is given by:

$$r = \frac{1}{1 + 0.03 \left(\frac{P}{0.01} \right)^{-\beta} l^m} \quad (2.37)$$

with

$$m(F, l) = 1 + \Psi(F) \log_e l \quad (2.38a)$$

and

$$\Psi(F) = 1.4 \times 10^{-4} F^{1.76} \quad (2.38b)$$

where $F(GHz)$ is the frequency, the β coefficient is given as a result of a best fit by:

$$\left. \begin{array}{ll} l < 50km & \\ \beta = 0.45 & \text{for } 0.001 \leq P(\text{percent}) \leq 0.01 \\ \beta = 0.6 & \text{for } 0.01 \leq P(\text{percent}) \leq 0.1 \\ l \geq 50km & \\ \beta = 0.36 & \text{for } 0.001 \leq P(\text{percent}) \leq 0.01 \\ \beta = 0.6 & \text{for } 0.01 \leq P(\text{percent}) \leq 0.1 \end{array} \right\} \quad (2.39)$$

The effective path length reflects the spatial inhomogeneity. Its frequency dependence which appeared in the reduction coefficient r equation (2.38b) results from both the non uniformity of the rain along the radio link path and the non linear dependence of the specific attenuation rain rate [4].

2.8.3 The Crane Attenuation Models

The Crane attenuation models, after Robert K. Crane, are popular for satellite links but also have terrestrial models. They were developed in the late 1970s and 1980s to provide a statistical relationship between rain rate model predictions and path attenuation predictions for use on either

Earth-space links or terrestrial paths. There are three versions of the Crane models. The Global Crane model was developed in 1980. In 1982 the two-component Crane model was developed that used a path- integrated technique. A volume cell contribution and a debris contribution for a path were computed separately and added to provide a link calculation. As a refinement of the 2-component model, the revised two-component model was introduced in 1989 that includes spatial correlation and statistical variations of rain within a cell [2], [22].

2.8.3.1 Global (Crane) Attenuation Model

The global, or Crane attenuation model, was developed for use on either Earth-space or terrestrial paths. It is based entirely on geophysical observations of rain rate, rain structure, and the vertical variation of atmospheric temperature [2]. The prediction of surface point rain rate is only the first step in a model for the prediction of attenuation [28]. Rain is characteristically inhomogeneous in the horizontal, and a statistical model is required to provide an estimate of the effect of the homogeneity on the estimation of attenuation [2], [28]

The simplest path profile for rain rate which, when integrated produces the observed median power law relationship, is the derivative of the power law relationship with respect to the path length. The observations were numerically differentiated to obtain this simplest profile model. This is accomplished by a piecewise representation of the path profile by exponential functions. An adequate model results when two exponential functions are used to span the 0 to 22.5 km distance range, one from 0 to $\delta(R)$ km, the other from $\delta(R)$ to 22.5 km [2], [28]. The resulting model for attenuation on a horizontal or terrestrial (or path-integrated) rain rate is given by [2]:

$$A_T(R, D) = \gamma(R) \left(\frac{e^{y\delta(R)} - 1}{y} + \frac{e^{-zD} - e^{-y\delta(R)}}{z} e^{\alpha B} \right) \quad \delta(R) < D < 22.5 \quad (2.40)$$

$$A_T(R, D) = \gamma(R) \left(\frac{e^{y\delta(R)} - 1}{y} \right) \quad 0 < D < \delta(R) \quad (2.41)$$

where

$$A_T = \text{horizontal path attenuation (dB)}$$

R = rain rate

D = path length (km)

$\gamma(R)$ = specific attenuation, = kR^α (dB / km)

and the remaining coefficients are the empirical constants of the piecewise exponential model:

$$B = \ln(b) = 0.83 - 0.17 \ln(R)$$

$$c = 0.026 - 0.03 \ln(R) \quad (\text{km}^{-1})$$

$$\delta(R) = 3.8 - 0.6 \ln(R) \quad (\text{km}^{-1})$$

$$u = \frac{B}{\delta(R)} + c \quad (\text{km}^{-1})$$

$$y = \alpha u \quad (\text{km}^{-1})$$

$$z = \alpha c \quad (\text{km}^{-1})$$

This model provides a prediction of the attenuation or path integrated rain rate given the equiprobable value of rain rate [2].

2.9 Chapter Summary

This chapter has covered the basic propagation fundamentals for electromagnetic waves passing through different propagation media. Also different propagation losses on terrestrial radio paths were also studied. The effect of rain on radio links as it leads to a rain induced attenuation on terrestrial line-of-sight links was also reviewed. This chapter also shows the various existing rain attenuation models: ITU-R Model, Moupfouma Model and the Global Crane Model as it applies to this research work for different regions around the world.

The next chapter focuses on the various works that have been done by different authors on rain rate and rain attenuation prediction in different parts of the world.

Chapter Three

Previous Work Done

In this chapter, the previous work done by various authors on rain rate and rain attenuation predictions on regional basis will be reviewed. Also the work done on global radioclimatological modeling will be covered. This chapter will also look into the ITU-R view on the prediction of rain rate and rain attenuation prediction on terrestrial line-of-sight links.

3.1 ITU-R View

From the ITU-R perspective, recommendation 837 [38], divides the whole globe into fifteen climatic rain zones by using the median cumulative distribution of rain rate for the rain climatic region [38]. This shows the rain intensity for the various climatic zones (see Fig 3.1, 3.2 and 3.3). These are to be utilized to obtain the rain intensity for estimating attenuation due to rain on both terrestrial and earth satellite microwave links for areas without adequate data on the cumulative rain intensity distribution [30].

According to the ITU-R classification, Southern Africa has six rain zones, namely: C, D, E, J, K, and N of which South Africa has five. These are: C, D, E, K, and N. However, these ITU-R designations are not necessarily adequate [30]:

- The entire sub-continent has been designated by two types of rain climate by the ITU-R (K and N), Sakar et al. [39], [30] have shown that the entire Indian sub-continent can be divided into 10–12 types of rain climatic zones.
- Although Brazil is classified by ITU-R into two rain climates (N and P), Migliora et al [40], [30] reported rain rate measurement in 11 rain climatic zones in Brazil.
- While according to ITU-R, China is designated by 5 types of rain (E, F, G, H, K), Zang et al [41], [30] were able to obtain 12 rain climatic zones for China.

Therefore there is great need to redefine the ITU-R regional rain climatic zones based on the actual local data [30] especially in the tropical climates.

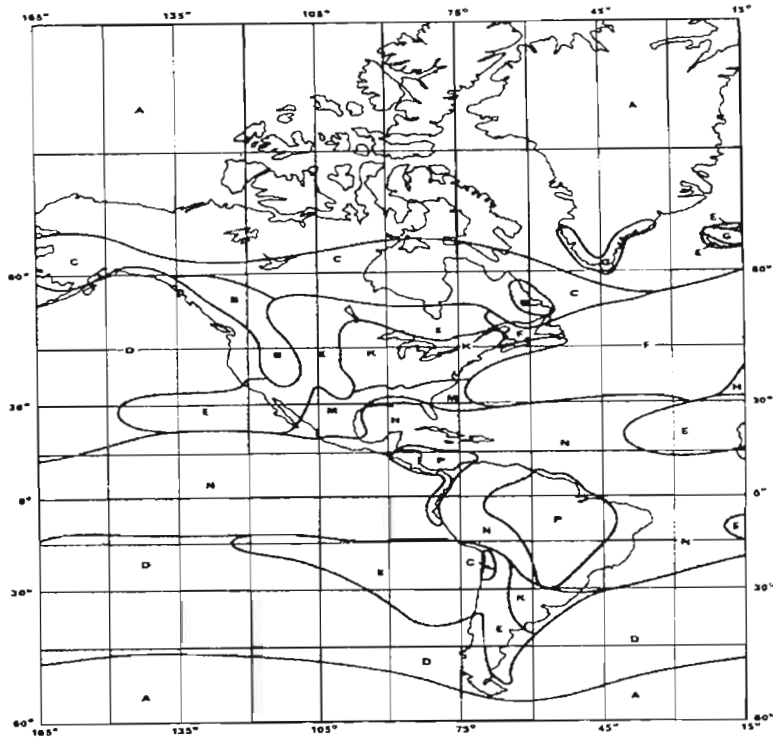


Fig 3.1 ITU-R rain climatic zone boundaries in America [38]

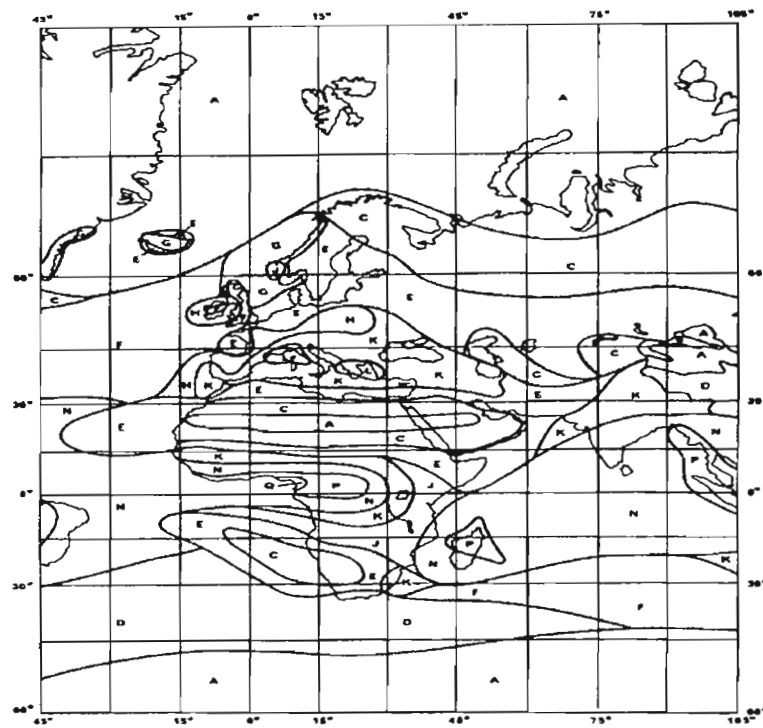


Fig 3.2 ITU-R rain climatic zone boundaries in Europe and Africa [38]

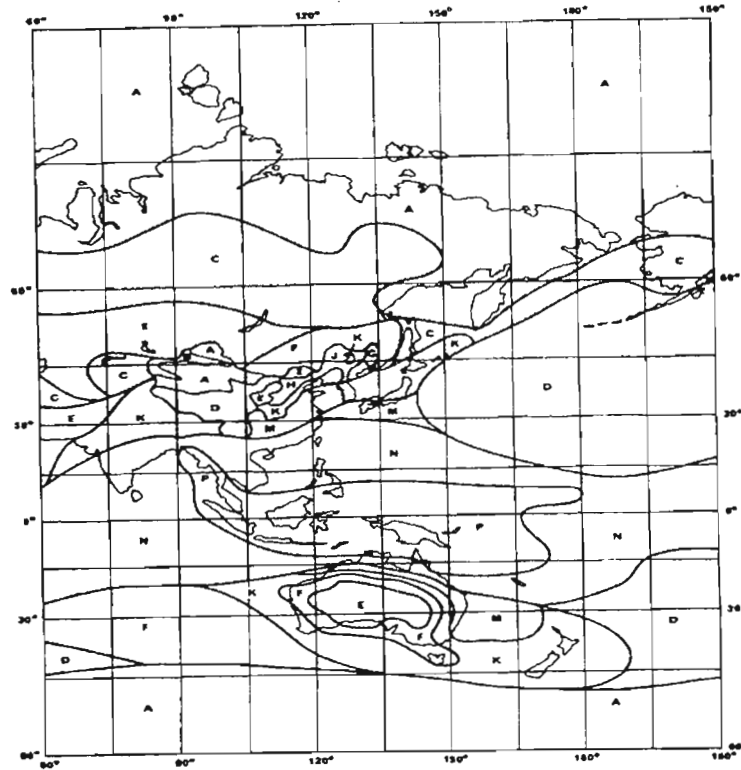


Fig 3.3 ITU-R rain climatic zone boundaries in Asia [38]

3.2 Global Studies on Radioclimatological Modeling

Olsen [21] provides a summary of global work on radioclimatological modeling. In his submission, extensive use of digital microwave and millimeter radio links in the communications networks of various countries over the last decades has resulted in a renewed interest in methods of predicting the effects of precipitation on radio propagation. Most current predictions of tropospheric propagation effects are made either for the average worst month or the average year. However, the radio-climatological frameworks for such predictions are more than thirty years old for clear-air effects and more than twenty years old for precipitation effects. A recent effort by international community to update the radioclimatological data base for tropospheric propagation predictions has involved an increase in the number of meteorological stations included in the analysis, the introduction of new potential prediction variables, and improved mapping and other presentation procedures. The purpose of his submission is primarily in twofold: (i) to present a review of recent progress in global radioclimatological modelling, and (ii) to address the question of what radioclimatological measurements and modelling will be required in future [21].

The global ITU-R radioclimatic models of point rain rate distributions within discrete rain zones have been available for prediction of annual cumulative distributions of rain attenuation on terrestrial and earth-space line-of-sight links since early 1970's. Such models have also been used for prediction of interference due to rain scatter into terrestrial and earth-space systems sharing the same frequencies since the early 1970's.

The work of Crane has considerably influenced the zonal models of the ITU-R, and the Crane models [2], [21], [28] as been used extensively in the United States, although to a lesser extent in other parts of the world. The work by Segal has also considerably influenced the ITU-R zonal models, and provided a systematic approach for obtaining a specific number of rain zones in Canada that have sufficiently large data bases of short-integration-time data [6], [21],[42]. One of the values of the zonal approach is that it allows spectrum regulators to perform systems calculations for a small number of somewhat representative situations.

Because of the discrete nature of the zonal approach and its inherent lack of precision to some degree, however, various other attempts have been made to predict point rain rate distributions, or statistics on such distributions, at specific points within a region. Such approaches have normally used measured rain rate distributions for as many locations in a region as possible, and then fitted contour maps for particular parameters of the distribution. Perhaps the first successful approach of this type was that of Segal for Canada [42], which employed contour maps of two parameters of the rain rate distribution, based on data for forty-seven locations within Canada and adjacent regions of the United States. Watson et al [43], later mapped rain rates exceeded for 0.1% and 0.01% of an average year based on data for four hundred locations within Europe. Moupfouma [44], developed two more general global models using two parameters, one of which was conveniently the rain-rate exceeded for 0.01% of the time. The ITU-R (and its predecessor, the CCIR), has provided a global contour map of the rain rate exceeded for 0.01% of the year since 1982 [45], although it was derived in part from use of the zonal model, at least at the early stages. The accuracy of the global map of the ITU-R has of course always been quite variable because of the lack of data for several regions of the world including Africa.

Another attempt to avoid the zonal approach was made by Rice and Holmberg [46], who developed a model employing three basic long-term parameters: the average annual rainfall (mm), the ratio of the thunderstorm to total rain, and the average annual number of days with rainfall of 0.25 mm or more. Although rain rate distributions have been the prime focus of

radioclimatological modelling because of their major contribution to the prediction of the propagation effects, other meteorological characteristics have also been of interest. The other meteorological parameter for which a climatic dependence has been attempted is the height of the 0°C isotherm. Results of the various studies at low latitudes in particular, have been reviewed by Ajayi [30]. All these results have been translated into several ITU models over the last decades.

Radioclimatological modelling has primarily been with respect to annual and worst-month predictions of propagation characteristics, in particular cumulative distributions. There have been speculations about the possible climatic variability of the raindrop size distributions at the surface, and the horizontal and vertical structure of rain for many years [21].

The existing global ITU-R prediction techniques for predicting cumulative distributions of rain attenuation on terrestrial [37] and earth-space [47] links in fact do not assume climatologically constant raindrop size distributions and horizontal structure for a given rain rate, although the latter may be true only at 0.01 % exceedance (since translation of the attenuation exceeded to other percentages of time is totally empirical, the implicit assumptions about horizontal structure at these occurrences are not fully evident) [21].

Accurate determination of climatological variations of the precipitation variables may require the deployment of ground-based sensors (e.g., distrometers, radars) in a number of locations around the globe, similar to the network of rain gauges currently in operations [21]. A few more accurate ground-based measurements of drop size distributions and rain structure in tropical regions in particular, would be quite helpful. This is because additional propagation measurements will verify and improve current climatological-based models [21].

3.3 African Scenario

McCarthy et al. in 1994, [30] presented the cumulative distribution (CD) of rainfall rate obtained in Doula (Cameroun), Ile-Ife (Nigeria), and Nairobi (Kenya) during the two years of joint radiometric measurement campaign in Africa. Although the total rain accumulation were highest in Doula, the convective factor which was lower than that of Ile-Ife, made the rain rate exceeded for 0.01% of the year comparable at Doula and Ile-Ife. The rainfall CDs in Doula and Nairobi show that the rain climate is not well described by the ITU-R predictive distributions. The rainfall

CD in Nigeria is between those of rain climate N and P as predicted by the ITU-R. Ajayi and Ezekpo [48] used the Rice Holmberg [46] technique to predict short integration time (1 minute) rainfall rate from long term precipitation data from thirty-seven stations in Nigeria over a period of thirty years.

As a result of the rapidly varying nature of rainfall at a given point, the cumulative rainfall rate distribution measured will be dependent on the sampling time of rain gauge [30]. In radio wave prediction techniques, an integration time of one-minute is used. This is because rainfall rate measured with high resolution rain gauge, say 1-2 min time resolution will resolve the small but significant rain cells because longer averaging times will miss the peak-rain-rate values. Therefore 1-min accumulation or averaging time is a reasonable compromise. This is because it removes the fluctuations caused by the measurement process but maintains the important geophysical variations [2]

Segal [6] has defined a conversion factor, $\rho_\tau(P)$ for converting data obtained with a gauge having an integration time of τ minutes to equivalent one minute statistics [6]:

$$\rho_\tau(P) = R_1(P) / R_\tau(P) \quad (3.7)$$

Where R_1 and R_τ are the rainfall rates exceeded with equal probability P , for the two integration times. $\rho_\tau(P)$ is also given by the power law:

$$\rho_\tau(P) = a.P^b \quad (3.8)$$

over the range $0.001\% \leq P \leq 0.03\%$.

Watson et al. [49] considered the conversion factor C_R and C_e for rain gauge integration times in the range of 10 seconds to 60 minutes, where:

$$\begin{aligned} C_e(R) &= e_T / e_\tau \\ C_R(t) &= R_T / R_\tau \end{aligned} \quad (3.9)$$

and where C_e refers to the ratio of the exceedances (with the same probability P) for a given rain rate R measured using gauges with integration times T and τ ; $C_R(t)$ refers to the ratio of rain rates exceeded for a given percentage of time t as measured by rain gauges with integration times T and τ . Here, $C_R(t)$ depends on the percentage of time considered [50], [49]. The conversion factors C_R and C_e obtained by Ajayi [50], using the rain rate data obtained from a fast response rain gauge with an integration time of 10 seconds are based on Watson's method [46]. It has also been found that a power law relationship exists between the equiprobable rain rates of two integration times. The power law relationship is given by [30]:

$$R_\tau = aR_T^b \quad (3.10)$$

where R is the rain rate, τ is the integration time at which the rain rate is required, and T is the integration time at which the rain rate is available

In the work by [50], the result obtained between 1 minute and 5 minutes integration time rain rates obtained in Ile-Ife has been compared with the result obtained by Flavin. Falvin [51] examined the effective 6 minutes and 1 minute cumulative distributions of rain rate for four locations in Europe, three in United States, one in Canada and five in Australia and obtained the following relationship:

$$R_1 = 0.990R_6^{1.054} \quad (3.11a)$$

where R_1 is the 1 minute rain rate, R_6 the equiprobable 6 minutes rain rate value. And that Ajayi and Ofoche, the relationship is given as:

$$R_1 = 0.991R_5^{1.098} \quad (3.11b)$$

where R_1 is the 1 minute rain rate, R_5 the equiprobable 5 minutes rain rate value.

Table 3.1 gives the coefficients a and b for required rain rates for different integration times. The coefficient a may not be very dependent on climate, while the dependence of b on climate may require further investigation. Therefore it is possible that a universal equation may be applicable between 1 minute rain rate and 5 minutes or 6 minutes equiprobable rain rate [50].

Table 3.1 Coefficients for $R_{\tau} = aR_T^b$, for $\tau = 1$ minute [47]

Integration Time T (Min)	Value Of Coefficient	
	a	b
2	0.872	1.055
5	0.991	1.098
10	1.797	1.016
20	4.311	0.853

3.4 Asian Scenario

In Indian, Sakar et al [39] have produced a reference data manual for rain rate distributions over the Indian sub-continent making use of the heavy rainfall data of five minutes and fifteen minutes available at thirty-five different geographical regions in Indian, as well as the fast response rain gauge.

The rapid response rain gauges with ten seconds integration time were used to measure rain rate in Delhi, Shillong, Calcutta, Bombay and Tirupati. The rain rates are 130 mm/h, 128 mm/h, 130 mm/h, 120 mm/h, and 80 mm/h respectively at 0.01% probability level considering all months [39]. The recordings indicate many features similar to those encountered in amplitude variations of microwave and millimeter radio waves.

In [39], the year-to-year variability of rainfall rate over Delhi and Calcutta were shown. The year-to-year variation in rainfall rate is large in Delhi compared to that at coastal station such as Calcutta. Whilst five years data may provide useful and reliable statistics at Calcutta, about ten years of data may be required in Delhi. Govindarajan [30] reported the rain climatic zones for Indian obtained from routine hourly rainfall data from twenty six meteorological stations for ten years and Sakar et al. [39] have produced the cumulative rainfall rate distributions for seventeen stations in India. In addition to the simultaneous measurements of rainfall rates with propagation experiments, analyses of the statistics of rainfall rates have been made by [41] based on data from several hundreds of conventional meteorological stations all over China.

As a result of the rapidly varying nature of rainfall at a given point, the cumulative rainfall rate distribution measured will be dependent on the sampling time of rain gauge [30]. In radio wave prediction techniques, an integration time of one-minute is used.

From the measurements made in Xinxiang, Nanjing and Guangzhou in China for the conversion of rainfall rate statistics with different integration times, Zhang and Hu [41] expressed the conversion factor of the statistics for 10 minutes to 1 minute as based on the Segal conversion factor in equation (3.8):

$$\rho_{10}(P) = aP^b \quad (3.17)$$

where P is the percentage of time for which the rainfall rate is exceeded. Table 3.2 shows the parameter a and b obtained in the three locations.

Table 3.2 Rainfall rate integration time conversion parameters in China [30]

Location	a	b
Xinxiang	1.0357	-3.54×10^{-2}
Nanjing	1.1006	-3.52×10^{-2}
Guangzhou	1.0496	-5.87×10^{-2}

The cumulative distribution of rainfall rate for different integration times from 10 seconds to 1 hour in India is also shown in [39]. The power law derived by using rain data taken simultaneously by using rain gauges having integration times of 10 seconds and 15 minutes over New Delhi is [30], [39]:

$$R_{10 \text{ seconds}} = 2.567 R_{15 \text{ minutes}}^{0.852} \quad (3.18)$$

The above relation will be valid even for other stations within the same limits as the values of the constants, a and b do not change drastically in Indian different regions [30].

3.5 European Scenario

In the European region, Pawlina-Bonati and Emilio Matricciani have characterized the structure and occurrence of convective and stratiform rain inferred from long term point rain rate data. In their work [52], they confirm that point rain rate time series is collected by rain gauge over a long period (like ten years) with good time resolution (one minute) may be successfully used for the modelling of horizontal extension of rain for various rain rates and for two main rain types:

convective and stratiform the synthetic storm rule of conversion of time to space originally thought for stronger convective rain cells, is adapted to weak stratiform rains, assuming decreasing advection speed values for lower rain rates, in order to match the corresponding radar statistics. Generally rain areas featuring the convective activity tend to be larger (at the lowest detectable rain rate contour) than the rain areas of weaker stratiform rain [52].

In [53], Pawlina-Bonati stated that the prediction of main propagation parameters for the radio systems operating in high and very high frequencies can be improved through better knowledge of the space-temporal structure of rain. The extremely variable in time and space process, like rainfall, does not encourage simplifications. Yet, sat-com system designer is forced to adopt certainly oversimplified, but acceptable models of complex reality. To perform well the model have to use parameters based on the (best known) local radio climatic data. In particular there is a demand for the accurate statistics of rain “cell” sizes, life-cycles and shapes, of the occurrence of different rain types (from widespread drizzle to hurricane, from stratiform to convective), of predominant motion of rainy areas.

Models of propagation impairments are always based on some knowledge of the spatial (and temporal) structure of rain. Different types of rain show different partial spatial structure and thus different impact on radio system. Propagation data are rarely use directly in system design, but employed to test propagation prediction models and to find proper values of model parameters. Rain “cells” are the compact areas of locally intensified precipitation, may be identified by a given intensity contour. Those exceeding 10-20 mm/h are definitely convective in nature [53]. In [54], the spatial distribution of rain along the path is investigated, describing the size of both rainy patches (at several intensity levels) and separations among them. In particular the size distribution of rainy intervals is derived and compared to the statistics obtained for the same region from rain gauge data and from two independent collections of rain “cells” identified on horizontal radar maps.

The same link simulation is then used to describe the “multi-cell” problem, i.e. the occurrence of several cells along the link. The description is supplied in terms of fraction of the link filled with the rain of a given intensity, and as the probability to find indicated number of cells of this intensity. Both results represent the input to the prediction models sensitive to the rain structure [54].

Rain intensity statistics were measured at TESTCOM Prague from 1992 to 1998 (7 years). These distributions are compared with a set of rain intensity measured in Albacete (18 years), Avila (10 years), Burgos (10 years), Granada (16 years), Lerida (10 years), Logrono (10 years), Madrid (20 years), Molina (15 years), Oviedo (10 years), Soria (10 years), Tarragna (8 years), Valladolid (10 years), and Zaragoza (10 years) in Spain. The sites selected in Spain correspond to continental climate regions, excepting Tarragona (Mediterranean climate) and Oviedo (Maritime climate) [55]. Cumulative distributions of average 5-minute rain intensities for the average year obtained in Prague are compared with the distributions for Madrid and Granada, as well as with distributions calculated in accordance with ITU-R recommendations [55].

Logarithmic differences of average 5-minute rain intensities were applied for rain intensity distributions obtained in Spanish sites and Prague for both the average year and monthly cumulative distributions. Degree of similarity between the measured distributions for Spanish sites and Prague was assessed. Comparison of rain rate exceedances duration was done for eight Spanish sites and Prague. Logarithmic differences of monthly variability of exceedances durations and diurnal variability of exceedances are obtained to compare between rain events measured in several sites in Spain and Prague [55].

Rain intensity data from rain gauge records 1992-2002 in Prague are statistically processed and the cumulative distributions of average n -minute ($n=1, 2, 5, 10, 15, 20, 30, 40, 60, 120, 240, 360$) rain intensities for the average year and the average worst months, relations between them, monthly and diurnal dynamic characteristics of rain events were obtained [56]. Their work also describes a detailed study of several properties of rainfall events over a period of 11 years as well as the dependence of average 1-minute rain intensities on average n -minute rain intensities. Besides, dynamic characteristics of rain events were obtained [56].

Since the cumulative rainfall rate distribution measured will be dependent on the sampling of the rain gauge, and in radio wave prediction techniques an integration time of one minute is used. Therefore, based on equation (3.7) and (3.8), for Europe, when $\tau = 10$ minutes, $a = 0.86$ and $b = -7.3 \times 10^{-2}$ [30].

3.6 South America Scenario

In Brazil, Assis and Dias [57] presented a modified ITU-R rain attenuation model for low latitude areas, for both terrestrial and slant paths. The rain attenuation prediction model currently adopted by ITU-R [37] appears to be inadequate for tropical regions. Once this model has a basic reference, the precipitation rate exceeded for 0.01% of an average year ($R_{0.01}$), the empirical expression used for scaling to other percentages of time causes an overestimation of the predicted rain attenuation in the range from 0.01 to 0.001% [58]. Based on the experimental data from low latitude areas, a modified scaling expression to overcome this problem was proposed in their work [50].

Also the statistical modelling of the cumulative probability distribution function of rainfall rate in various sites in Brazil has been presented in the work done [31]. The sites chosen for this presentation are located in the cities of Belem (1°S), Manaus (6°S), Recife (8°S), Rio de Janeiro (23°S), and Sao Paulo (23°S). These sites are within equatorial and tropical regions of the country and were chosen to provide a wide view of rainfall behaviour in Brazil. The aim of their work is to obtain the probability density function (pdf) of rainfall rate based on the data collected in several sites located throughout Brazilian territory. The location of the sites span over 22 degrees of latitude and represent 2 types of equatorial and 3 types of tropical climates. In some of the sites presented, the measurement campaigns were carried out for several years and the year-to-year variations are presented [31].

Modelling the rainfall induced attenuation is a paramount issue concerning the system designer, even more so in the tropical and equatorial regions of the planet, where intense rainfall events are common [31]. Efficient methods to evaluate attenuation using the statistics of rainfall may therefore be the answer to this problem. A fundamental step in constructing such method is to obtain a form of for the probability density function of rainfall rate, from which a form for the probability density function of attenuation can be derived based on the intrinsic relationship between attenuation and rainfall rate.

The year-to-year variation of the cumulative distribution function of rainfall indicated that the nature of widespread, long duration rain events does not tend to change appreciably over the years. Results also indicate that the ITU-R expectations for the rainfall rate distribution in

climates P and N tend to overestimate the measured values for the sites studied. The ITU-R climates rain distributions will thus provide conservative estimates for attenuation [30], [31].

Mello et al. [59], gives the conversion factors for converting 5 minutes to 1 minute integration time rain rate at various probability levels obtained for five stations in Brazil. The paper also gives the regression coefficients using equation (3.2) obtained for the five stations compared with the values from Segal [30]. This is shown in Table 3.3 [30], [59]

Table 3.3 Regression coefficients for locations in Brazil [30].

Locations	ITU-R Climate	Regression Coefficients					
		Segal		Burgueno		Bosota	
		a	b	a	b	a	b
Belem	P	1.45	0.046	2.14	0.86	0.190	0.37
Manaus	P	1.41	0.042	2.15	0.86	0.226	0.42
Rio	N	1.61	0.073	2.49	0.82	0.149	0.57
Brasilia	N	1.02	-0.020	0.88	1.02		
Santa Rita	N	1.02	-0.041	0.74	1.12		

3.7 North America Scenario

A large database of nearly instantaneous observations is potentially available in the archives of the U.S. National Weather Service in the form of unanalysed strip chart recordings. Bodtmann and Ruthroff [60] obtained and analysed data for five years of observations at 20 locations in the United States. The time resolution of the data, however was limited, the observations represented rain rate values averaged over time intervals of the order of 2-4 minutes. For the estimation of attenuation along a path, the specific attenuation at each point along the path is required and one-minute rain rate averages are needed for the prediction [2].

Rice and Holmberg [46] devised approximations procedures for the estimation of instantaneous rain rate distributions from available excessive precipitation data. The excessive precipitation data reported up through 1972 consisted of the highest 5-minutes, 10-minutes and longer accumulations with an average 5-minutes rain rate in excess of 76.2 mm/h, an average 10-minutes rain rate in excess of 45.7 mm/h [46]. Rice and Holmberg processed the excessive precipitation

data and the hourly data available from the National Weather Service. Experience with varying the integration interval for processing instantaneous rain rates at the smaller percentages of the year has shown that averaging affects mainly the higher rain rates at the smaller percentages of the year [2]. In the 0.1-1% of the year interval, the distribution function for hourly observations provides a good estimate for the distribution function for 1-minute averaged rain rate. The Rice-Holmberg model, therefore, should produce a good estimate of rain rate distribution in the 0.1% range [2].

Crane in processing excessive precipitation data from 15 stations in New England and Eastern New York state, found that the mean and the variance of data pooled from 7 years and 15 stations were statistically identical to the mean and variance for 24 years at one of the stations (Boston). This result implies that the regional maps are useful for the representation of rain rate distribution data. The results also suggest the use of data pooled from a region to provide improved statistical estimates for the distribution function [2].

In the development of the empirical parameters for their model and its dependence on total rain accumulation and thunderstorm accumulation, pooled data from stations within each of the ten climate regions for the United States; the climate regions were defined on the basis of temperature, terrain height, average rain accumulation, and vegetation but not on the basis of a similarity in rain rate distributions. A subsequent comparison of the model distribution functions produced for each climate region resulted in the reduction of the number of rain climate regions required to describe the pooled rain rate distributions to five (the five climate regions originally embraced by the CCIR-now ITU-R. These climate regions, although fashioned for the United States, were then employed to describe rain climate regions for the entire globe [2]. Dutton expanded the number of rainfall zones in the United States to 19 based on mappings of the independent parameters in the Rice-Holmberg model [2].

In the development of a global rain-rate climate model for use in communication system design, the number of regions chosen to represent the expected variation in rain rate was expanded from five to eight to better emphasize variation with latitude. The globe was initially divided into four latitude bands: arctic, mid-latitude, sub-tropics and tropics. A wet and dry climate zone was to be associated with each band. The eight regions were labeled A through H, going from dry to wet for each latitude band from the pole to the equator. A was arctic dry and H tropical wet but, in the sub-tropics, the designation was reversed with E wet and F dry [2].

The available measured instantaneous rain rate distributions were then pooled (combined) for each of the climate regions. A review of the data available in 1978 when the model was initially constructed showed a progressive variation in rain rate at smaller percentages of occurrence across the data-rich mid-latitude region D. Region D was further subdivided into three regions, D1-D3, with D1 driest and D3 wettest. By 1982, significant amounts of new data were published for Canada by Segal. The climate map was then revised by addition of two new sub-regions; B1 and B2, then an adjustment of contour region boundaries near the U.S.-Canadian border were made [2].

All these, produce an improvement over the ITU-R rain climatic zones in the northern hemisphere especially in the northern America because of the local measurements and data accumulation made in the geographical areas. They were able to divide the world into a number of climate zones as that of the ITU-R , but in the absence of locally obtained data in some other parts of the world, the model suffers the same drawbacks like that of the ITU-R [23].

3.8 Chapter Summary

This chapter has focused on the previous work done by various authors on rain rate and rain attenuation measurements and predictions in different regions around the world. The ITU-R perspective was also studied and the global radioclimatological modeling was also reviewed.

The next chapter of this research work will aim at utilizing the actual local rain rate statistics measured in a broad range of geographical locations in the Republic of South Africa to predict the cumulative distributions of the rainfall-rate intensities for each location and to determine the rain climatic zones based on the actual local data.

Chapter Four

Prediction of Rainfall-rate Statistics

This chapter aims at utilizing the actual local rain rate statistics measured in a broad range of geographical locations in the Republic of South Africa to predict the cumulative distributions of the rainfall-rate intensities for each location and to determine the rain climatic zones based on the actual local data. This chapter also focuses on the effect of integration time on rain rate statistics measured with higher integration time and how to determine the conversion factor coefficient a and b for South Africa. Also, the comparison of the rainfall-rate intensities is analysed to show the annual variations of the rainfall-rate statistics in different geographical locations.

4.1 Rain Rate Statistics Measurement in South Africa

Since rainfall is a natural and time-varying phenomenon that varies from location-to-location and from year-to year, estimate of rain attenuation on a terrestrial radio path are usually derived from the available information on rain rate observed in the geographical area considered [30].

For the purpose of this study, a one-hour rainfall-rate statistics measured by the South Africa Weather Services (SAWS) in different climatic regions for the year 2000-2004 for twelve different meteorological stations were processed and utilized. These then give a 5-year rainfall-rate statistics for twelve different geographical locations in South Africa (see map in Fig 1.2). Table 4.1 shows the twelve geographical locations with their corresponding climatic regions.

In addition, one-minute rainfall-rate statistics was also measured at the University of KwaZulu-Natal (Howard College Campus), Durban, for a period of one year (2004). All these data were pooled together and processed to estimate the cumulative distribution of rainfall-rate in South Africa.

4.2 Effect of Integration Time on Rain Rate Statistics

Daily rainfall accumulations are universally recorded and hourly data are also fairly widely available by national weather bureaus [6]. This is because global national weather services are

established to satisfy more traditional requirements such as those of agriculture, hydrology and forest management. But the precipitation data requirements of the radio communications communities are generally more demanding than the hourly data available.

Table 4.1 The 12 geographical locations and their corresponding rain climatic zones (source: South Africa Weather Service) [20].

Locations	Geographical Coordinates		Climatic Regions (SAWS)
	Latitude South	Longitude East	
Durban	29°.97'	30°.95'	Coastal Savannah
Richards Bay	28°.78'	32°.02'	Coastal Savannah
Cape Town	33°.97'	18°.60'	Mediterranean
Brandvlei	30°.47'	20°.48'	Desert
East London	33°.03'	27°.83'	Savannah
Ladysmith	28°.57'	29°.77'	Inland Temperate
Newcastle	27°.77'	29°.98'	Inland Temperate
Vryheid	27°.78'	30°.80'	Inland Temperate
Pretoria	25°.73'	28°.18'	Temperate
Bloemfontein	29° ⁰ .10'	26° ⁰ .30'	Steppe
Ulundi	28° ⁰ .30'	31° ⁰ .42'	Inland Savannah
Pietermaritzburg	29° ⁰ .63'	30° ⁰ .40'	Inland savannah

Rainfall rate measured with high resolution rain gauge; say one to two minutes time resolution will resolve the small but significant rain cells. Gauges with longer averaging times will miss the peak-rain-rate values. Therefore for the prediction of attenuation on a variety of terrestrial or Earth-space paths, a one-minute accumulation or averaging time is a reasonable compromise. It removes the fluctuations caused by measurement process, but maintains the important geophysical variations [2]. Also, Ajayi and Ofoche determined that the use of one-minute rain rates gives the best agreement with the ITU-R stipulations for the design of microwave radio links [50]. Therefore, there is a great need to convert the available one-hour rain rates measured by the South Africa Weather Service to a one-minute rain rate [20].

From the 5-year rain rate data measured with an integration time of 60 minutes for the twelve different locations in South Africa, the Segal [6] and the Ajayi [50] approaches were used to determine the conversion factor and to convert from 60-minute integration time to an effective 1-

minute integration time (see Chapter 3). From these, the power law relationship was determined for South Africa. The coefficients a and b were determined for Durban in South Africa. Note that the conversion is only effected for Durban for the year 2004, but was not available for the other 11 sites in South Africa. Therefore, this was then used to generalize for other locations in South Africa which is consistent with the approach of Ajayi and Ofoche, where conversion data for Ile-Ife was used [50]. This results in a linear scatter plot of data points, in which a simple power law fits. This is shown in Fig. 4.1. (where Ln refers to natural logarithm). Therefore, for Durban in South Africa, the relationship is determined from Fig. 4.1 as:

$$R_{1\text{min}} = 9.228R_{60\text{min}}^{0.8207} \quad (4.1)$$

Therefore, the coefficient $a=9.228$ and $b=0.8207$.

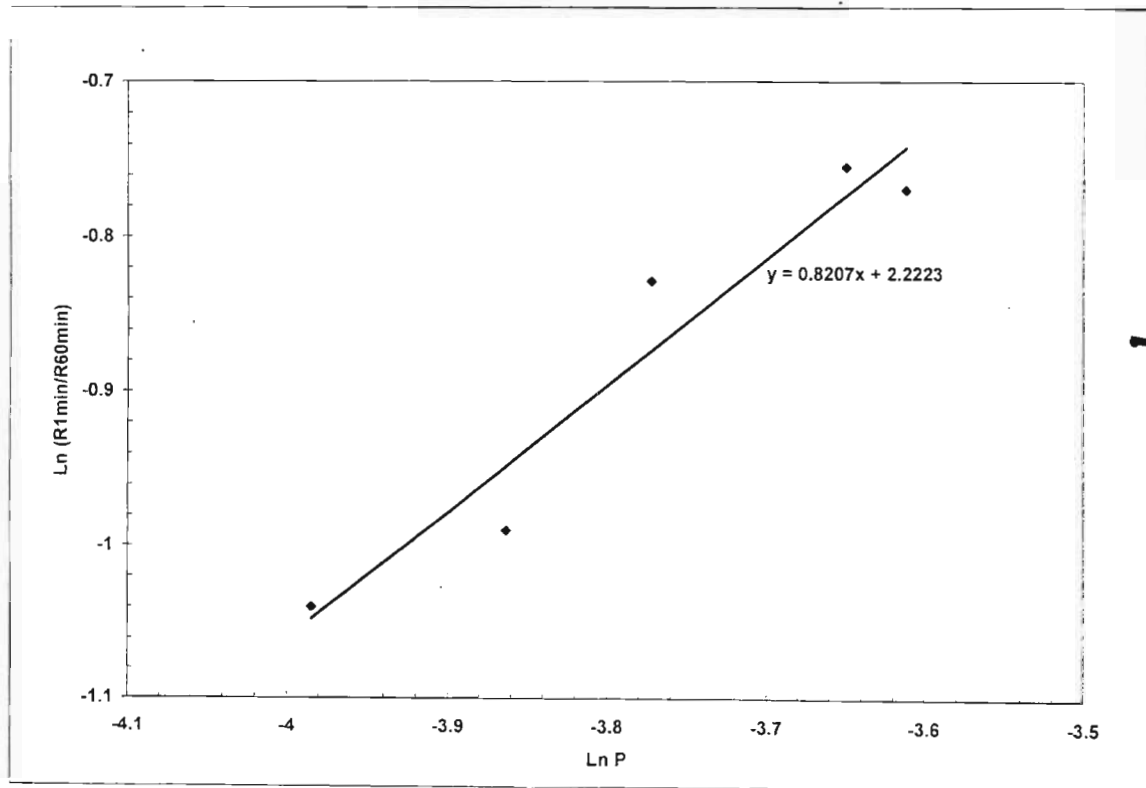


Fig. 4.1 Determination of coefficient a and b for Durban, South Africa

Thus, the Durban coefficients of a and b in equation (4.1) are used to convert other 60-minute rain rate data from other locations in South Africa to an effective 1-minute integration time [20]. As a matter of interest, the results obtained between 1-minute and 60-minute integration time rain

rates in Durban from January 2000 to December 2004 were compared with those obtained by Ajayi and Ofoche [50], [20]. The latter examined the effective 1-minute, 2-minute, 5-minute, 10-minute, and 20-minute cumulative distributions of rain rate for Ile-Ife, Nigeria from September 1979 to December 1981 [20].

The 60-minute coefficients are obtained through extrapolation. Table 4.2 shows a comparison between the Durban coefficient of a and b and the corresponding coefficients obtained for Ile-Ife in [50], [20]. Linear extrapolation gives $a=11.565$ for Ile-Ife for 60-minute integration time, while a logarithmic extrapolation gives $b=0.7982$. These are quite close to the Durban values in equation (4.1). It has been reported that the coefficient a may not be very dependent on climate, while the dependence of b on climate may require further investigation [50].

Table 4.2 Comparison of coefficients a and b for Durban, South Africa, with the measurements in Ile-Ife, Nigeria ($\tau = 1$ minute)

Integration time T		Value of Coefficient	
Station	T (minutes)	a	b
Ile-Ife	2	0.872	1.055
Ile-Ife	5	0.991	1.098
Ile-Ife	10	1.797	1.016
Ile-Ife	20	4.311	0.853
*Ile-Ife	60	11.565	0.798
Durban	60	9.228	0.8207

*Extrapolation values

Fig. 4.2 shows for Durban (using 2004 data), the values of equiprobable rain rate for integration time of 1-minute and 60-minute for occurrence probability of 0.1% or less. Fig 4.2 confirms the power law relationship between equiprobable rain rates of two different integration times, as they are based on raw data. Fig 4.2 shows that the longer integration time hides the probable rainfall peaks, during which the highest outages take place. Therefore outage probabilities and fade margins would be inaccurately determined if the 60-minutes integration data are used [20].

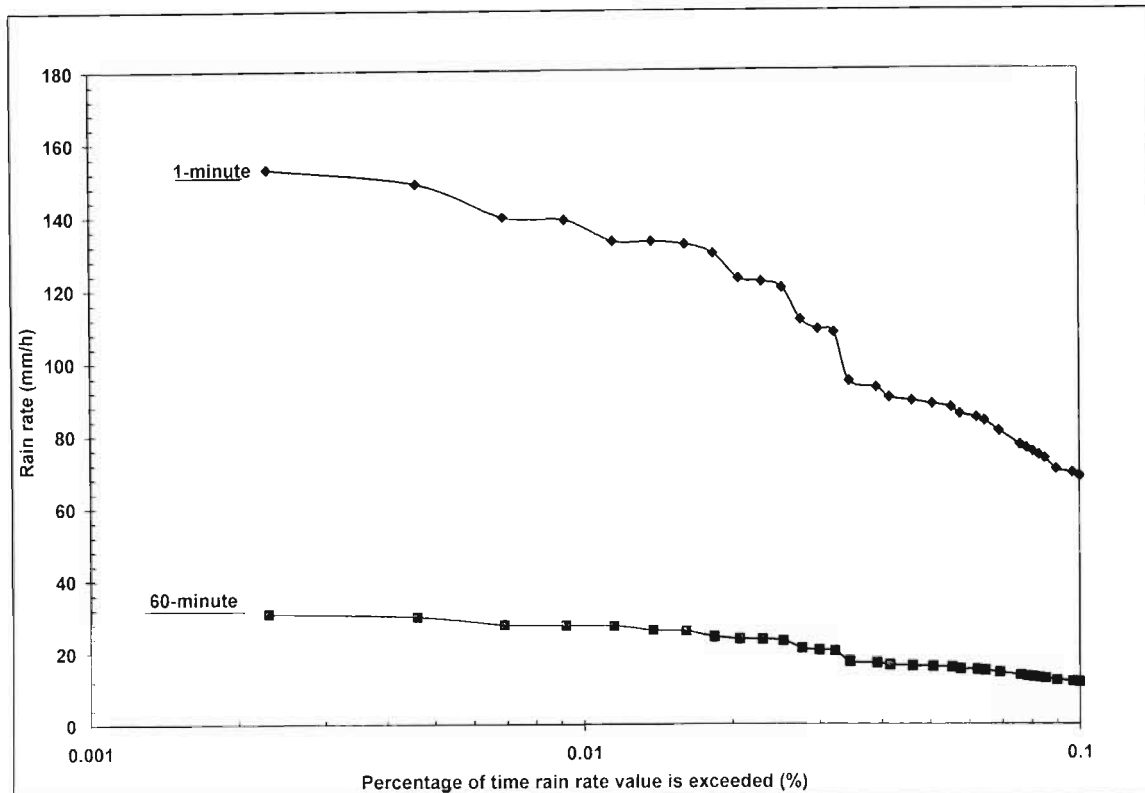


Fig 4.2 Cumulative distribution of rain-rate for Durban for 1-minute and 60-minute integration times

4.2 Comparison of Rain Rate Statistics for Different Geographical Locations

The rain rate statistics for 12 locations in South Africa over a period of 5 years were compared. It has been reported that the main factors that cause the differences in the annual rain intensities in South Africa are the influence of the South Atlantic Ocean, Indian Ocean, and the topography [16], [17], [18],[19]. The combination of these effects causes the differences in the annual rain intensities among the South Africa climatic regions. The rainfall is unreliable and unpredictable throughout the country. Large fluctuations around the regions are compared in Figure 4.3, 4.4 and 4.5 which are based on conversion to 1-minute integration times. The locations are then classified according to the South Africa climatic regions (see Table 4.1) [20]. The yearly 1-minute integration time rain rate statistics at 0.01% exceedance of the time for each location within the same climatic regions are compared. These give the variation in the annual rain intensity for the entire period of 5 years.

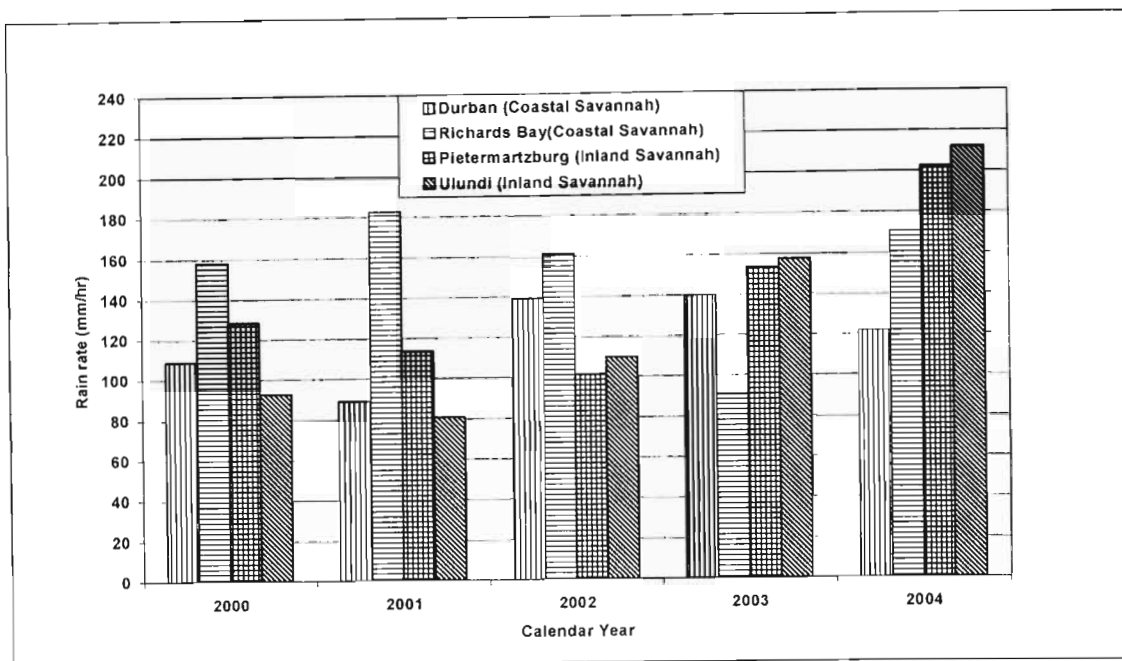


Fig. 4.3 Variation in the annual rain intensity (mm/h) exceeded for 0.01% of the time for South Africa (Coastal & Inland Savannah Regions)

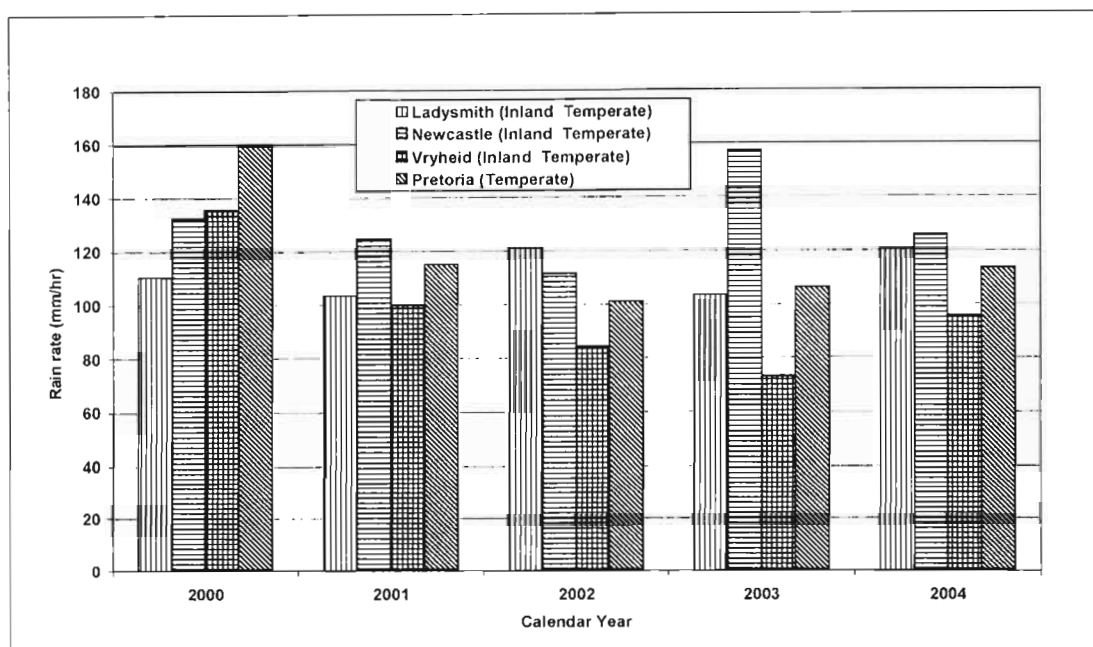


Fig.4.4 Variation in the annual rain intensity (mm/h) exceeded for 0.01% of the time for South Africa (Temperate and Inland Temperate Regions)

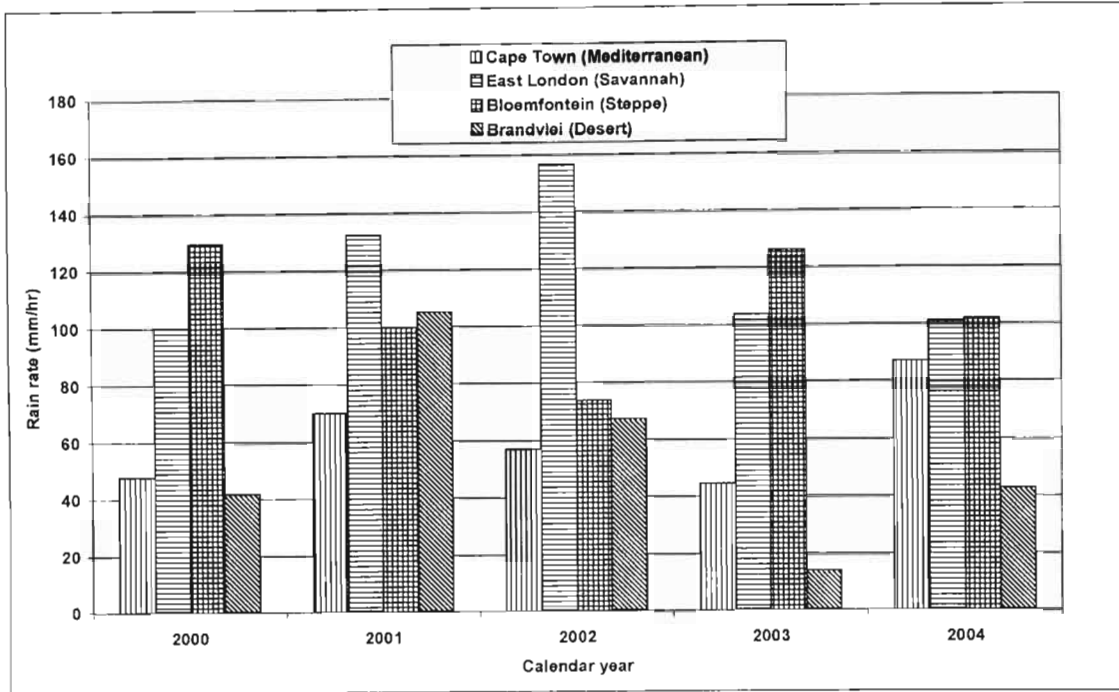


Fig. 4.5 Variation in the annual rain intensity (mm/h) exceeded for 0.01% of the time for South Africa (Mediterranean, Steppe, Savannah and Desert Regions)

In Fig. 4.3, Richards Bay consistently records the highest yearly rain rate in the initial three years (2000-2002), with a peak of 182.66 mm/h in 2001. Over these three years, Durban records the second highest of 139.66 mm/h in 2002, while Pietermaritzburg has a high value of 126 mm/h in 2000 and 115 mm/h in 2001. Despite the fact that Durban and Richards Bay lie in the same climatic region, there are differences in the rain intensity from year to year. The highest rain rate in the zone was recorded in the year 2004 with values of 211.38 mm/h and 202.16 mm/h for Ulundi and Pietermaritzburg, respectively. For three consecutive years, (2002 to 2004) Ulundi records a progressive increment in rain rate, as is also applicable to Pietermaritzburg. And for two consecutive years 2000-2001, a decrement in rain rate is recorded in both locations. A measure of differences is also noticed between the two locations in this climatic region but the differences are not as large as that of the Coastal Savannah [20].

In Fig. 4.4, the yearly rain rate variations for temperate and inland temperate regions were plotted. It was observed that Newcastle and Pretoria recorded the two highest rates of 160mm/h (in 2000) and 157mm/h (in 2003), respectively. Vryheid recorded the lowest rates in this category, with a minimum rate of 76mm/h in 2003. On the other hand, the rain intensity in

Ladysmith appears to be roughly uniform over four years between 2001 and 2004, with a mean value of 103mm/h. As already stated, Pretoria has a high rate of 160mm/h in 2000 while the rain intensities for 2001 and 2004 are quite close (115mm/h and 113mm/h, respectively), with the corresponding values for 2002 and 2003 also remaining almost the same at 101mm/h and 106mm/h, respectively [20].

Finally, in Fig. 4.5, four different climatic zones were compared. They are; Mediterranean, Savannah, Steppe and Dessert. East London in the savannah zone records the highest two rates over the five years, namely, 133 mm/h in 2001 and 157mm/h in 2002. This is followed by Bloemfontein in the Steppe zone, which records two similar highs in 2000 (130mm/h) and 2003 (127mm/h). Note that there is a discernible periodicity for Bloemfontein (with almost similar rates in 2000 and 2003, followed by similar ones in 2001 and 2004) and Cape Town. However, there is no obvious pattern for East London and Brandvlei (desert region). Cape Town which lies in the Mediterranean region of South Africa has its highest rain intensity of 87.04mm/h in the year 2004, with rain intensities in the other years being relatively low. Rain rate in the year 2000 and the year 2003 are almost the same (47.7mm/h and 44.5mm/h respectively) [20].

East London has its highest rain rate of 156.97mm/h recorded in year 2002. Year 2003 and 2004 appears to have the same rain rates value of 103.2mm/h and 100.72mm/h respectively. The lowest rain rate was recorded in the year 2000 at 99.83mm/h. Bloemfontein which lies in the steppe region of South Africa has its maximum rain rate of 129.54mm/h recorded in the 2000. It is seen that the rain rate gradually decreases from 2002. In 2003, there is a rise in the rain rate to a value which is almost the same as that recorded for the year 2000 and for 2004 the rain rate value decreases again to a value close to one recorded for the 2001. Brandvlei which lies in the desert region of South Africa is seen to have an irregular and unpredictable type of rain intensity. On average Brandvlei has low rain intensities as compared to other climatic regions in South Africa, with its highest peak of rain intensity of 105.2 mm/h recorded in 2001 and lowest rain rate of 13.67mm/h recorded in 2003. It is also observed that year 2000 and 2004 have almost identical rain rate values of 41.25 mm/h and 42.34 mm/h respectively [20].

The 5-year rain statistics with 1-minute integration time for the 12 locations in different climatic regions at 0.01% exceedance of the time are compared in Fig. 4.6. It is seen that Richards Bay which lies in the coastal savannah has the highest rain intensity, followed by Ulundi, Pietermaritzburg and Durban. Ulundi and Pietermaritzburg lie in the Inland area of Coastal

Savannah region. The high rain peaks that occur in these areas are mostly due to Indian Ocean influence in the region. The moist Indian Ocean air masses which are the chief source of the rain over most of the countries gradually losses their moisture as they move towards the western interior [20], [18].

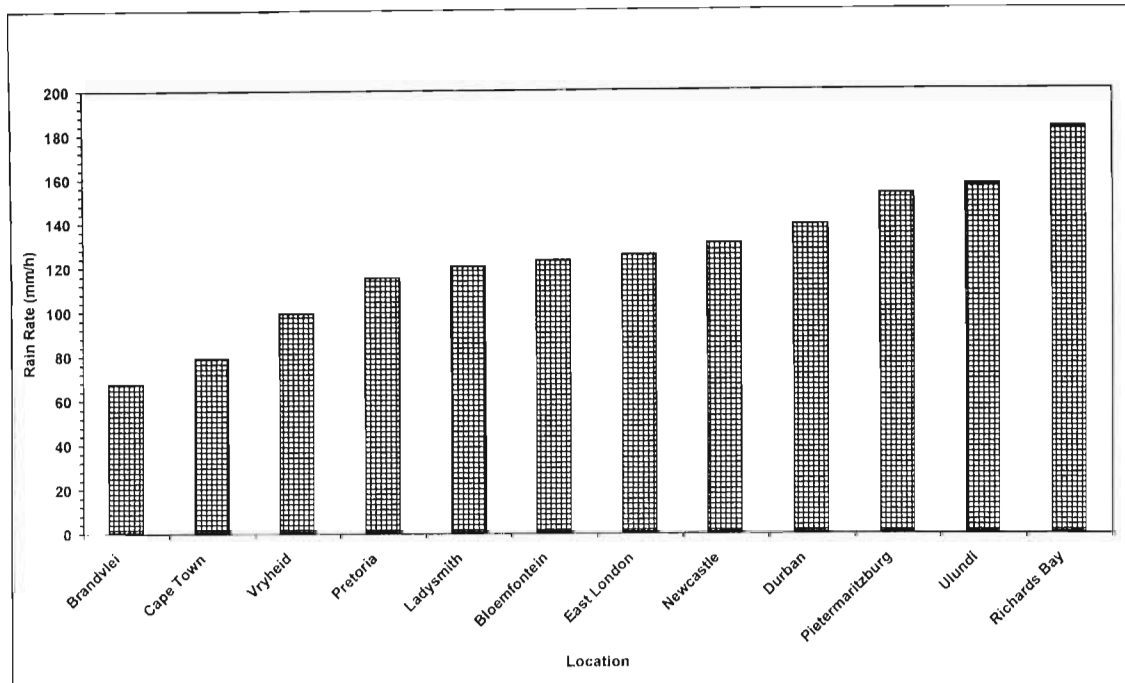


Fig. 4.6 Comparison of the 5-year rain intensity (mm/h) for 12 locations in South Africa Exceeded for 0.01% of the Time

The very lowest rain fall occur on the west coast, with Brandvlei which is found in the desert area showing the lowest rain intensity. Cape Town which lies in the Mediterranean climate is seen to have low rain fall intensity, similar to that of Brandvlei which lies in the desert region of South Africa. This is because Cape Town is situated towards the western coast of South Africa ,and its rainfall mostly occurs during winter (June through August) as opposed to other places in South Africa which have their rain fall during summer (November through March) [16], [20].

One therefore concludes that the north-eastern area of South Africa (which has the coastal Savannah and Inland Savannah climate zones) have higher rain rates than the north-western parts (which have Mediterranean and desert climate zones). In addition, it can be observed in Figures 4.3-4.5 that there is a peak quasi-periodicity every 3-4 years, as observed by Tyson et al [19], [20].

4.3 Cumulative Distribution of Rain Intensities for Different Geographical Locations

Cumulative distributions (CD's) of five-year 1-minute rain intensities for the twelve geographical locations in South Africa are plotted in Fig. 4.7. The cumulative distribution is based on rain intensities and percentages of time; the higher the rain intensity the lower the corresponding percentage of time recorded, while the lower the rain intensity the higher the percentage of time.

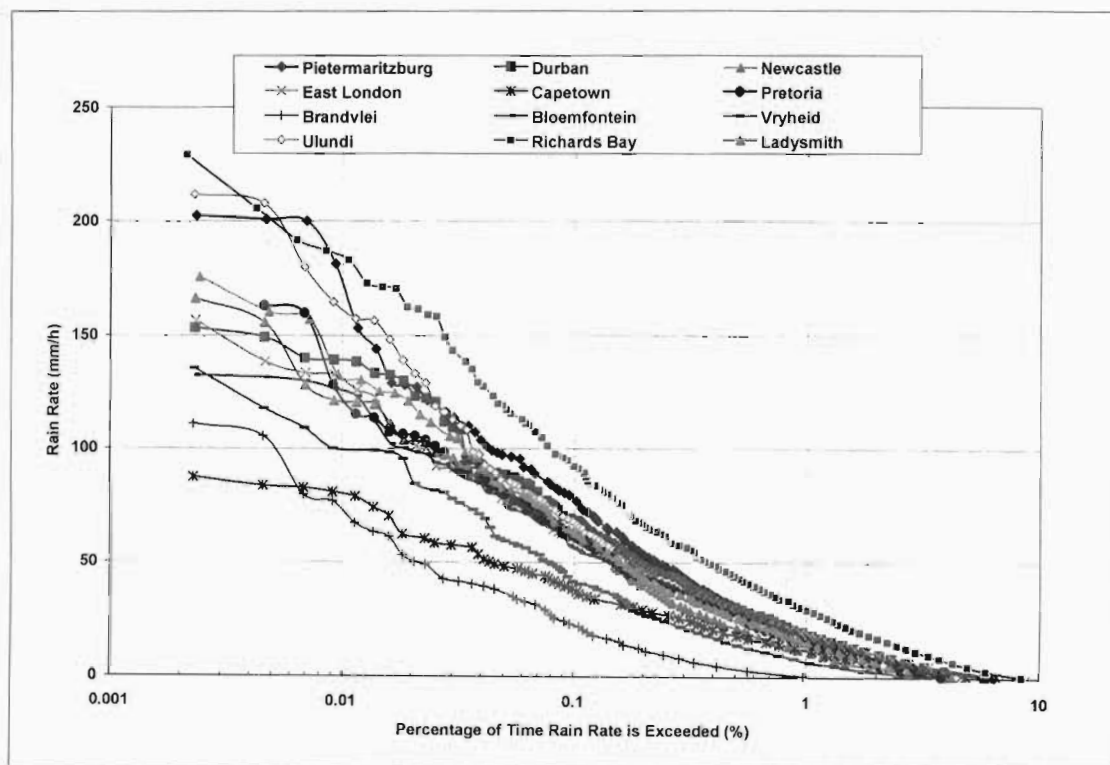


Fig 4.7 Cumulative distribution of rain intensities for South Africa for an average of 5 years

For Durban, at the higher time percentage of 0.1%, the rain rate recorded is 68.98 mm/h; while for the lower time percentage 0.01%, the rain rate is 138.83 mm/h. Therefore, the rain intensity for time percentage differences between 0.1% to 0.01% is 69.85 mm/h. Also for Richards Bay, at the higher time percentage of 0.1%, the rain rate recorded is 91.65 mm/h; while for the lower time percentage 0.01%, the rain rate is 182.66 mm/h. Therefore, the rain intensity for time percentage differences between 0.1% and 0.01% is 91.01 mm/h. At higher time percentage of 0.1% for Pietermaritzburg, the observed rate is 79.55 mm/h, with the difference in rain intensities between 0.1% and 0.01% being 73.37 mm/h. Similarly for Ulundi, at higher time percentage of 0.1%, the

observed rain rate is 67.02 mm/h, with the difference in rain intensities between 0.1% and 0.01% being 89.99 mm/h. This difference is almost close to that of the Richards Bay which lies in the coastal savannah.

For Newcastle, at 0.1% of time percentage the rain intensities is 63.07 mm/h and at the lower time percentage of 0.01% the rain intensity is 130.39 mm/h. The rate difference between 0.1% and 0.01% is 67.32 mm/h. Also for Ladysmith, at higher time percentage of 0.1%, the rain rate recorded is 62.07 mm/h and for the lower time percentage of 0.01%, the rain rate is 120.11 mm/h. The difference was recorded to be 58.04 mm/h. Vryheid also records 41.25 mm/h at the higher time percentage of 0.1% with the difference in rain intensities between 0.1% and 0.01% to be 57.68 mm/h. This difference is found to be close to that of Ladysmith which lies in the same inland temperate. In the case of Pretoria, the distribution shows that at 0.1% the rain intensities is 61.07 mm/h and 0.01% has 114.90 mm/h. The rain rate difference between 0.1% and 0.01% of the time is 53.83mm/h.

For Cape Town, it was observed that at the higher time percentage of 0.1% the rain intensity is 37.95 mm/h while at the lower time percentage of 0.01% the rain intensity is 78.60 mm/h. The rain intensity difference at higher and lower time percentage is 40.65 mm/h. This difference is almost close to that of Brandvlei. For East London, the time percentage of 0.1% has a rain intensity of 61.07% mm/h, while at 0.01% the rain intensity is 125.27 mm/h. The difference in rain intensity between 0.1% and 0.01% is 64.20 mm/h. At the higher time percentage of 0.1 % the rain intensity is similar to Pretoria. In Bloemfontein at higher percentage of 0.1%, the rain intensity is 56.01 mm/h, while at the lower time percentage of 0.01% the value is 122.70 mm/h. The difference between the higher and lower time percentage recorded gives an intensity of 66.69 mm/h. Finally, for Brandvlei, at higher percentage of 0.1% the rain intensity is 25.19 mm/h, while at the lower time percentage of 0.01%, the intensity is 67.02 mm/h. The rain intensity difference between the higher and lower time percentages is 41.83 mm/h, which is close to the difference in Cape Town.

It can also be observed here that the north-eastern area of South Africa have higher rain rates than the north-western parts and thus more prone to rain attenuation.

4.5 Determination of South Africa Rain Climatic Zones

ITU-R classifies the rain climatic zones of southern Africa into six rain zones, namely; C, D, E, J, K, and N of which South Africa has five. These are; C, D, E, K, and N [38]. However, these ITU-R designations are not necessarily adequate, as discussed in the previous chapters for the case of India, China, and Brazil [30]; therefore there is need to redefine the ITU-R regional climatic zones based on the actual local data.

From the 5-year actual rain data for 12 different geographical locations which is converted into 1 minute integration time in South Africa, a compiled table of 1 minute rainfall rate distribution at 1.0%, 0.3%, 0.1%, 0.03% and 0.01% probability level (percentage of time ordinate exceeded) for five years is shown in Table 4.3.

Table 4.3 Rain intensity exceeded (mm/h) for the 12 selected geographical locations in South Africa.

Percentage of time (%)	Lady smith	Durban	Richards Bay	Cape town	Vryheid	Bloem fontein
1.0	16.29	18.93	28.79	12.17	6.07	14.95
0.3	35.7	41.25	57.03	25.2	21.49	34.58
0.1	62.07	68.98	91.65	37.95	41.25	56.01
0.03	95.32	108.75	143	57.03	77.65	89.92
0.01	120.11	138.83	182.66	78.60	98.93	122.7
Percentage of time (%)	Pretoria	East London	Ulundi	Brandvlei	Newcastle	Pietermaritzburg
1.0	14.95	18.93	14.95	2.46	12.17	18.93
0.3	35.71	36.83	34.58	9.22	31.14	43.43
0.1	61.07	61.07	67.02	25.19	63.07	79.55
0.03	98.03	90.74	112.27	42.33	105.2	113.15
0.01	114.90	125.27	157.01	67.02	130.39	152.92

The rain intensity exceeded (mm/h) for the 12 selected geographical locations in South Africa are compared with the ITU-R rain climatic zone table (see Table 2.2) [38]. The errors obtained by comparing each location against different ITU-R climatic zones are determined; the ITU-R zone that gives the least recorded error value for each geographical location is chosen as the location's

rain climatic zone [20]. The resulting climatic rain zones are shown in Table 4.4. From the local data measured by South Africa Weather Services for 12 locations, four climatic rain zones are determined, namely, N, M, P and Q. Hence three “additional” rain climatic zones are added to ITU-R rain Climatic zone for South Africa [20]. Hence, three additional rain climatic zones are added to ITU-R rain climatic zone for South Africa.

Table 4.4 Proposed rain climatic zone for 12 geographical locations in South Africa

Location	ITU-R P.837-1	ITU-R P.837-4	Proposed zone
Durban	L	M	P
Richards Bay	N	M	P
Cape Town	E	E	N
Brandvlei	D	D	M
East London	K	K	Q
Ladysmith	K	L	Q
Newcastle	K	L	P
Vryheid	K	L	N
Pretoria	K	L	Q
Bloemfontein	K	L	P
Ulundi	L	L	P
Pietermaritzburg	L	L	P

One therefore concludes that ITU-R zoning underestimates the precipitation in each zone, as evidenced by the fact that the “new” zones have higher precipitation rates than the zones prescribed by Recommendation P.837. As more data is gathered a fuller picture of these recommendations will emerge.

4.6 Chapter Summary

The actual local rain rate statistics measured by the South Africa Weather Services for 12 different locations over a period of 5-year have been utilized to study the effect of integration time on the cumulative distribution of rain rate for South Africa in this chapter. Also, comparison of the 5-year rain rate statistics exceeded for 0.01% of the time for the different geographical locations were studied which shows the variability of the rain rate statistics from location-to-location and from year-to-year. In this chapter also, additional climatic rain zones (N, M, P and

Q)are determined for South Africa, as against the ITU-R classifications of C,D, E, K and N based on the available 60-minute rain data (converted to 1-minute integration time). Thus, an additional three rain zones have been identified for South Africa.

Since the rain rate statistics varies from location-to-location and from year-to-year, and it has been observed that the north-eastern area of South Africa have higher rain rates than the north-western parts and thus more prone to rain attenuation, the next chapter of this work will study the effect of rain rate statistics at these various locations on terrestrial SHF radio link design.

Chapter Five

Rain Attenuation Prediction and Modeling

Rainfall is a natural and time varying phenomenon, therefore the estimate of rain attenuation is usually derived from the available information on rain rates observed in the geographical area considered [4,], [30]. As indicated by Moupfouma [4], the excess attenuation due to rainfall becomes one of the most important limits on the performance of any line-of-sight (LOS) microwave links above a certain threshold of frequency. In temperate climates, this frequency threshold is about 10 GHz, while in the tropical climates (equatorial climate particularly), since raindrops are larger than in temperate climates, the incidence of rainfall on radio links becomes important for frequencies as low as 7 GHz [4], [5].

In this chapter, the specific rain attenuation (dB/km) for the twelve different geographical locations is computed based on the available rain rate data. Also the path attenuation (dB) for these locations is subsequently estimated by using the existing models on the available local rain data. This chapter also focuses on the prediction of rain attenuation model from the signal attenuation level measurements recorded over a period of one year in Durban, South Africa. From there, a suitable rain attenuation model is proposed for the Republic of South Africa.

5.1 Computation of Specific Rain Attenuation on Terrestrial Line-of-Sight Links

The specific rain attenuation γ_R (dB/km) for the twelve geographical locations (shown in Fig 1.2) in South Africa were computed based on the global ITU-R model [36]. Using the actual local rain rate data from these locations, the rain rate $R_{0.01}$ exceeded for 0.01% of the time was determined from the cumulative distributions of their rainfall-rate for an integration time one-minute (see chapter 4). This is determined for all the years (from 2000-2004) and averaged over the period of five years [31]. Also, the ITU-R [38] average rain rate $R_{0.01}$ values exceeded for 0.01% of the time with one-minute integration time of the average year for South Africa were utilized to compute the specific attenuation for these locations. Table 5.1 shows the cumulative distribution of the rain rate statistics at 0.01% exceedance value.

Table 5.1 Annual rain rate statistics for each location at 0.01% exceedance value ($R_{0.01}$)

Locations	2000 (mm/h)	2001 (mm/h)	2002 (mm/h)	2003 (mm/h)	2004 (mm/h)	2000-2004 (Average)	ITU-R P.837-1 (Average)
Durban	108.75	88.82	138.83	139.66	121.84	119.58	60
Richards Bay	157.82	182.66	161.07	90.75	170.74	152.61	80
Ladysmith	110.51	103.42	120.97	103.42	120.11	111.69	50
Newcastle	132.09	124.48	111.39	157.01	125.27	130.01	50
Vryheid	135.47	99.83	84.25	72.86	95.31	97.54	50
Pietermaritzburg	127.84	113.15	100.73	152.92	202.16	139.36	60
Ulundi	92.57	80.49	109.63	157.01	211.38	130.22	60
East London	99.83	132.09	156.19	103.42	100.72	118.45	42
Cape Town	47.7	69.96	57.03	44.5	87.04	61.25	22
Pretoria	159.45	114.90	100.73	106.09	113.15	118.86	50
Bloemfontein	129.54	99.83	73.83	126.13	101.63	106.19	50
Brandvlei	41.25	105.2	67.02	13.67	42.34	53.90	19

From the power law relationship of specific attenuation γ_R stated in equation (2.28), the values of k and α coefficients used for the computation of the specific attenuation for both horizontal and vertical polarization for these twelve geographical locations are adopted from ITU-R [36] (see Table 2.1). Hence, the specific attenuation for the twelve locations was computed.

5.1.1 Results and Discussion from the Various Locations

The specific rain attenuation for both horizontal and vertical polarization for all the geographical locations are plotted for frequencies of up to 55 GHz. Fig 5.1 shows the plot for Richards Bay which lies in the Coastal Savannah of South Africa with the highest average rain rate of 152.61 mm/h statistics at 0.01% exceedance level for 1-minute integration time from the actual measurements for all the five years. Also, shown in the plot is the ITU-R average rain rate statistics at 0.01% exceedance level for 1-minute integration time of 80 mm/h. Observing this graph keenly, it is seen that the ITU-R tends to under-estimate the specific rain attenuation for all the five years considered and the one averaged over the whole five years. Also as expected, the attenuation produced by the horizontal polarization tends to be slightly higher than that of the vertical polarization. Table 5.2 gives the values at which the ITU-R rain attenuation prediction

under-estimate the attenuation predicted based on the actual local rain measurement done in Richards Bay over the period of five years at frequencies 10 GHz to 50 GHz.

Fig 5.2 shows the plots of Cape Town in the Mediterranean region of South Africa with the average measured rain rate statistics exceeded for 0.01% exceedance level of 61.25 mm/h and that of the ITU-R at 22 mm/h at 1-minute integration time. It is also seen here that the ITU-R

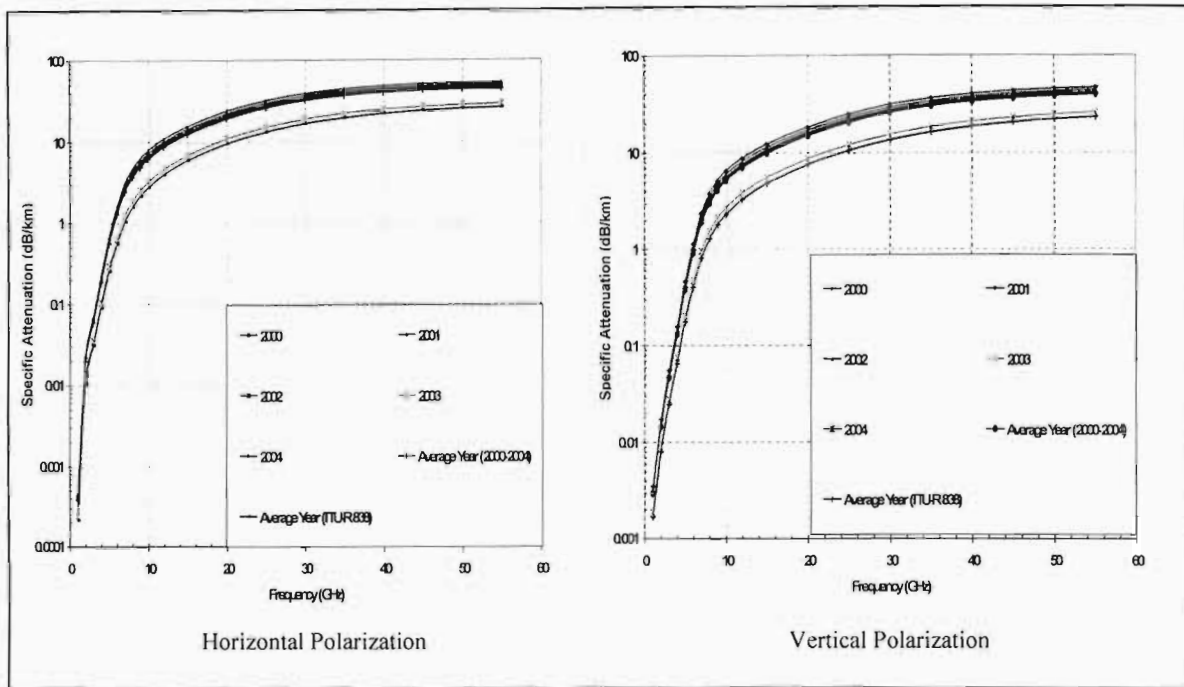


Fig 5.1 Specific rain attenuation for horizontal and vertical polarization in Richards Bay; taking rain rate exceeded for 0.0% of the time

Table 5.2 Values by which the ITU-R under-estimate the specific rain attenuation for Richards Bay

Frequency (GHz)	ITU-R Under-estimate Values (dB/km)	
	Horizontal Polarization	Vertical Polarization
10	3.43	2.83
20	9.61	7.31
30	15.20	11.97
40	17.94	14.98
50	18.62	16.28

prediction for the specific attenuation was under-estimated for each year and the one averaged over the whole five years. It is again noted that the attenuation produced by the horizontal polarization tends to be slightly higher than that of the vertical polarization. Table 5.3 gives the values by which the ITU-R rain attenuation prediction under-estimates the attenuation predicted based on the actual local rain measurement done in Cape Town over the period of five years at frequencies 10 GHz to 50 GHz.

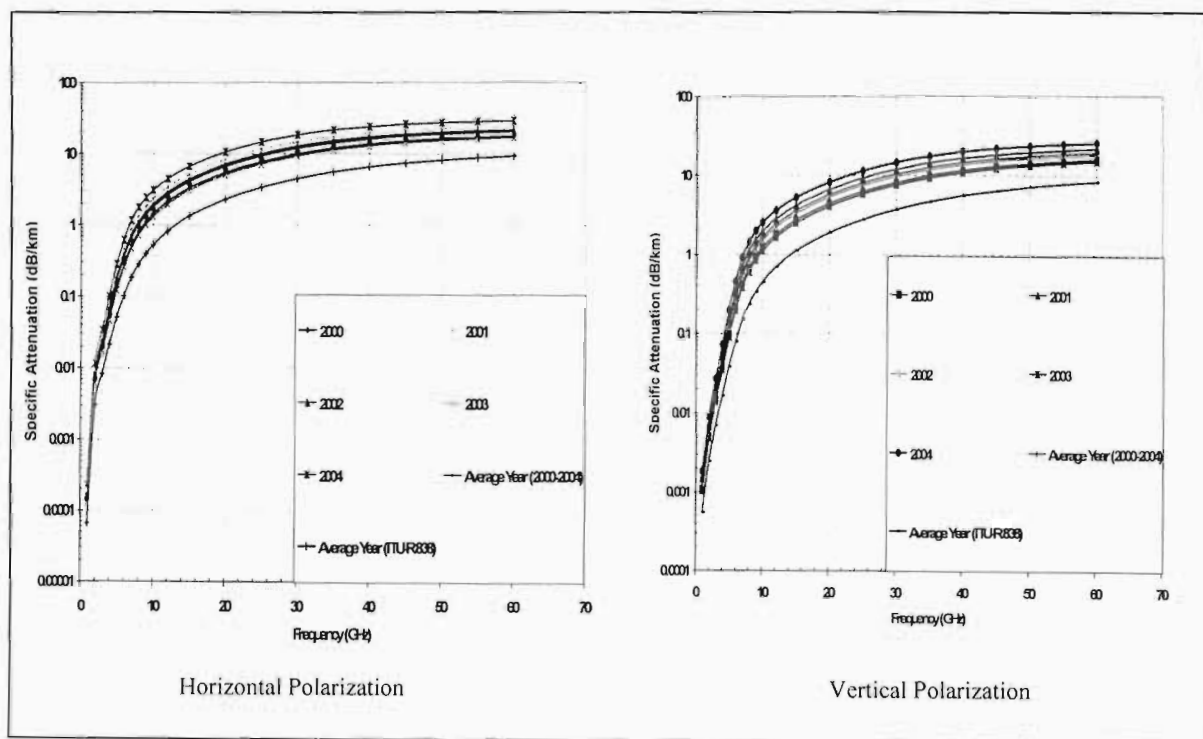


Fig. 5.2 Specific rain attenuation for horizontal and vertical polarization in Cape Town; taking rain rate exceeded for 0.01% of the time

Table 5.3 Values by which the ITU-R under-estimate the specific rain attenuation for Cape Town

Frequency (GHz)	ITU-R Under-estimate Values (dB/km)	
	Horizontal Polarization	Vertical Polarization
10	1.40	1.16
20	4.67	3.63
30	8.04	6.49
40	10.33	8.72
50	11.51	10.08

Fig 5.3 shows the graph of the specific rain attenuation for Pretoria which lies in the temperate climatic region of South Africa. From the ITU-R , the average rain rate statistics exceeded for 0.01% of the time at 1-minute integration time is estimated to be 50 mm/h, while from the local actual measurement taken in this geographical location over an average of five years, the rain rate exceeded for 0.01% of the time at 1-minute time is 118.86 mm/h. It is seen from this graph that prediction for the specific rain attenuation is under-estimated for each year and for the averaged-five years by the ITU-R. Table 5.4 shows the values by which the specific rain rate is under-estimated.

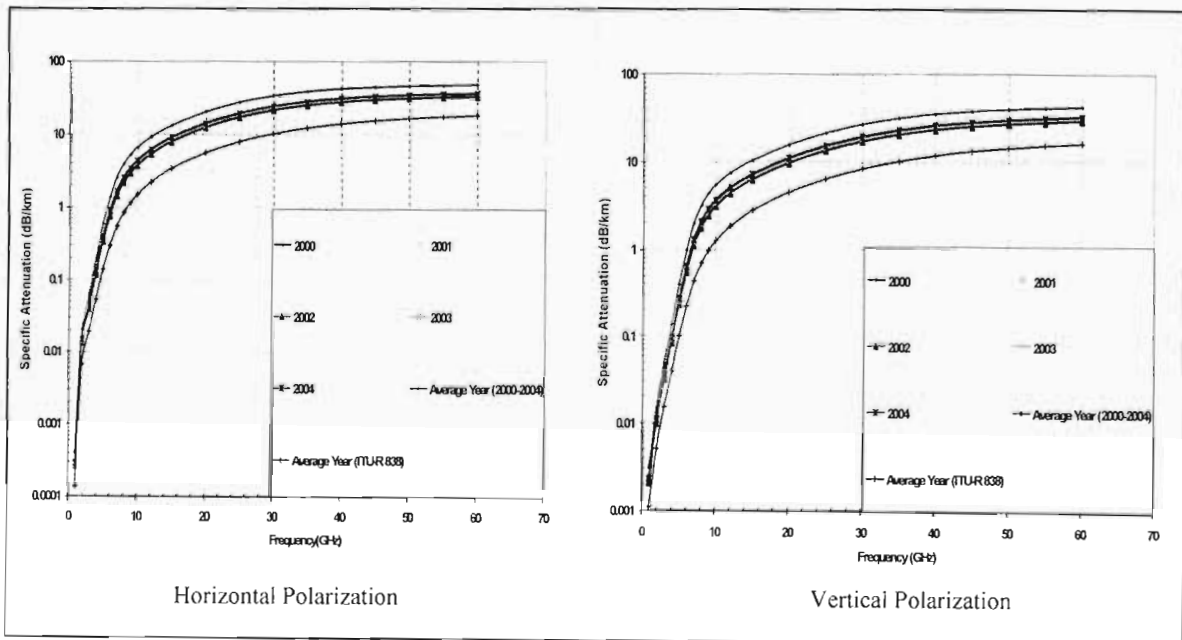


Fig. 5.3 Specific rain attenuation for horizontal and vertical polarization in Pretoria; taking rain rate exceeded for 0.01% of the time

Table 5.4 Values by which the ITU-R under-estimate the specific rain attenuation for Pretoria

Frequency (GHz)	ITU-R Under-estimate Values (dB/km)	
	Horizontal Polarization	Vertical Polarization
10	2.97	2.47
20	8.81	6.78
30	14.31	11.36
40	17.36	14.55
50	18.42	16.11

Fig 5.4 shows the graph of Brandvlei which is classified as a desert region in South Africa. The ITU-R records a average rain rate statistics of 19 mm/h for a 1-minute integration time at 0.01% exceedance value while 53.9 mm/h was recorded from the actual rain rate measurement taken from this geographical area for an average of five years for 1-minute integration time at 0.01% exceedance level.

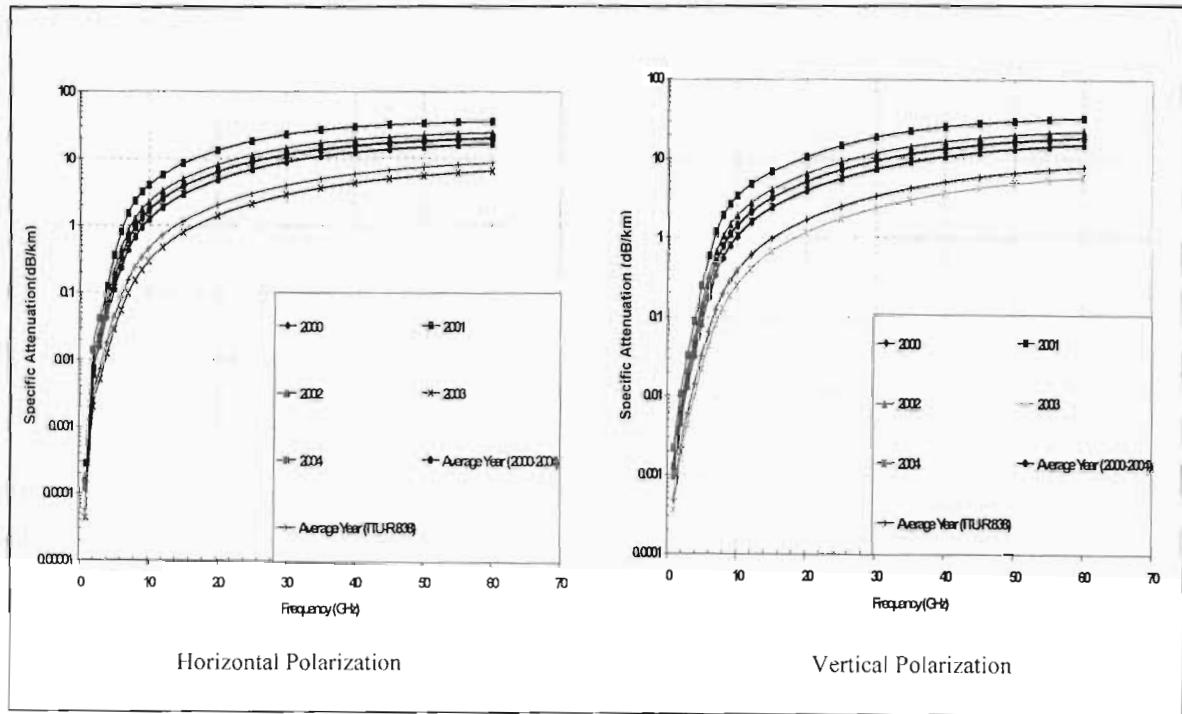


Fig. 5.4 Specific rain attenuation for horizontal and vertical polarization in Brandvlei; taking rain rate exceeded for 0.01% of the time

Table 5.5 Values by which the ITU-R under-estimate the specific rain attenuation for Brandvlei

Frequency (GHz)	ITU-R Under-estimate Values (dB/km)	
	Horizontal Polarization	Vertical Polarization
10	1.19	0.99
20	4.10	3.25
30	7.13	5.77
40	9.23	7.83
50	10.4	9.12

Looking at Fig 5.4 keenly and comparing the specific rain attenuation predicted for both the horizontal and vertical polarization by the ITU-R and from the actual local measurement, it can be seen that for the year 2003, the ITU-R tends to over-estimate the specific rain attenuation. For this year 2003, the over-prediction values for the horizontal polarization at 10 GHz, 20 GHz, 30 GHz, 40 GHz and 50 GHz are: 0.15 dB/km, 0.58 dB/km, 1.07 dB/km, 1.48 dB/km, 1.75 dB/km respectively. And for vertical polarization the over-prediction values are: 0.13 dB/km, 0.47 dB/km, 0.88 dB/km, 1.26 dB/km and 1.54 dB/km at 10 GHz, 20 GHz, 30 GHz, 40 GHz and 50 GHz respectively. But averaging the specific rain attenuation computed from the actual measurement over the period of five years, ITU-R under-estimates these values. And these values are shown in Table 5.5.

Fig. 5.5 shows the specific rain attenuation for both horizontal and vertical polarization for Durban using the actual rain rate statistics measured in Durban for a period of five years and the average ITU-R rain rate statistics for 1-minute integration time at 0.01% exceedance level. For the whole five years (2000-2004), ITU-R under-estimates the specific rain attenuation for each year and the specific rain attenuation averaged over the whole five years. Table 5.6 shows the values at which the specific rain rate is under-estimated by using the ITU-R rain statistics.

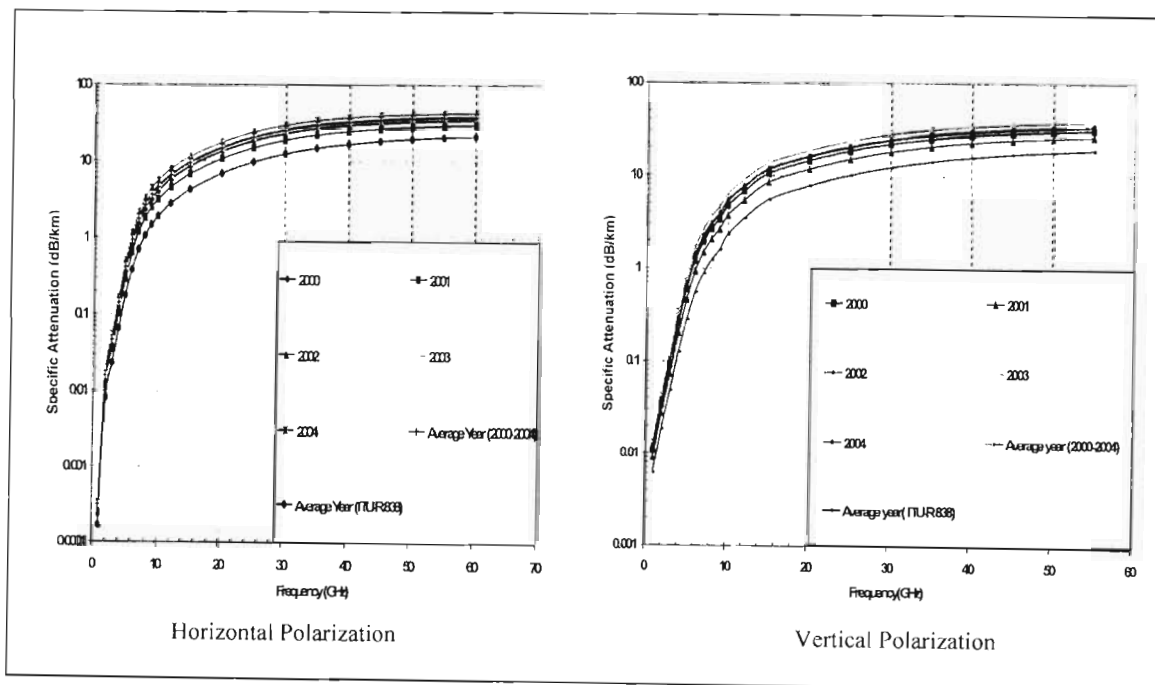


Fig. 5.5 Specific rain attenuation for horizontal and vertical polarization in Durban; taking rain rate exceeded for 0.01% of the time

Table 5.6 Values by which the ITU-R under-estimate the specific rain attenuation for Durban

Frequency (GHz)	ITU-R Under-estimate Values (dB/km)	
	Horizontal Polarization	Vertical Polarization
10	2.93	2.62
20	7.93	7.67
30	12.4	11.38
40	14.95	13.3
50	15.79	14.12

From Fig. 5.1 to Fig. 5.5, it is observed that the ITU-R average rain rate statistics utilized to compute the specific rain attenuation under-estimated the values of the rain attenuation for all the geographical locations considered when compared with the actual local rain statistics measured at the different locations for each year. Except for Brandvlei in the year 2003 where the ITU-R tends to over-estimate the rain attenuation, on average for the whole five years, it is seen that ITU-R prediction under-estimates it. Looking at all these inadequacies, it can be conclusively said that these ITU-R designations are not necessarily adequate [30]. As mentioned earlier, an adequate estimate of rain attenuation are usually derived from the available information on rain rates observed in the geographical area considered [4].

It is also observed that, appreciable rain attenuation becomes noticeable between 5 GHz to 7 GHz upwards. Looking at frequencies below 5 GHz, the differences in the specific rain attenuation averaged over the whole five years and that of the ITU-R are not so conspicuous, which corroborates the earlier statement by Moupfouma [4] that the incidence of rainfall on radio links in the tropical regional (equatorial climate particularly) becomes important for frequencies as low as 7 GHz.

The plots of the specific rain attenuation and the values at which the specific rain attenuation is under-estimated by using the ITU-R average rain statistics as compared with the actual average rain rate statistics over a 5-year period for the remaining geographical locations are shown in the Appendix A of the appendices.

5.2 Estimation of Path Attenuation Using Different Existing Models on the Available Local Rain Data

From the earlier sections in this chapter, the specific rain attenuation (reduction per unit length) predicted for each geographical location based on the average point rain rate statistics exceeded for 0.01% of the time with an integration time of 1-minute may not be too adequate for the estimation of attenuation along a radio link path [2], [28]. This is because the spatial inhomogeneity present in rain makes it unlikely that the reference rainfall rate will extend uniformly over the length of the transmission path, unless this is very short [12]. The longer the path, the less likely it is that rain will extend the full length of the path. And also, there is non-uniformity of rain along a radio links path and the non-linear dependence of the specific rain attenuation [2], [4], [28]. Because of this, certain authors have used the concept of equivalent path-averaged rain rate which is obtained by multiplying the point rain rate for the time of percentage of interest by a reduction factor, while other authors used an effective path length. The value of which is obtained by multiplying the actual path length by a reduction coefficient, and rain intensity over this effective path length is assumed to be constant [24].

In this section, an estimation of the rain induced attenuation on a line-of-sight (LOS) path will be calculated using different existing models based on the average point rain rate statistics exceeded for 0.01% of the time with an integration time of 1-minute. This will result in a path attenuation $A_{0.01}$ (in dB) exceeded for 0.01% of the time for radio path lengths of up to 22 km. This will be tested at different frequencies for all the twelve geographical locations.

The existing models to be tested on the available local rain rate data are:

1. The ITU-R long-term statistics of rain attenuation model [37]
2. The Moupfouma model [4], which is an improvement of rain attenuation prediction method for terrestrial microwave links
3. The Global Crane model [2], [28].

These three models have been formulated based on the available local propagation data and have been extended to other parts of the world. The theories and the guiding equations for all these three models have been clearly stated and shown in Chapter Two (section 2.8) of this work.

5.2.1 Results and Discussion of the Existing Models on the Available Local Data

The Fig. 5.6-Fig. 5.9 below show the plots of the three models using the actual local measurements recorded for each geographical location situated at different climatic regions at different frequencies. A lower frequency of 10 GHz and a higher frequency of 40 GHz will be shown for five different locations in this chapter to really observe how these three existing models behave at different rain rate values and different frequencies. The plots of other frequencies and the remaining geographical locations will be shown in Appendix B of the appendices.

Fig 5.6 shows the rain attenuation exceeded for 0.01% of the time for Richards Bay at 10 GHz and 40 GHz with a radio path length ranging from 1 km to 22 km for the three models. Richards Bay which lies in the Coastal savannah of South Africa has the highest average rain rate statistics of 152.61 mm/h at 0.01% exceedance level from the actual measurements averaged over a period of five years. This rain rate measurement gives different attenuation values along the propagation

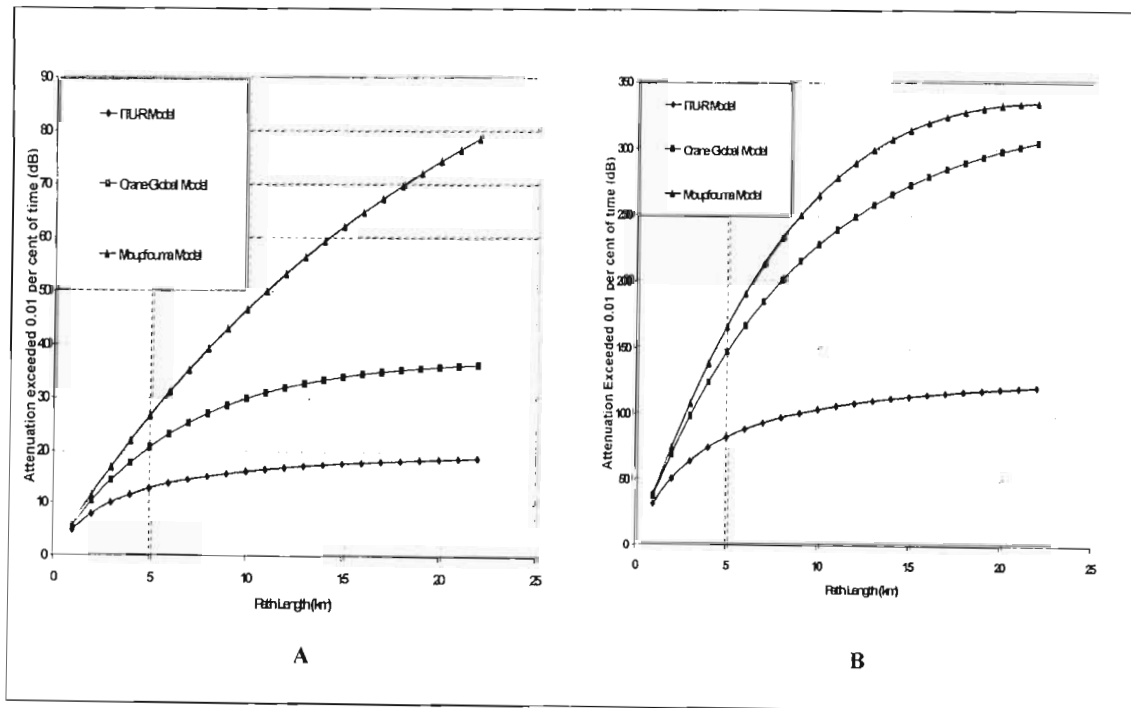


Fig. 5.6 Rain attenuation prediction models for terrestrial line-of-sight links for Richards Bay for frequencies 10 GHz (A) and 40 GHz (B)

path when used on the existing models. It can be seen that the ITU-R model gives a very low attenuation value exceeded at 0.01% of the time $A_{0.01}$ for frequencies 10 GHz and 40 GHz when compared to other two models. At 10 GHz, and at this high rain rate of 152.61 mm/h, the differences in these three existing models are so conspicuous while at 40 GHz and using the same rain rate value the results of the Crane Global model and Moupfouma models tends to be more closer to each other.

Fig. 5.7 shows the plots of rain attenuation exceeded for 0.01% of the time on the three existing models for Cape Town. Cape Town which is located in Mediterranean region of South Africa with an average rain rate statistics of 61.25 mm/h recorded over a period of five years gives different attenuation results when tested on the three existing models. Out of these three models, the ITU-R gives the lowest attenuation values at both frequencies (10 GHz and 40 GHz). It is also observed that differences in the results of these attenuation models on the propagation measurements recorded in Cape Town is not so wide as compared to that of Richards Bay which

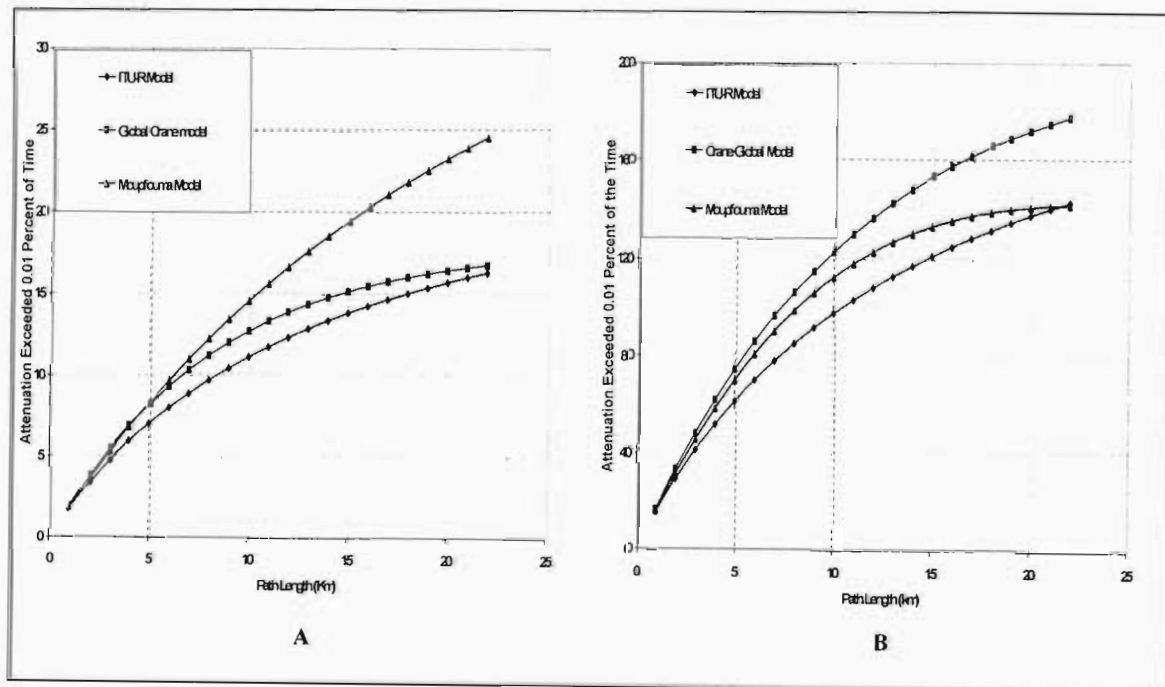


Fig. 5.7 Rain attenuation prediction models for terrestrial line-of-sight links for Cape Town for frequencies 10 GHz (A) and 40 GHz (B)

has a very high rain rate statistics. At 10 GHz, the ITU-R attenuation results and that of Crane Global tends to get closer as the path length increases while that of Moupfouma increases. Looking at the 40 GHz plots, the Moupfouma model behaves in a different way, as the path length increases, the results of the ITU-R model and that of the Moupfouma tend to get closer while that of the Crane model increases and gives the highest rain attenuation along the radio link paths.

The rain attenuation exceeded for 0.01% of the time at 10 GHz and 40 GHz over a path length ranging from 1 km to 22 km in Pretoria which is situated in the temperate region of South Africa is shown in Fig. 5.8. Pretoria which has an average rain rate statistics of 118.86 mm/h recorded over a period of five years give different attenuation results when used on the available models. At 10 GHz and 40 GHz, ITU-R gives the lowest attenuation values over the propagation path. At 10 GHz, the differences in the attenuation values amongst these three models are so wide and look similar to that of the Richards Bay. While at 40 GHz, ITU-R attenuation values are still very low as compared to the other two remaining models, Moupfouma model gives the highest attenuation values for Pretoria and the results of the Crane Global model tends to be very close to the Moupfouma model.

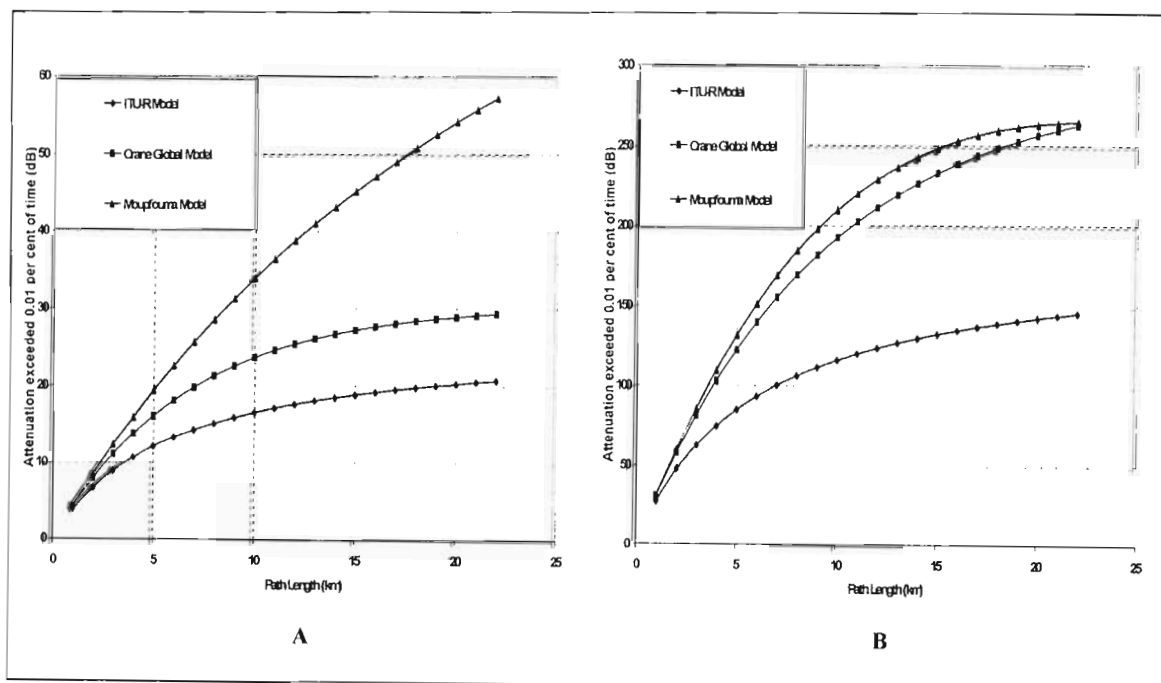


Fig. 5.8 Rain attenuation prediction models for terrestrial line-of-sight links for Pretoria for frequencies 10 GHz (A) and 40 GHz (B)

Fig. 5.9 shows the behaviour of the three available models on a path length that ranges between 1 km to 22 km to predict the rain attenuation exceeded for 0.01% of the time for Brandvlei. Brandvlei which is found in the desert region of South Africa with an average low rain rate statistics of 53.9 mm/h recorded over a period of five years resulted in different attenuation values when used on the three existing models. At 10 GHz, ITU-R still gives the lowest attenuation values along the propagation path, but the Crane Global model, which tends to give the highest attenuation values here, overlaps with that of the Moupfouma model at a path length of 11 and 12 km and bends a little bit more downward than that of the Moupfouma. The attenuation results of Moupfouma model at this point is seen to increase as the path length increases.

At 40 GHz, the Crane Global gives the highest attenuation results along the propagation length. The ITU-R model gives the lowest attenuation results up to a path length of 18 km and the curve of the Moupfouma gradually bends downwards below that of the ITU-R one to produce a lower attenuation results.

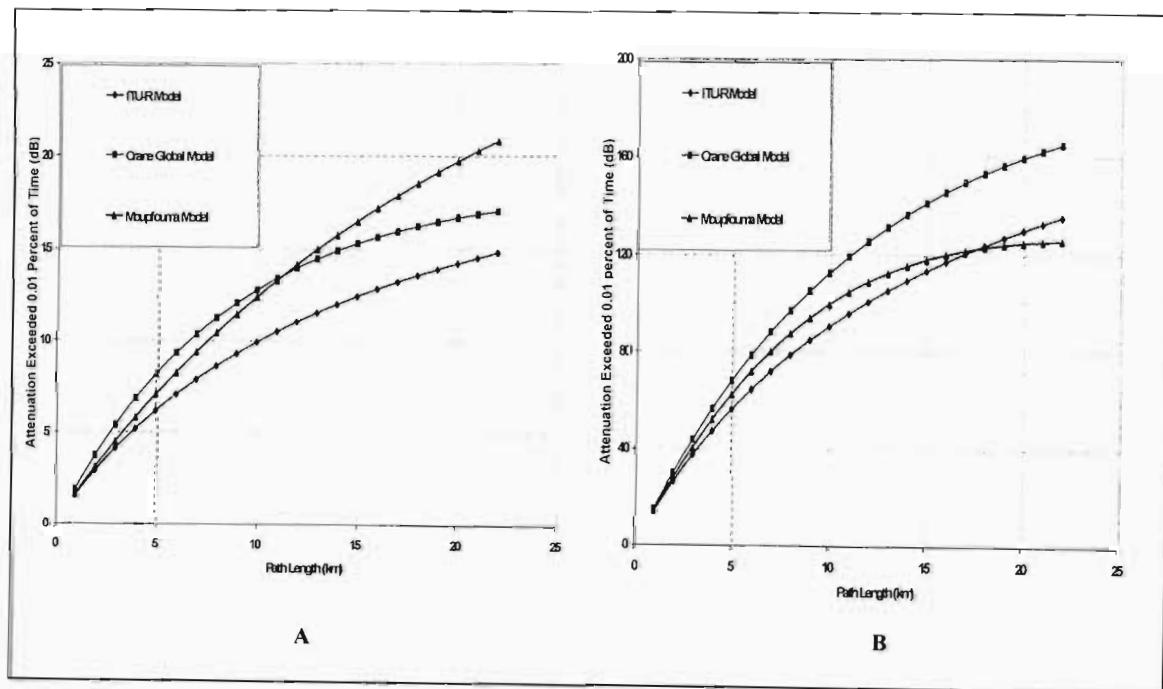


Fig. 5.9 Rain attenuation prediction models for terrestrial line-of-sight links for Brandvlei for frequencies 10 GHz (A) and 40 GHz (B)

Looking at Fig. 5.10, the attenuation exceeded at 0.01% of the time for Durban based on the three available models produce similar results to those of Richards Bay and Pretoria. Durban which also lies in the Coastal Savannah region of South Africa with an average rain rate statistics of 119.58 mm/h (which is very close to that of Pretoria (118.86 mm/h)) produces an attenuation result that seems very close to that of Pretoria and Richards Bay when used on the three available models. At both frequencies (10 GHz and 40 GHz), the ITU-R model produces the lowest attenuation values, followed by the Crane Global model and the Moupfouma model gives the highest attenuation prediction along the propagation paths. At frequency of 10 GHz, the attenuation differences between the Moupfouma and the remaining two other models are too wide while at 40 GHz, the differences between the attenuation values produced by the Crane Global model and Moupfouma model are not so wide as that of the ITU-R.

In conclusion, it can be seen that these three existing models behave differently from each other. And it can be observed that these behaviours depend on the values of the rain rate statistics, the operating frequencies, the radio path lengths and other propagation measurements. ITU-R which

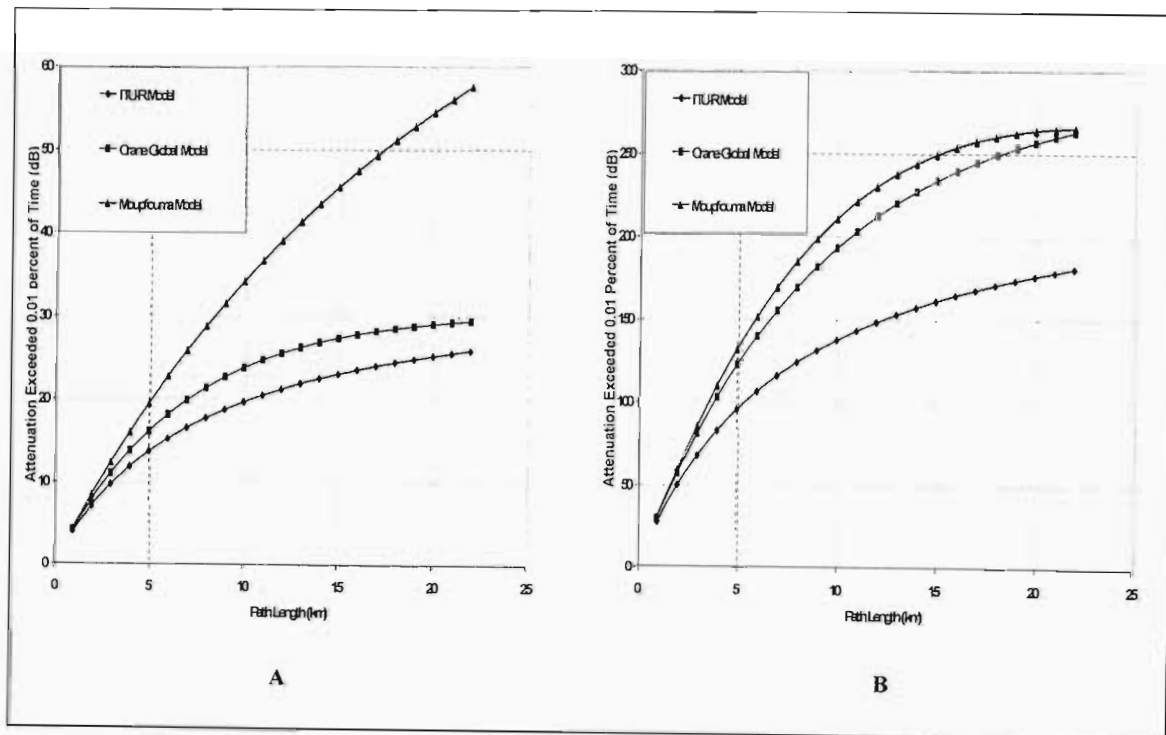


Fig. 5.10 Rain attenuation prediction models for terrestrial line-of-sight links for Durban for frequencies 10 GHz (A) and 40 GHz (B)

gives the lowest attenuation values on all the geographical locations in South Africa can easily be inferred from the non-availability of the propagation data from the Southern hemisphere. ITU-R used mainly the northern hemisphere temperate zones data to predict their model and they extend it to other part of the globe [23]. For the Crane Global model, which follows after Robert K. Crane [2], [28], the work was developed in the same temperate zones as that of the ITU-R, but covers a wider area; however this model still suffers the same set back because of lack of locally obtained data. The Moupfouma model, after Fidele Moupfouma, extends this work to the southern hemisphere and tried to produce an improvement over the ITU-R model [4]. But unfortunately the attenuation produced by this model seems to be inadequate for South Africa being a country that has various rain climatic regions. All these tested models, especially the Crane Global model and the Moupfouma model give a pointer to predict a suitable attenuation model along a terrestrial LOS links for South Africa with the available locally measured propagation data.

5.3 Prediction of Rain Attenuation Model for South Africa from Measurements

Due to the inadequacies produced from all the existing rain attenuation models when used on the average rain rate measurement in each of the twelve geographical locations, the signal attenuation level measurements over a period of one year in Durban by Naicker et al. is utilized to predict and model for rain attenuation on a terrestrial line-of-sight links in South Africa [61]. This line-of-sight link was established between the Howard College and Westville campuses of the University of KwaZulu-Natal separated by a 6.73 km path length and centered at an operating frequency of 19.5 GHz [61]. The link passes over both hilly (near Westville) and suburban (near Cato Manor) terrain. The transmitter station was setup on the roof of the Science building at the Westville campus and the corresponding receiver station was established on the roof the Electrical Engineering building in the Howard College campus. This provides sufficient clearance for the link. The path clearance from the first Fresnel ellipsoid and the line-of-sight path are shown in Fig 5.11. An aerial map of the link showing the distance between the two base stations is provided in Fig 5.12. Also, the various terrestrial link parameters are shown in Table 5.7.

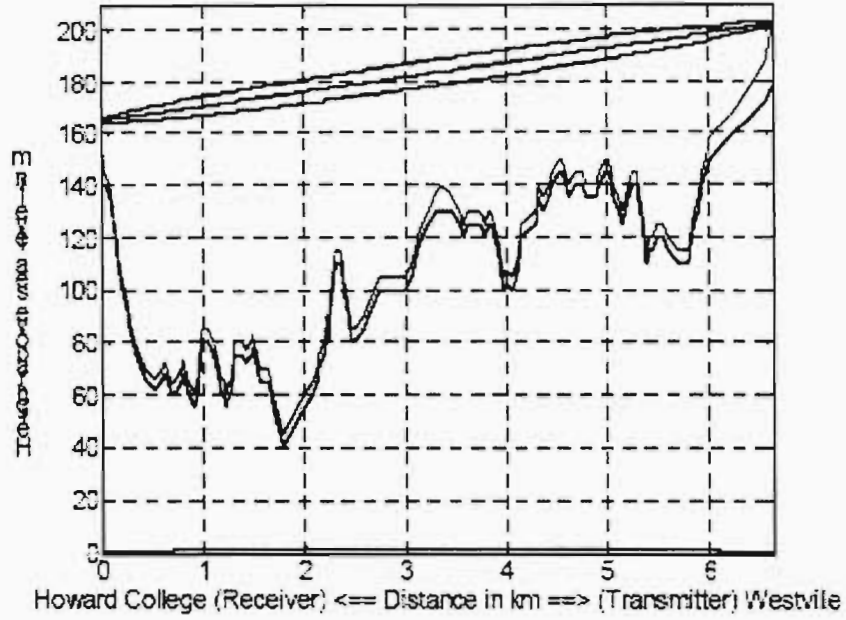


Fig 5.11 The path profile for the 6.73 km terrestrial line-of-sight link from the Howard College campus to the Westville campus [61]

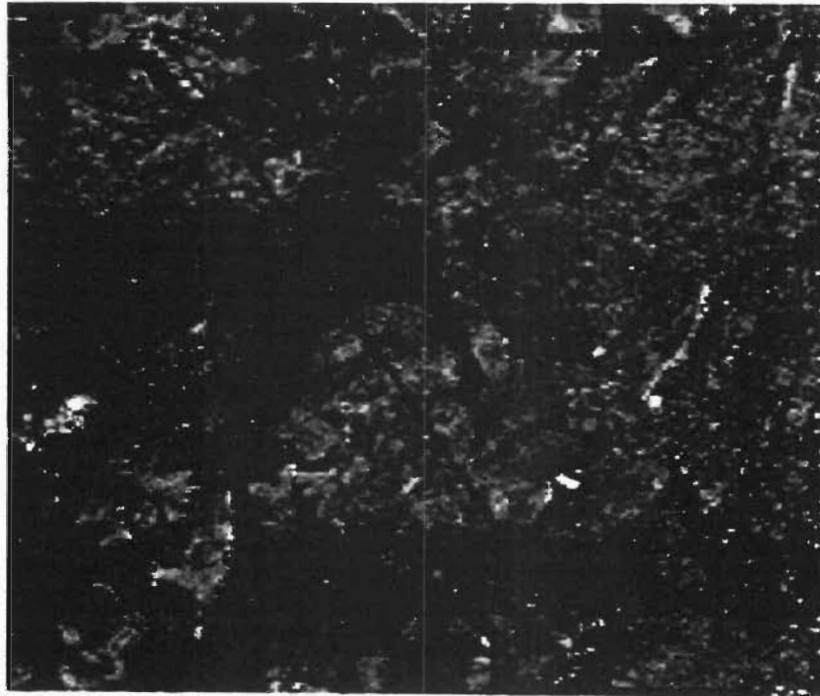


Fig. 5.12 An aerial photograph of the 6.73 km line-of sight terrestrial link [61]

Table 5.7 Terrestrial link parameters [61]

Parameter	Description
Path Length	6.73 Km
Height of transmitting antenna above the ground	24 m
Altitude of transmitter station	178m
Height of receiving antenna above the ground	20m
Altitude of receiver station	145m
Carrier frequency	19.5 GHz
Bandwidth under investigation	200 MHz
Transmitting power	10-100 mW
Transmitting/receiver antenna gain	38.6 dBi
Transmitting /receiver antenna beamwidth ¹	1.9 degrees
Free space loss	135 dBm
Total cabling and connection losses	≅ 2.2 dB
Clear air attenuation	1 dB
Receiver Bandwidth	100 kHz-1 GHz

From these link parameters stated in Table 5.7, the received signal level (RSL) was determined using a transmitting power of 100 mW (20 dBm) so as to have an idea of the power that will be received at the receiver end of the link when there were no rains. (Assuming the effective earth radius factor $k=4/3$ for Durban).

Calculating for the power received P_r :

$$P_r = P_t - FSL + G_{rant} + G_{tant} - Losses \quad (5.1)$$

where:

P_t = Power transmitted

FSL = Free space loss

G_{rant} = Receiver antenna gain

G_{tant} = Transmitted antenna gain

Therefore,

$$P_r = 20dBm - 135dB + 38.6dBi + 38.6dBi - 2.2dB - 1dB \quad (5.2)$$

$$P_r = -41dBm .$$

¹ The beamwidth of an antenna is the angle enclosing the main lobe or twice the angle between the boresight direction and a reference power on the main lobe of the antenna pattern [24].

Therefore, the power received P_r , expected at the receiver end of the link when a transmitting power of 100 mW is employed between Howard College and Westville campuses should be $\cong 41dBm$ when there are no rains to cause any rain induced attenuation.

5.3.1 Signal Attenuation Measurements in Durban for the Various Months

The signal level measurements and its corresponding 1-minute rain rate statistics were recorded over a period of ten calendar months in Durban for the year 2004: February, March, April, May, June, August, September, October, November and December. This data was analyzed, processed and the average signal level for the non-rainy days for each month was determined. There were no rains in the months of May, June and August, therefore, the signal attenuation recorded for those three months are assumed to be due to other attenuating factors like fog, obstructions, trees, vegetations, hills, tall buildings etc. Fig 5.13 shows the values of the average signal level for the non-rainy days which can also be referred to as the non-rain faded average values.

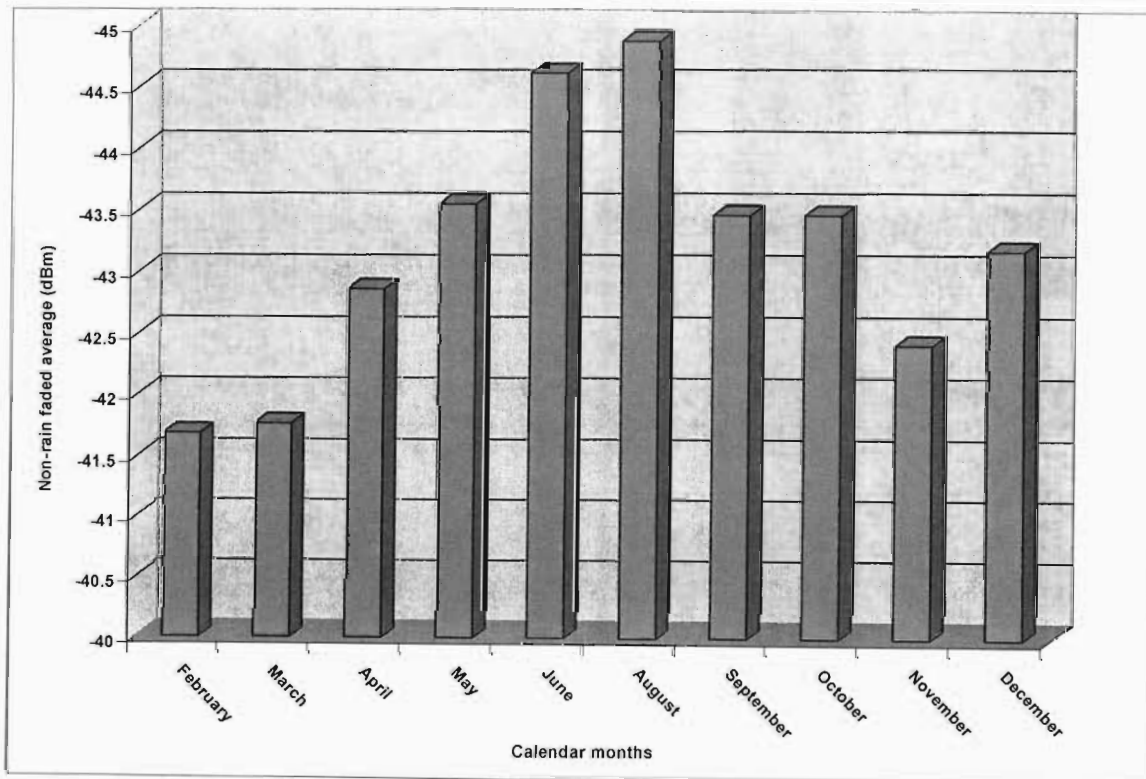


Fig. 5.13 Non-rain faded average signal values for 10 months in 2004

From Fig. 5.13, the non-rain faded average for February and March is -41.68 dBm and -41.76 dBm respectively while that of April is -42.86 dBm which tend to be higher than that of the other two months and relatively higher than the expected received signal level. For the months of May, June, and August which is normally referred to as the winter months in South Africa [16], [18], a very high non-rain faded average values of -43.55 dBm, -44.61 dBm, and -44.87 dBm are recorded respectively. Since there are no rains in these three months that means other factors are responsible for this high signal level. Taking into considerations other factors discussed in the second chapter of this work, and Durban being a location that has a hilly terrain, this high signal level may be due to obstructions along or near the propagation path. Note that while an effective earth radius factor, k value of $4/3$ is assumed in this design, the correct design value of k for Durban should be 1.21 [62]. The diffraction gain or signal attenuation in clear air in Durban for a radio link between Sherwood and Umlazi has been estimated to be -44.50 dBm when an effective earth radius factor, k exceeded 99.9% of the time of 0.50 is utilized to design the link [62]. One thus concludes that these high non-rain faded signal levels for these winter months can be caused by k -factor fading.

The months of September, October, November and December which are regarded as summer months in seasonal variation in South Africa [16], [18], are said to have an abundant low stratus cloud and fog particularly during summer in the east coast of South Africa [18]. And Durban, lying in the coastal side of South Africa has the tendency of being influenced by this fog and low stratus cloud which in turn can affect any signal level even when there are no rains. According to Crane [24], cloud or fog attenuation at frequencies lower than 10 GHz can be ignored but at a frequency of 30 GHz, the attenuation may approach 3 to 4 dB. Also looking at Fig 2.4 in Chapter 2, fog attenuation at 20 GHz can be estimated to approximately 2 dB/km or less [12]. Therefore, for the months of September, October, November and December having a slightly high average non-rain faded average of -43.46 dBm, -43.46 dBm, -42.41 dBm and -43.17 dBm respectively can be caused by the presence of these foggy patches.

5.3.2 Rain Attenuation Modeling in Durban at 19.5 GHz from Measurements

Having determined the non-rain faded average for the months in the year 2004 from the actual signal level measurements recorded between the two radio transmitting paths, now, the rain induced attenuation can be modeled for months that had rains for the year 2004. This is done for

the months of February, March, April, September, October, November and December. The three existing models, namely, ITU-R model, Crane Global model and the Moupfouma model, are used on the link parameters such as the path length of 6.73 km. This enables us to determine the effective path length between the links; then, at the carrier frequency of 19.5 GHz and the measured rain rate at 1-minute integration, we determine the attenuation values that will be predicted by these models. These are then compared with the actual attenuation measurements recorded for these months. Logarithmic and power estimation models are then used to fit the measurement data. Fig 5.14- Fig 5.20 shows the modeling of rain attenuation in Durban from the actual measurements.

5.3.3 Discussion for Rain Attenuation Measurements

In figures 5.14-5.20, y refers to path attenuation (dB) and x refers to the rain rate (mm/h). Fig 5.14 shows the rain attenuation models for the month of February in Durban at a frequency 19.5 GHz from the actual measurements and the other existing models. The attenuation values predicted from these other existing models tend to be lower than the ones from the actual measurements. From these actual attenuation measurements, the path attenuation is seen to increase as the rain rate increases until it gets to a rain rate of above 20 mm/h, and at this point, there is slight downward movement of the actual attenuation measurement curve. The highest rain rate measured in this month was 21 mm/h and its corresponding signal attenuation value was 14.93 dB. Also for Fig 5.15, the rain attenuation models for the month of March are shown. For this month, the maximum rain rate recorded was 19 mm/h, and the attenuation measured at this point was 11.48 dB. In this month, the attenuation predicted by the Crane model tends to be very close to the actual measured attenuation values. The power estimation model and the logarithmic estimation model derived from the actual attenuation tend to overlap over the Crane model curve.

The path attenuation recorded from the actual measurements for the month of April (Fig 5.16) is considerably low compared to the months of February and March. The month of April records its highest attenuation level of 5.94 dB at a rain rate of 17 mm/h. The highest rain rate recorded in this month was 20 mm/h with an attenuation of 3.169 dB. From this figure, the crane model is seen to predict a very high attenuation as compared with the actual attenuation measurements. The Moupfouma model, ITU-R model, the power and the logarithmic estimation model predicted from the actual attenuation model curves are seen to overlap upon each other for this month

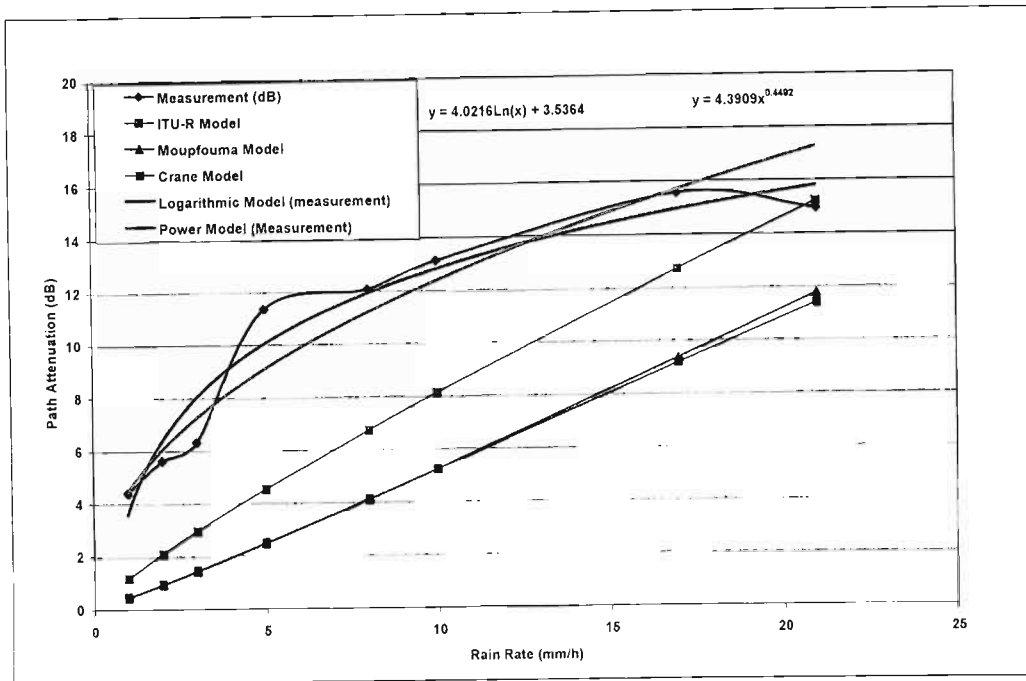


Fig 5.14 Rain attenuation in Durban for February: Measurement and Models at 19.5 GHz

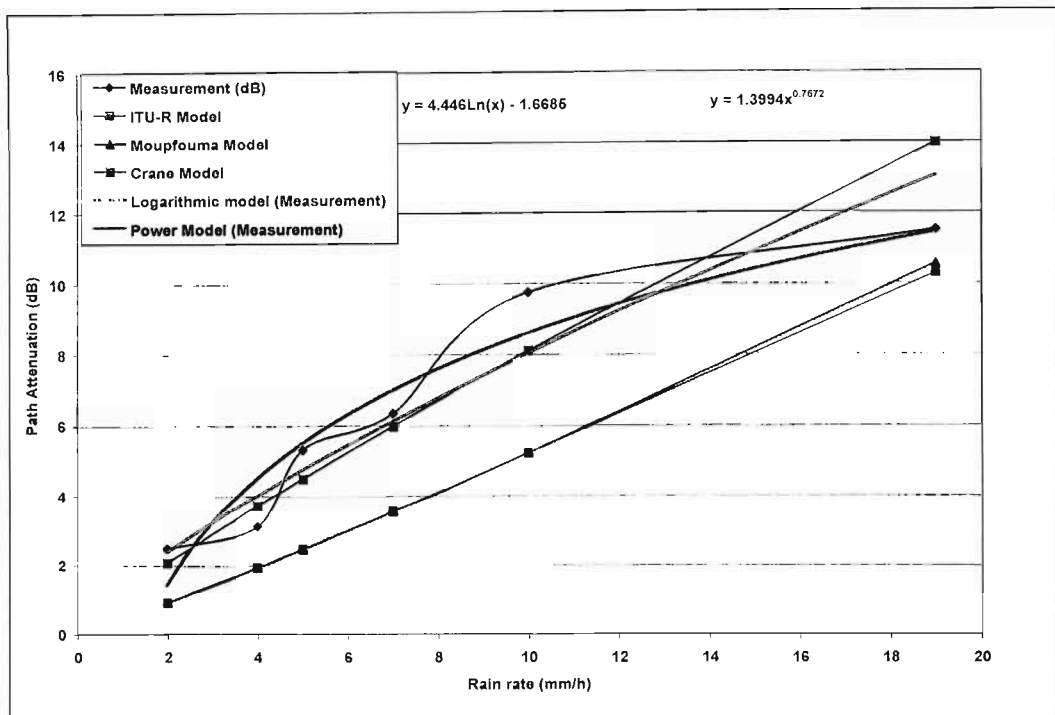


Fig 5.15 Rain attenuation in Durban for March: Measurement and Models at 19.5 GHz

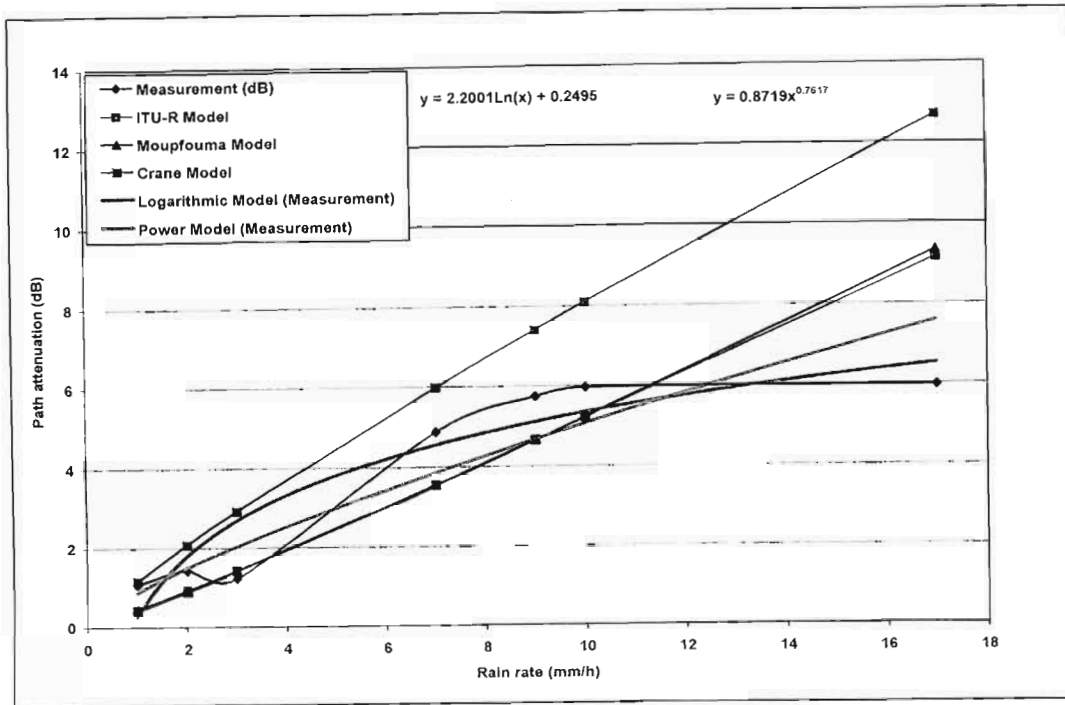


Fig 5.16 Rain attenuation in Durban for April: Measurement and Models at 19.5 GHz

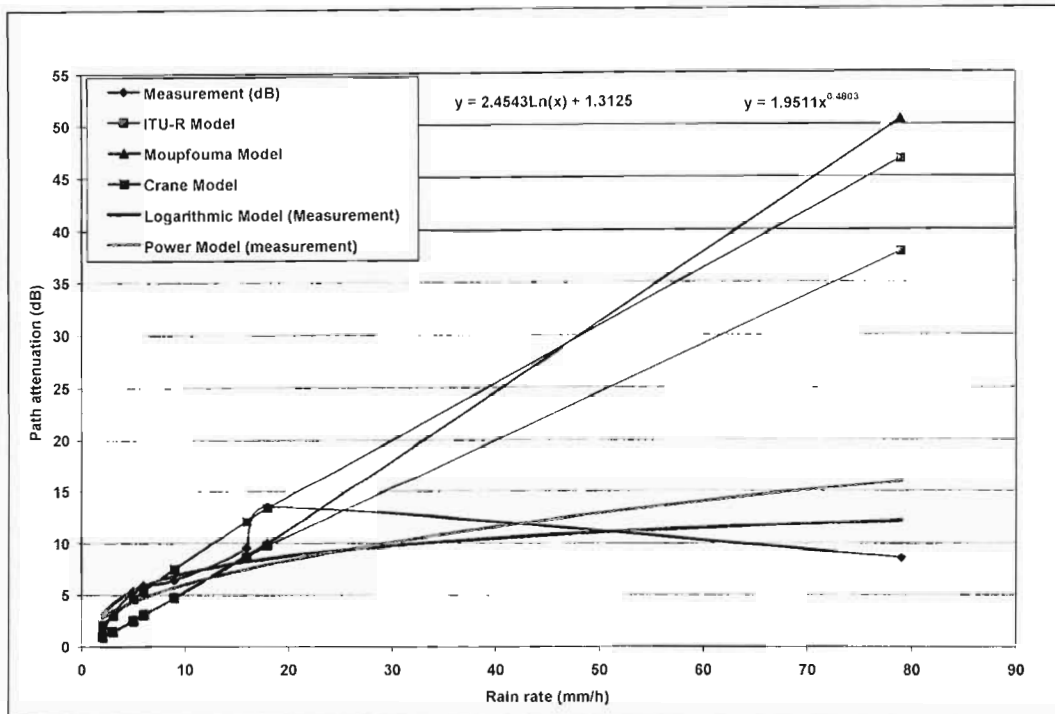


Fig 5.17 Rain attenuation in Durban for September: Measurement and Models at 19.5 GHz

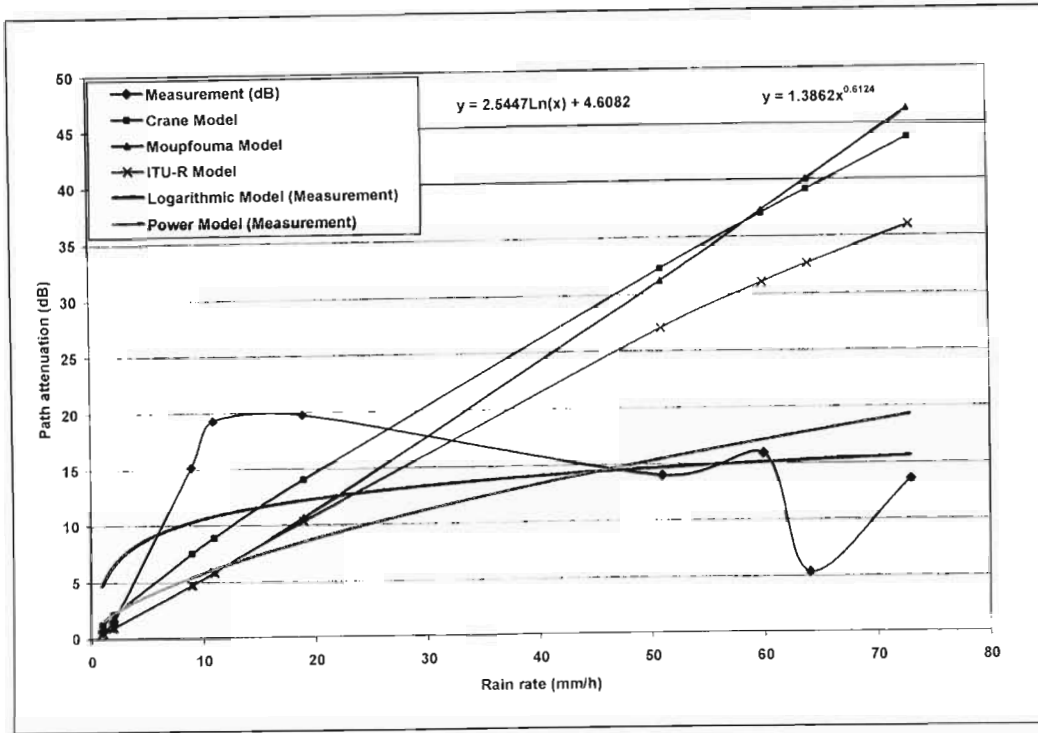


Fig 5.18 Rain attenuation in Durban for October: Measurement and Models at 19.5 GHz

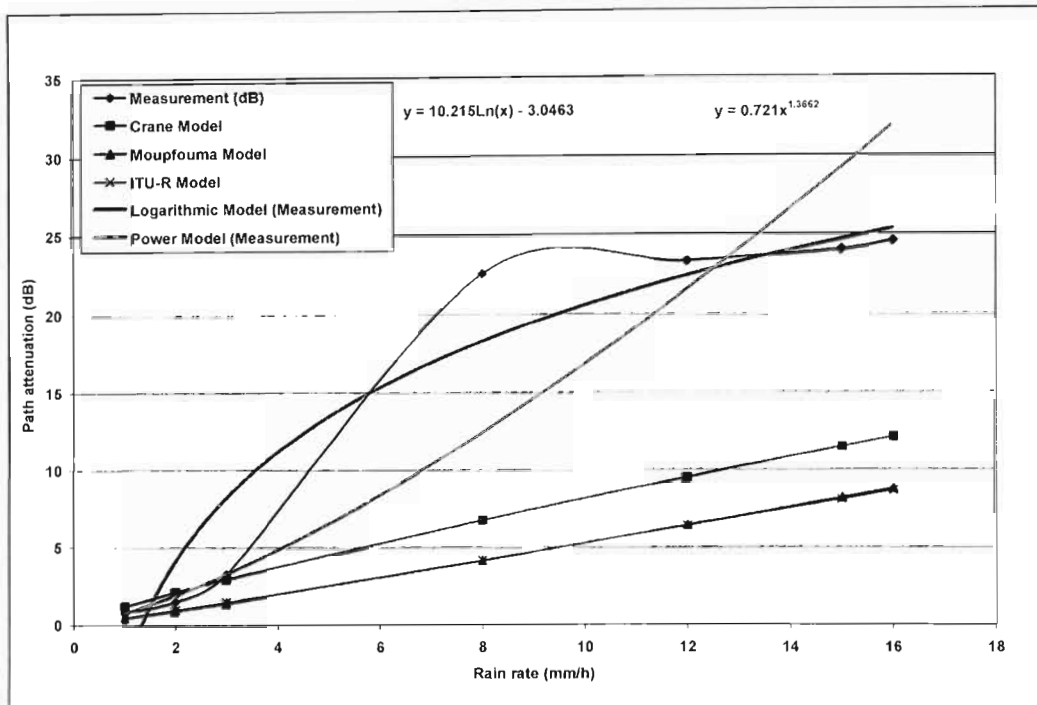


Fig 5.19 Rain attenuation in Durban for November: Measurement and Models at 19.5 GHz

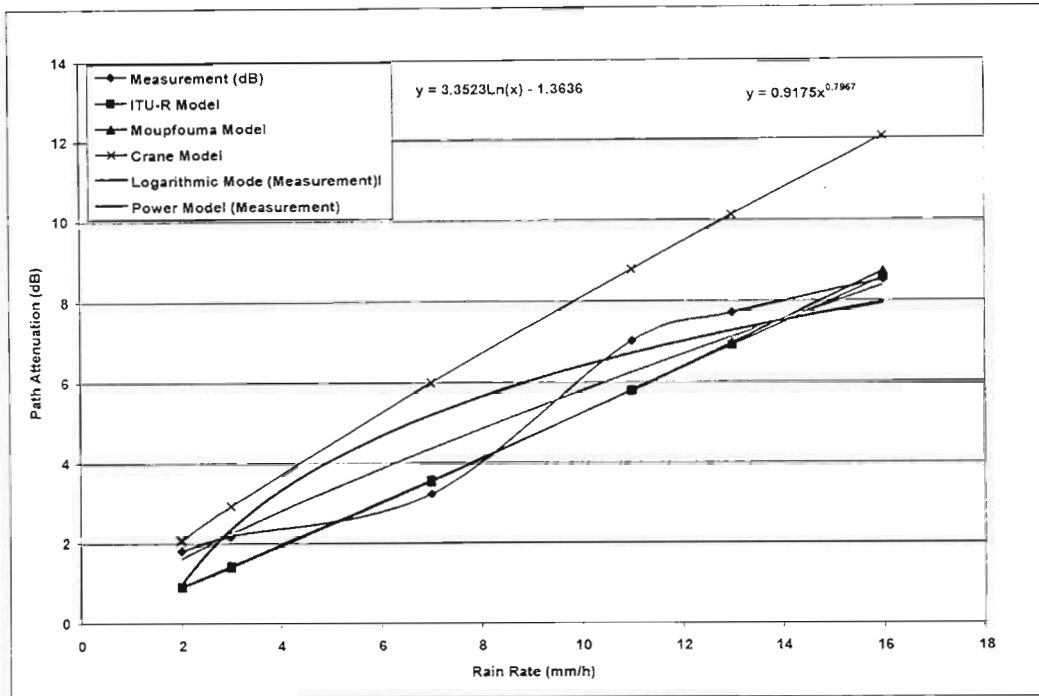


Fig 5.20 Rain attenuation in Durban for December: Measurement and Models at 19.5 GHz

For the month of September (Fig 5.17), the highest rain rate measured was 79 mm/h with a corresponding low signal attenuation of 8.5 dB. From this figure, it is also observed that at lower rain rate, there is a corresponding increase in the path attenuation values as the rain rate also increases until after a rain rate of 18 mm/h when it is observed that there is a sharp bend on the rain attenuation curve from the actual measurements. The behaviour of the rain attenuation in the month of October in Durban at a frequency of 19.5 GHz is shown in Fig. 5.18. The maximum rain rate recorded in this month was 73 mm/h with its corresponding rain attenuation signal level of 13.45 dB. At a rain rate of 19 mm/h, the highest signal attenuation value of 19.69 dBm was recorded for the month and afterwards, it was also observed that there is a sharp bend in the actual attenuation measurement curve.

Fig 5.19 shows the signal attenuation models and measurements recorded for the month of November. At low rain rates of 1 mm/h, 2 mm/h and 3 mm/h, correspondingly low attenuation values were measured. But at a higher rain rate of about 8 mm/h very high attenuation values were recorded. The highest rain rate recorded for this month was 16 mm/h with a corresponding signal attenuation of 24 dB. The attenuation values from the existing three model shows a little bit of agreement with the measured values at lower rain rates but at a higher rain rate, the existing three models gave lower attenuation values. For the month of December (Fig 5.20), the signal

attenuation measurement recorded shows a considerable increase as the rain rate increases. The maximum rain rate recorded for this month was 16 mm/h with its corresponding signal attenuation of 8.5 dB. The Crane model is seen to show higher attenuation values than the actual measurements for this month. The Moupfouma model, ITU-R model, the power estimated model and the logarithmic estimated model derived from the actual measurements are seen to overlap on each other.

From the measurements, Fig 5.14-Fig 5.20, it is observed that the highest rain rate was recorded in the summer months. These months are September and October with rain rate of 79 mm/h and 73 mm/h respectively. The highest rain attenuation for the link was recorded in the month of November with a value of 24.51 dB followed by 19.69 dB recorded in the month of October. Table 5.8 gives the summary of the highest rain attenuation values at a frequency of 19.5 GHz for a propagation path of 6.73 km path length and their corresponding rain rates recorded for months with rains in the year 2004 in Durban. It is also observed from the above figures that as the rain rate increases, the path attenuation signal level increases, but as the rain rate goes above 18 mm/h, a decrement in the path attenuation signal level is observed and an anomalous behaviour of the signal level is also observed as seen in Fig. 5.17 and Fig. 5.18. The reasons for this behaviour along a propagation path length will be explained in sub-section 5.3.3.1.

Table 5.8 The highest rain attenuation values and their corresponding rain rates recorded in Durban for year 2004 (6.73 km at 19.5 GHz)

Months	Path attenuation (dB)	Rain rate (mm/h)
February	15.54	17
March	11.48	19
April	5.94	17
September	13.46	18
October	19.69	19
November	24.51	16
December	8.5	16

5.3.3.1 The Behaviour of Point Rain rate along Radio propagation Path Lengths

Most attenuation prediction methods use the concept of an equivalent rain cell with uniform rain that should produce the same path attenuation as the random rain clusters [53]. The ITU-R path attenuation prediction model and other authors have used the concept of an effective path length d_{eff} which is determined by multiplying the actual path length d of the link by a reduction factor r , as indicated in Chapter 2 [4], [37]. This effective path length reflects the high degree of spatial inhomogeneity present in a rain cell, simply because it is unlikely that reference rain rate will extend uniformly over the length of transmission path unless this propagation path length is very short [12]. The longer the path, the less likely it is that rain will extend the full length of the propagation path.

In [53], the spatial distribution of rain along a propagation path is investigated and this describes the size of both rainy patches (at several intensity levels) and separations among them. These statistics are obtained through the scanning of large number of horizontal radar rain maps collected at Spino d'Adda along thousands of simulated links in two principal directions [53], [54]. Fig 5.21 thus shows the resulting typical dimension of rain cells (in km) for varying rain rates [53].

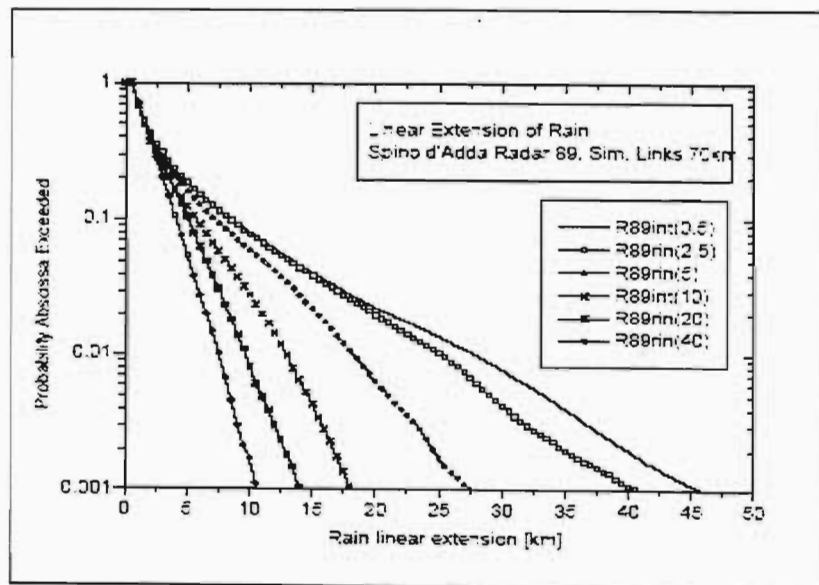


Fig 5.21 Extension of rain exceeding a given intensity, from 0.5 mm/h to 40 mm/h [53]

From this figure, a rain rate of 0.5 mm/h extends over a path of about 45 km, 10 mm/h extends over a 40 km path and it goes on like that until it gets a 40 mm/h rain rate and this only covers a 10 km path length. From this example, it can be inferred that the higher the precipitation rate, the lower path length it will cover and vice-versa

Taking a closer look at the measurements recorded in Durban, South Africa, with a path length of 6.73 km, the rain attenuation produced by the lower rain rates tends to increase as the rain rate increases. This is to say, the lower rain rates extends uniformly along the 6.73 km propagation paths and an accurate measurement is taken at the receiver end of the transmitting station. But at higher rain rate, the rain may not be able to cover the entire propagation path length of 6.73 km as seen in the example shown in Fig 5.21. Therefore, the rain attenuation recorded at these high rain rates reflects a corresponding diminution of the effective path length. Note that, the effective path length is introduced to incorporate the effect of non-uniformity of rain along any propagation path length. Therefore, the higher the rain rate (above 18 mm/h), the smaller the coverage radius or rain cell size. This may therefore explain the reduced attenuation at higher rain rates.

5.4 Statistical Analysis of the Rain Attenuation Models Predicted from the Measurements in Durban

The logarithmic estimation model and the power estimation model that was used to fit in the attenuation measurements in Durban was analysed and tested by using a statistical tool known as the chi-square χ^2 statistics. The table in Appendix C in the Appendices is used for the interpretation of the chi-square and to determine threshold values for the chi-square test at either 1% or 5% level of confidence for the various months analysed.

The chi-square statistics is given by:

$$\chi^2 = \sum_{R=1}^N \frac{(M_R - P_R)^2}{P_R} \quad (5.3)$$

where

$$M_R = \text{measured value}$$

P_R = predicted value

N = number of measurements

The measured values in this context are the signal attenuation measurements recorded in Durban at 19.5 GHz for a path length of 6.73 km. The predicted values are the values that are predicted by the logarithmic estimation and the power estimation model. And the numbers of measurements depict the number of times the signal attenuation measurements are made. In a chi-square statistics problem, the degrees of freedom ($N - 1$) for the number of measurements recorded in each month must be determined so that the threshold values for the chi-square test at each level of confidence will be analysed. Table 5.9 shows the equations predicted by the logarithmic estimation model, the power estimation model (as shown in Fig. 5.14-Fig. 5.20), the chi-square statistics results and the degrees of freedom for each month.

Table 5.9 Equations predicted by the Logarithmic and Power models

Calendar months	Degrees of freedom ($N - 1$)	Logarithmic model equation	Chi-square statistics: (Log. model)	Power model equation	Chi-square statistics: (Power model)
February	7	$y=4.0216\text{Ln}(x)+3.5364$	0.8876	$y=4.3909x^{0.4492}$	1.1485
March	5	$y=4.4446\text{Ln}(x)-1.6685$	1.4287	$y=1.399x^{0.7572}$	0.8235
April	6	$y=2.2001\text{Ln}(x)+0.2495$	3.7904	$y=0.8719x^{0.7617}$	1.3851
September	7	$y=2.4543\text{Ln}(x)+1.3125$	5.3929	$y=1.9511x^{0.4803}$	9.3861
October	8	$y=2.5447\text{Ln}(x)+4.6085$	28.1008	$y=1.3862x^{0.6124}$	73.3293
November	6	$y=10.215\text{Ln}(x)-3.0463$	1.0326	$y=0.721x^{1.5662}$	11.1266
December	5	$y=3.3523\text{Ln}(x)-1.3636$	1.5468	$y=0.9175x^{0.7967}$	0.4722

From Table 5.9, the month of February with 7 degrees of freedom has a computed chi-square statistics of 0.8876 and 1.1485 for the logarithmic and power models respectively. The threshold values for the chi-square test at 1% and 5% level of confidence when the degrees of freedom is 7 are 18.4753 and 14.0671, respectively, (as shown in Appendix C) and these are larger than the values predicted by the logarithmic and power model, hence we can accept the hypotheses of these two models at both 1% and 5% level of confidence. The chi-square statistics value of the logarithmic model having a smaller value than the power model gives a better fit to the measured

attenuation values. Hence, the logarithmic model is accepted for the prediction of rain attenuation in this month.

For the month of March with a degree of freedom of 5, the computed chi-square statistics shown in Table 5.9 for both models are smaller than the threshold values for the chi-square test at 1% and 5% level of confidence when the degree of confidence is 5 (see appendix C), therefore the hypotheses for these two models can be accepted at 1% and 5% level of confidence. The chi-square statistics for the power model being smaller than the logarithmic model, therefore, for the month of March, the power model is accepted. April, with 6 degrees of freedom and computed chi-square statistics of 3.7904 and 1.3851 for the logarithmic and power model respectively is smaller than the chi-square test threshold values at both 1% and 5% level of confidence. Hence, the hypotheses of these two models can be accepted. The power model gives a better fit to the attenuation measured values because of its lower chi-square statistics to the one predicted by the logarithmic model.

For September with 7 degrees of freedom with computed chi-square statistics of 5.3929 and 9.3861 for both the logarithmic model and power model, are smaller than the threshold values for the chi-square test at 1% and 5% level of confidence when the degree of confidence is 7 (see appendix C), therefore the hypotheses for these two models can be accepted at 1% and 5% level of confidence. The logarithmic model having a better fit to the attenuation measurements data than the power model because of its smaller chi-square statistics value is accepted for the attenuation prediction in the month of September. Also for October, with 8 degrees of freedom, the computed chi-square statistics of 28.1008 and 73.3293 for the logarithmic model and power model, respectively, are larger than the chi-square threshold values for both the 1% and 5% level of confidence; hence the hypotheses for both models are rejected.

For the November, the chi square statistics computed is 1.0326 and 11.1266 for the two models for degree of freedom equals 6. These values are smaller than the chi-square threshold test values at both 1% and 5% level of confidence; therefore, the hypotheses for these two models are accepted at 1% and 5% levels of confidence. The logarithmic model is accepted for the attenuation prediction for the month because of its smaller chi-square statistics. Also, for the month of December, for 5 degrees of freedom the computed chi-square statistics are 1.5468 and 0.4722 for the logarithmic and the power models respectively. The chi-square threshold test values for degree of freedom equals 5 (as shown in Appendix C) is larger than the computed chi-

square statistics at 1% and 5% level of confidence, therefore the hypotheses for these two models is accepted at both level of confidence. The power model is accepted to predict the attenuation for the month of December

Finally, from this statistical analysis, it can be observed that the month of October is the only month that gave rejected hypotheses for both 1% and 5% level of confidence. It was also observed that the month of February, September and November are the months that predicted that the logarithmic model curve gave a better fit to the measured attenuation data than the power model. The months of March, April and December are predicted by the power model curves.

5.5 Application of Rain Attenuation Predictions

As earlier stated in the first chapter of this work, accurate and a fairly precise propagation measurements are essential for the proper prediction of rain induced attenuation on propagation paths. Therefore at this point, the attenuation predicted by the logarithmic and the power models computed from the actual signal level measurements recorded in Durban, South Africa is used on the average 1-minute rain rate statistics exceeded for 0.01% of the time measured in Durban, South Africa (see Table 5.1). With this, the attenuation exceeded for 99.99% of the time will be determined for Durban and this can be estimated for the remaining eleven locations in South Africa using their average rain rate exceeded for 0.01% of the time at 1-minute integration time. Table 5.10 shows the rain attenuation model equations for each month computed from the actual signal level measurements at 19.5 GHz and a propagation path length of 6.73 km and their corresponding rain attenuation computed base on the average 1-minute integration time rain rate exceeded for 0.01% of the time.

The predicted rain attenuation values for a propagation path length of 6.73 km at a frequency of 19.5 GHz shown in Table 5.10 can then be utilized by terrestrial link designers in Durban and other parts of South Africa for the design of radio link systems. This will at the end gives a better performance and reduces the possibility of rain attenuation affecting services, and also confines the effect to very heavy and very infrequent rain periods

Table 5.10 Rain attenuation predicted for the year 2004 in Durban, South Africa in a typical path of 6.73 km.

Calendar Months	Predicted Model	Rain Attenuation at $R_{0.01}$ (dB)
February	$A=4.0216\ln(R)+3.5364$	22.78
March	$A=1.399R^{0.7572}$	52.36
April	$A=0.8719R^{0.7617}$	33.34
September	$A=2.4543\ln(R)+1.3125$	13.05
November	$A=10.215\ln(R)-3.0463$	45.82
December	$A=0.9175R^{0.7967}$	41.48

5.6 Chapter Summary

At the end of this chapter the specific rain attenuation (dB/km) for the twelve different geographical locations has been computed based on the available rain rate data. Also the path attenuation (dB) for these locations was estimated by using the existing models on the available local rain data. This chapter also focuses on the determination of rain attenuation model from the signal attenuation level measurements recorded over a period of one year in Durban, South Africa. And from there a suitable rain attenuation model was predicted for Durban. All the other existing models do not accurately predict rain attenuation in Durban.

Chapter Six

Conclusion

6.1 Conclusion

The importance of an accurate prediction of rain rate and rain attenuation on terrestrial line-of-sight links at millimeter wavelengths cannot be overemphasized in radio communication studies. In this report, rain rate and rain attenuation predictions for South Africa have been studied and proposed rain-induced attenuation models have been determined. Rain rates over a period of five years (2000-2004) for twelve different geographical locations; Durban, Richards Bay, Pietermaritzburg, Ulundi, Vryheid, Newcastle, Ladysmith, Pretoria, Cape Town, East London, Bloemfontein and Brandvlei in the Republic of South Africa has been utilized for the accurate prediction of rain rates statistics in South Africa.

The effect of integration time on the cumulative distribution of rain rate statistics for South Africa was studied. Also, comparison of the 5-year rain rate statistics exceeded for 0.01% of the time for the different geographical locations was studied; thus shows the variability of the rain rate statistics from location-to-location and from year-to-year. Richards Bay which lies in the coastal savannah of South Africa was found to have the highest average rain intensity of 152.61 mm/h, followed by Pietermaritzburg, Ulundi, and Newcastle with average rain intensities of 139.96 mm/h, 130.22 mm/h and 130.01 mm/h, respectively. Ulundi and Pietermaritzburg lie in the Inland area of Coastal Savannah region. The very lowest rain fall occur on the west coast, with Brandvlei which is found in the desert area showing the lowest average rain intensity of 53.90 mm/h.

In this study, additional climatic rain zones ; N, M, P and Q are determined for South Africa, as against the ITU-R classifications of C,D, E, K and N based on the available 60-minute rain data (converted to 1-minute integration time). Thus, an additional three rain zones have been identified for South Africa.

It is noted that the north-eastern area of South Africa have higher rain rates than the north-western parts and thus more prone to rain attenuation, therefore, the specific rain attenuation (dB/km) for the twelve different geographical locations were computed based on the available rain rate data. It

was observed that the ITU-R average rain rate statistics utilized to compute the specific rain attenuation under-estimated the values of the rain attenuation for all the geographical locations considered when compared with the actual local rain statistics measured at the different locations for each year. Also the path attenuation (dB) for these locations is subsequently estimated by using the existing models on the available local rain data. The behaviour of these existing models at different frequencies and propagation path lengths were observed and compared.

A suitable rain attenuation model was proposed for Durban from the signal attenuation level measurements recorded for a typical path length of 6.73km and at an operating frequency of 19.5 GHz over a period of one year in Durban, South Africa. A Logarithmic model and a Power model were predicted for each of the rainy months in the year 2004 and using a chi-square statistical analysis, the model that best fit the attenuation measurements was accepted. Hence, a Logarithmic model was proposed for the months of February, September and November and a Power model was proposed for March, April and December. The month of October which has a rejected hypothesis for both the Logarithmic and Power model due to its anomalies in the attenuation measurements can be further studied.

6.2 Recommendation for Future Work

As a result of the rapidly varying nature of rainfall from location-to-location and from year-to-year, the sites for rainfall data collection should be expanded to more geographical locations in South Africa over a longer period of years. This will in turn give a better precision and accuracy to the rainfall-rate predictions. Also a smaller integration time rain rate such as 10 seconds, 20 seconds, and 30 seconds should be sought after for a better prediction of rain attenuation models.

The signal attenuation measurements should also be expanded to more geographical locations in South Africa (not in Durban alone) and this should also be extended to cover a longer period of years. By doing this, the anomalies observed in some rainy months will be incorporated and a better attenuation prediction will be determined for the Republic of South Africa.

References

- [1]. M. Marcus and B. Pattan, "Millimeter Wave propagation-Spectrum Management Implications," *IEEE Microwave Magazine*, Vol. 6, No2, June 2005, pp. 54- 61.
- [2]. Robert K. Crane: *Electromagnetic Wave Propagation through Rain*, John Wiley, New York, 1996, Chapter1, 2,3,4.
- [3]. Roger L. Freeman: *Radio System Design for Telecommunications*, 2nd Edition, John Wiley, 1997, Chapter 1 & 9.
- [4]. Fidele Moupfouma, "Improvement of a Rain Attenuation prediction Method for Terrestrial Microwave Links," *IEEE Transactions on Antennas and Propagation*, Vol. AP-32, No. 12, December 1984, pp. 1368-1372
- [5]. F. Moupfouma and J. Tiffon, "Raindrop Size Distribution from Microwave scattering Measurements in Equatorial and Tropical Climates," *Electronic Letter*, Vol. 18, 1982, pp. 1012-1014.
- [6]. B. Segal, "The Influence of Raingage Integration Time on Measured Rainfall-Intensity Distribution Functions," *J. of Atmospheric and Oceanic Tech*, Vol. 3, 1986, pp.662-67
- [7]. D.S Upadhyay: *Cold Climate Hydrometeorology*, New Age International (P) Limited August, 1995, pp. 13-14
- [8]. Panter P.: *Communication Systems Design: Line-of-sight and Troposcatter Systems*, McGraw-Hill Inc., New York, 1972.
- [9]. G.P. Brasseur, John J. Orlondo and G.S Tyndall: *Atmospheric Chemistry and Global Change*, New York, Oxford University Press, 1999 Chapter 1
- [10]. Thomas A. Blair: *Weather Element*, Prentice-Hall, Inc. Eaglewood Cliffs, N.J. 1957, pp. 7-30, Chapters one and two
- [11]. Barry G. and Chorly J.R.: *Atmosphere, Weather and Climate*, 5th Edition, Chapman and Hall Inc, New York, 1987, Chapter 2.

- [12]. M.P.M. Hall, L.W. Barclay and M.T Hewitt: *Propagation of Radiowaves*, IEEE, London United kingdom, 1996, Chapter 1 and Chapter 4
- [13]. G. O. Ajayi, "Physics of Tropospheric Radiopropagation" *ICTP, Trieste, Italy*, Feb1989, pp. 11-12
- [14]. Carlos Salema: *Microwave Radio Links from Theory to Design*, John Wiley & Sons, Inc.,2003, Chapter two
- [15]. http://www.places.co.za/maps/north_west_map.html
- [16]. South Africa Climate and Weather, in <http://www.sa-venues.com/no/weather.htm>.
- [17]. P.D. Tyson: *Climatic Change and Variability in Southern Africa*, Oxford University Press Cape Town, 1986, Chapter one.
- [18]. Republic of South Africa 1989-1990: Official Year Book of the Republic of South Africa, 15th Edition, Bureau for information pp1-22
- [19]. P.D Tyson, R.A Preston-Whyte, R.E. Schulze: *The Climate of the Drakensberg* Natal Town and Regional Planning Commission, 1976, pp.50-60
- [20]. M.O. Fashuyi, P.A. Owolawi, T.J.O Afullo, "Rainfall Rate Modelling for LOS Radio Systems in South Africa," *Accepted for publication in the Transaction of South Africa Institute of Electrical Engineering*, March 2006
- [21]. R.L. Olsen, "Radioclimatological Modelling of Propagation Effects in clear-Air and Precipitation conditions: Recent Advances and Future Directions", in *Proceedings of Radio Africa '99 Conference*, Gaborone, Botswana, October 1999, pp. 92-106. ISBN-99912-2-151-4
- [22]. William Myers, "Comparison of propagation Models", *IEEE 802.16 Broadband Wireless Access Working Group*, 31 Aug, 1999, pp. 1-7
- [23]. Harry E. Green, "Propagation impairment on Ka-band SATCOM links in Tropical and Equatorial Regions", *IEEE Antennas and Propagation Magazine*, Vol. 46, No.2, April 2004, pp. 31-44.

- [24]. Robert K. Crane, *Propagation Handbook for Wireless Communication System Design*, CRC Press LLC. 2000 N.W, 2003, Chapter two
- [25]. David M. Pozar, *Microwave Engineering*, Second Edition, John Wiley and Sons, Inc., 1988, Chapter one
- [26]. T.J Afullo, "Microwave Circuits" Unpublished lecture note, University of KwaZulu-Natal, Durban, 2004.
- [27]. <http://www.telesat.ca/satellites/transmissions/rain-attenuation.htm>
- [28]. Robert K. Crane, "Prediction of Attenuation by Rain", *IEEE Transactions on communications*, Vol. Com-28, No.9, September 1980, pp. 1717-1733.
- [29]. Goldrish J. and Vogel, W.J., "Report A2A-98-U-0-021," *Applied Physics Laboratory*, John Hopkins University, Laurel, M.D, 1998.
- [30]. G.O Ajayi, S.Feng, S.M. Radicella, B.M Reddy (Ed): Handbook on Radiopropagation Related to Satellite communications in Tropical and Subtropical Countries. ICTP, Trieste, Italy 1996, pp.2-14
- [31]. E. Couto de Miranda, M.S. Pontes and L.A.R. da silva Mello, "Statistical Modelling of the Cumulative Probability Distribution Function of Rainfall Rate in Brazil", *Proceedings of URSI Commission F Open Symposium on Climatic Parameters in Radiowave Propagation Prediction*, Ottawa, Canada, 27-29 April, 1998, pp.77-80
- [32]. R.L. Olsen, D.V. Rogers and D.B. Hodge, "The aR^b Relation in the Calculation of Rain Attenuation, *IEEE Transaction Antennas Propagation*, AP-26, N.2, 1978, pp. 547-556
- [33]. Wei Zhang, Nader Moayeri, "Power-Law Parameters of Rain Specific Attenuation," *IEEE 802.16 Broadband Wireless Access Working Group*, 26 October, 1999, pp.1-8
- [34]. J. Ottis Laws and Donald A. Parsons, "The relationship of raindrop Size to Intensity, *Transactions, American Geophysical Union*, Vol. 24, 1943, pp. 452-460
- [35]. Ross Gunn and Gilbert D. Kinzer, "The Terminal Velocity of Fall for Water Droplets in Stagnant Air," *Journal of Meteorology*, Vol. 6, 1949, pp. 243-248

- [36]. Recommendation ITU-R 838-2 “Specific Attenuation Model for Rain for Use in Prediction Models,” Vol. 2003, P Series, *International Telecommunication Union*, Geneva, Switzerland, 2003
- [37]. Recommendation ITU-R 530-10, “Propagation Prediction Techniques and Data Required for the Design of Terrestrial Line-of-Sight Systems,” Vol. 2001, P Series, *International Telecommunication Union*, Geneva, Switzerland, 2001, pp.271-295
- [38]. Recommendation ITU-R 837-1, 2, 3, 4, “Characteristics of Precipitation for Propagation Modelling,” Vol. 1992-2003, P Series, *International Telecommunication Union*, Geneva, Switzerland, 2003.
- [39]. S.K. Sarkar, I. Ahmed and M.V.S.M. Prasad, H.M. Dutta and B.M. Reddy: Rain Rate Distributions over the Indian Subcontinent- Reference Data manual, 1992
- [40]. C.G.S. Migliora, M.S. Pontes and L.A.R. Silva Mello, “Rain Rate and attenuation Measurements in Brazil,” *Preprint of URSI Comm. F Open Symposium on regional Factors in Predicting Radiowave Attenuation Due to Rain*, Rio de Janeiro, Brazil, Dec. 1990, pp.8-13
- [41]. M.G. Zhang, D.Z. Hu, “Investigation of Rain Attenuation and Rain Rates Statistics in China and its Neighbouring Area,” Paper Submitted for [15], 1995
- [42]. B. Segal, “A New Procedure for Determination and Classification of Rainfall rate Climatic Zones”, *Ann. Telecommunications*, Vol.35, Dec. 1980, pp. 411-417.
- [43]. P. A. Watson, M.J. Leito, V. Sathiaselan, M. Gunes, J.P.V. Poiars Baptista, B.A. Potter, N. Sengupta, O. Turney and G. Brussard, “Prediction of Attenuation on Satellite-Earth Links in European Region,” *IEE Proceedings*, Vol. 134, pt. F, No. 6, 1987, pp. 583-596
- [44]. F. Moupfouma, “More about Rainfall Rates and their Prediction for Radio System Engineering,” *IEE Proceedings*, Vol. 134, Pt. H, 1987, pp. 527-537
- [45]. CCIR Recommendation 563-2, “Radiometeorological Data”, Vol. V, *Recommendations and Reports of the CCIR*, International Telecommunication Union, Geneva, Switzerland, 1982, pp. 96-122

- [46]. P.L. Rice and N.R. Holmberg, "Cumulative Time Statistics of Surface-Point Rainfall Rates," *IEEE Transactions, Communications*, vol.COM-21, 1973, pp. 1131-1136
- [47]. Recommendation ITU-R 618-5, "Propagation Data and Prediction Techniques Required for the Design of Earth-Space Telecommunication Systems," Vol.1997, P Series, *International Telecommunication Union*, Geneva, Switzerland, 1997, pp.305-323
- [48]. G.O. Ajayi, S.U.B.Ezekpo, "Development of Climatic Maps of Rainfall Rate and Attenuation for Microwave Application in Nigeria," *The Nigerian Engineer* **23**, No. 4, 1988, pp.13-30
- [49]. P.A. Watson, Sathiaselan and B. Potter: *Development of a Climatic Map of Rainfall Attenuation for Europe*, Post Graduate School of Electrical and Electronic Engineering, University of Bradford, U.K, Rep. No.300, 1981, pp. 134.
- [50]. G. O Ajayi and E.B.C. Ofoche, "Some Tropical rainfall rate characteristics at Ile-Ife for Microwave and millimeter Wave Application," *J. of Climate and Applied. Meteor.*, Vol. 23, 1983, pp 562-567
- [51]. R.K., Flavin, "Rain Attenuation Considerations for satellite Paths," *Telecom Australia Research Laboratories Report No 7505*, 1981.
- [52]. Emilio Matricciani, A. Pawlina Bonati, "Statistical Characterisation of Rainfall Structure and Occurrence for Convective and Stratiform Rain Inferred from Long-Term Point Rain Rate Data,"
- [53]. A. Pawlina- Bonati, "Essential Knowledge of Rain Structure for Radio Applications Based on Available Data and Models," *Proceedings of the 3rd Regional Workshop on Radio communication, Radio Africa '99*, Gaborone- Botswana , 25-29 October, 1999, pp.96-106, ISBN-99912-2-151-4
- [54]. A. Pawlina, M. Binaghi, "Rain Distribution along the Path: New Statistics of Cells and Cells separations from Radar Data," *Proceedings of URSI Commission F Open Symposium on Climatic Parameters in Radiowave Propagation Prediction, CLIMPARA '98*, Ottawa, Canada, 27-29 April, 1998, pp. 81-84.

- [55]. A.Bennarroch, P.Garcia del Pino, V.Kvicera, "Comparison of Rain rate statistics measured in Spain and Prague," *Cost Action 280 on Propagation Impairment Mitigation for Millimeter Wave Radio Systems*. Doc. PM3003S, 1st International Workshop , July 2002
- [56]. V. Kvicera, M.Grabner, M. Hlavaty, "Results of Statistical Processing of Rain Intensities in Prague from Period 1992-2002,"
- [57]. M.S. Assis and M.H.C. Dias, " Modified ITU-R Rain Attenuation Model for Low Latitude Areas," *Proceedings of URSI Commission F Open Symposium on Climatic Parameters in Radiowave Propagation Prediction, CLIMPARA '98*, Ottawa, Canada, 27-29 April, 1998, pp. 137-139
- [58]. M.S Assis, "Rain Attenuation in Terrestrial Paths," *ISRP ' 92*, Sapporo, Japan, Sept.1992
- [59]. Mello Silva, L.A.R., M.A.G.M. Maia, M.B.P Jimenez and M.S. Pontes, " Conversion to one-minute rainfall Rate Distributions for Different Integration Time Statistics", *Preprint of URSI Comm. F Open Symposium on regional Factors in Predicting Radiowave Attenuation Due to Rain*, Rio de Janeiro, Brazil, Dec. 1990.
- [60]. W.F. Bodtmann and C.L Ruthroff, "Rain Attenuation on Short Radio Paths: Theory, Experiment and Design," *Bell System Tech. Journal* **53**, pp. 1329-1349, 1974.
- [61]. K. Naicker and S.H. Mneney, "Propagation Measurements and Modeling for Terrestrial Line-of-Sight Links at 19.5 GHz," *IEEE Africon 2004*, Gaborone, Botswana, Vol. 01, pp.95-100, 15-17 Sept. 2004, ISBN: 0-7803-8605-1
- [62]. P.K Odedina and T.J.O Afullo, "Effective Earth Radius Factor (k-factor) Determination and its Application in Southern Africa," *Proceedings of the 2nd IASTED International Conference on Antennas, Radar, and Wave Propagation*, Banff, Alberta, Canada, pp. 222-227, July 19-21,2005, ISBN: 0-88986-505-1

APPENDICES

Appendix A: Computation of Specific Rain Attenuation

The plots of the specific rain attenuation and the tables that show the values at which the specific rain attenuation is under-estimated by using the ITU-R average rain statistics as compared with the actual average rain rate statistics over a 5-year period for the other geographical locations not shown in Chapter five are displayed in this section. This is also done for both horizontal and vertical polarization

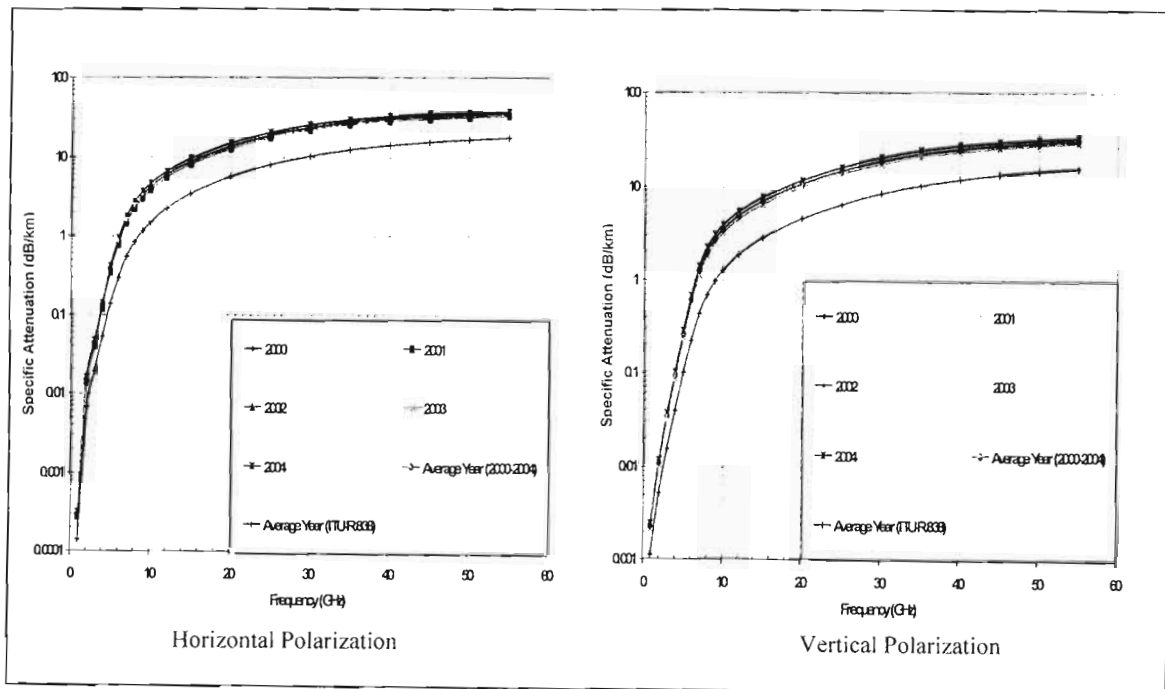


Fig. A1.1 Specific rain attenuation for horizontal and vertical polarization in Ladysmith taking rain rate exceeded for 0.01% of the time

Table A1.1 Values by which the ITU-R under-estimate the specific rain attenuation for Ladysmith

Frequency (GHz)	ITU-R Under-estimate Values (dB/km)	
	Horizontal Polarization	Vertical Polarization
10	2.63	2.19
20	8.97	6.06
30	12.81	11.57
40	15.59	13.07
50	18.74	14.51

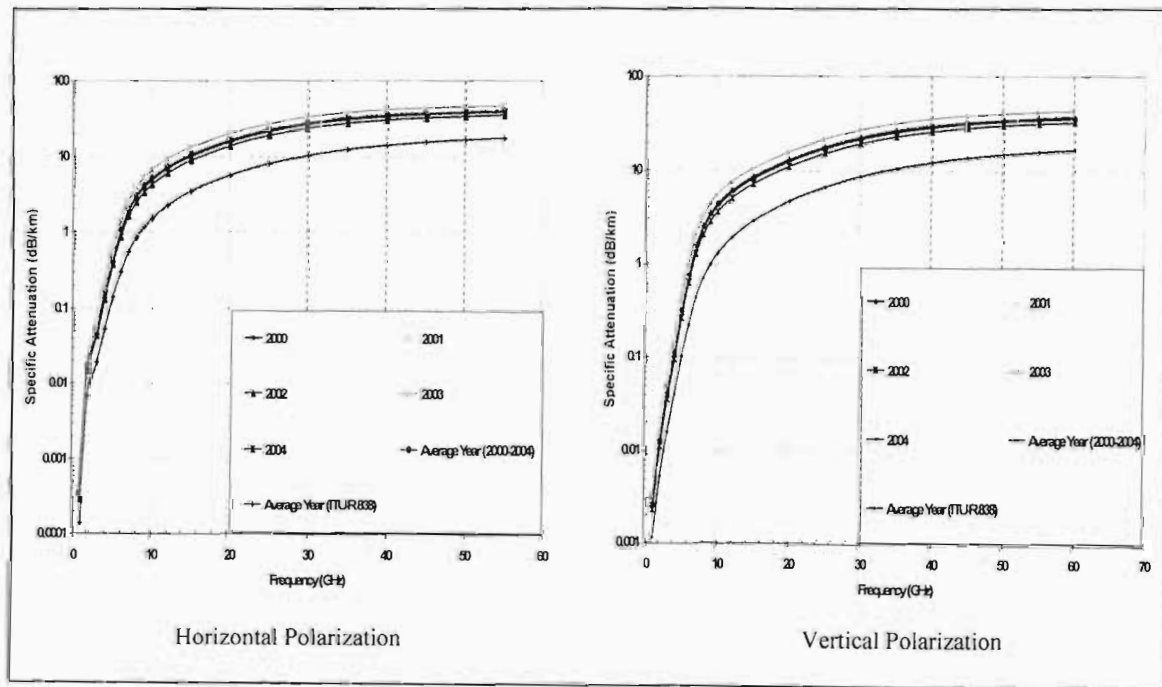


Fig. A1.2 Specific rain attenuation for horizontal and vertical polarization in Newcastle; taking rain rate exceeded for 0.01% of the time

Table A1.2 Values by which the ITU-R under-estimate the specific rain attenuation for Newcastle

Frequency (GHz)	ITU-R Under-estimate Values (dB/km)	
	Horizontal Polarization	Vertical Polarization
10	3.51	2.91
20	10.29	7.91
30	16.65	13.2
40	20.10	16.83
50	21.25	18.58

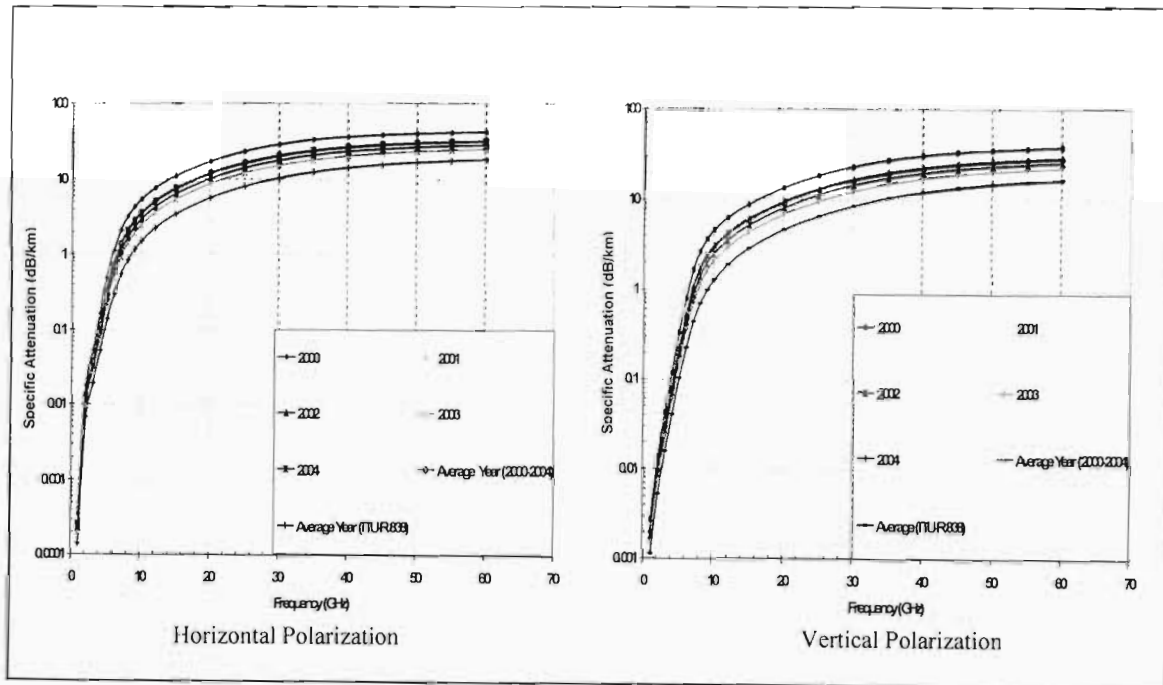


Fig. A1.3 Specific rain attenuation for horizontal and vertical polarization in Vryheid; taking rain rate exceeded for 0.01% of the time

Table A1.3 Values by which the ITU-R under-estimate the specific rain attenuation for Vryheid

Frequency (GHz)	ITU-R Under-estimate Values (dB/km)	
	Horizontal Polarization	Vertical Polarization
10	1.98	1.65
20	6.00	4.64
30	9.85	7.84
40	12.07	10.13
50	12.91	11.30

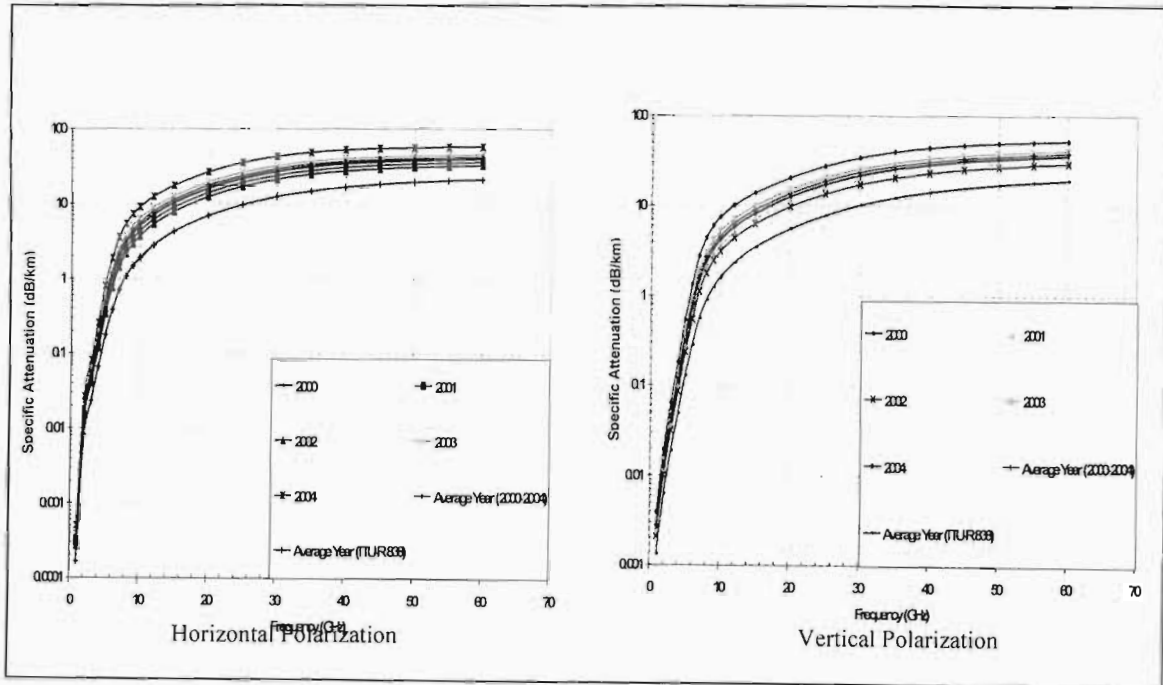


Fig. A1.4 Specific rain attenuation for horizontal and vertical polarization in Pietermaritzburg; taking rain rate exceeded for 0.01% of the time

Table A1.4 Values by which the ITU-R under-estimate the specific rain attenuation for Pietermaritzburg

Frequency (GHz)	ITU-R Under-estimate Values (dB/km)	
	Horizontal Polarization	Vertical Polarization
10	3.58	2.97
20	10.32	7.90
30	16.55	13.09
40	19.80	16.57
50	20.80	14.17

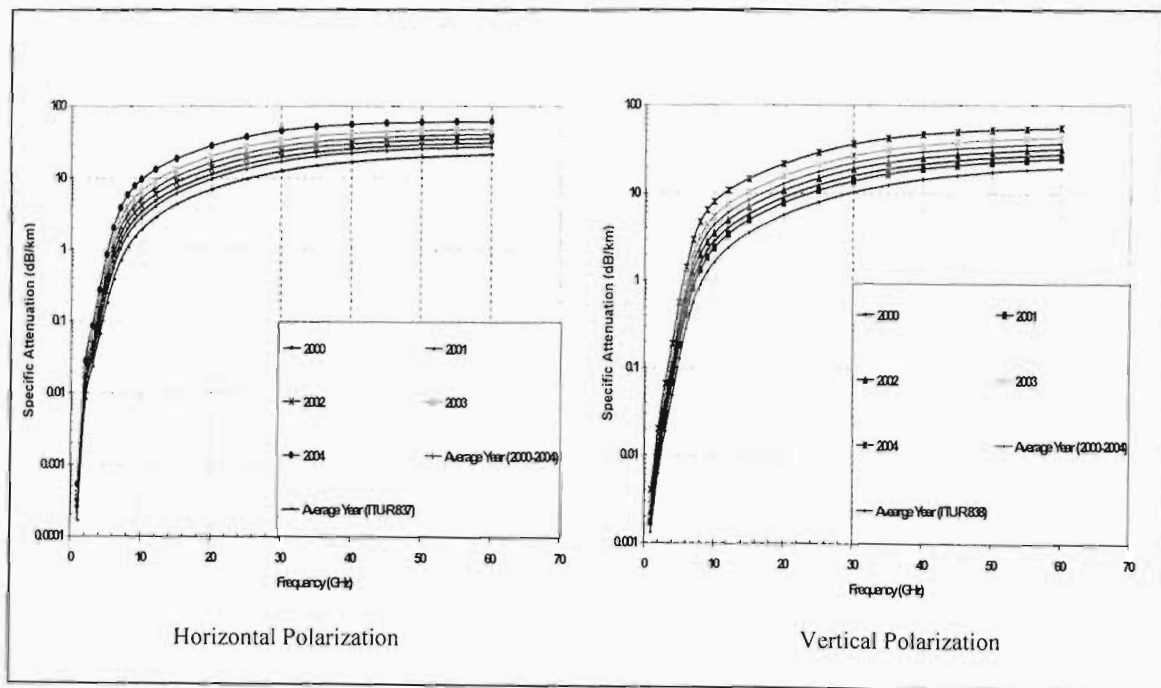


Fig. A1.5 Specific rain attenuation for horizontal and vertical polarization in Ulundi; taking rain rate exceeded for 0.01% of the time

Table A1.5 Values by which the ITU-R under-estimate the specific rain attenuation for Ulundi

Frequency (GHz)	ITU-R Under-estimate Values (dB/km)	
	Horizontal Polarization	Vertical Polarization
10	3.13	2.60
20	9.09	6.98
30	14.63	11.58
40	17.57	14.71
50	18.49	16.17

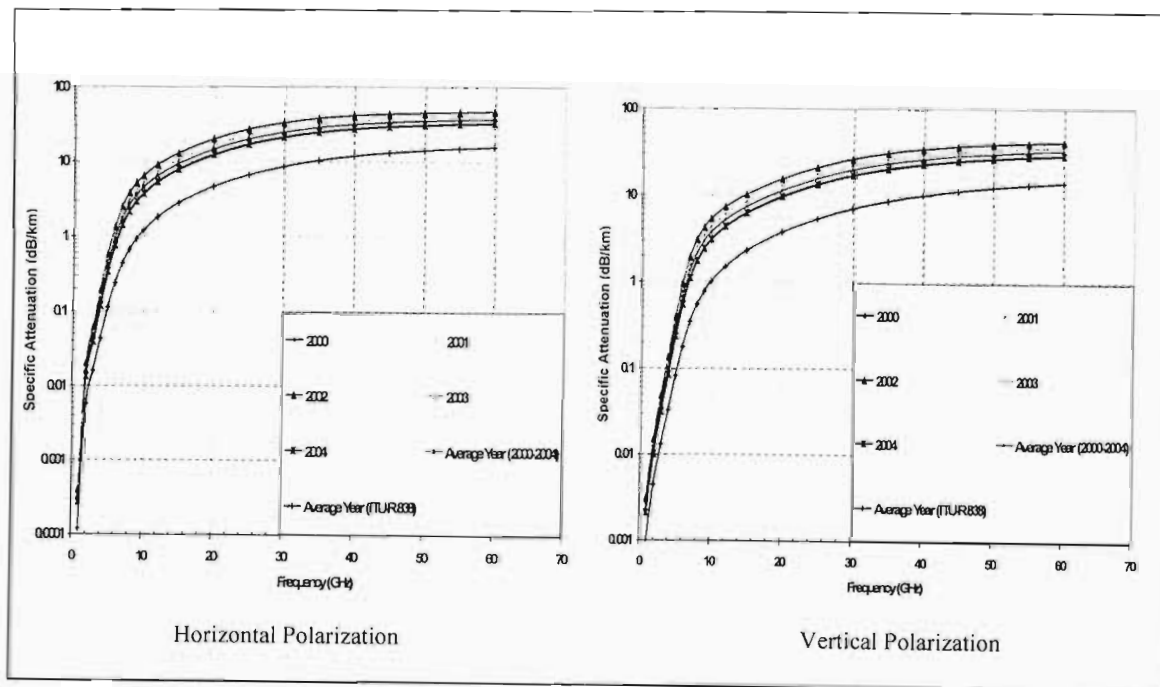


Fig. A1.6 Specific rain attenuation for horizontal and vertical polarization in East London; taking rain rate exceeded for 0.01% of the time

Table A1.6 Values by which the ITU-R under-estimate the specific rain attenuation for East London

Frequency (GHz)	ITU-R Under-estimate Values (dB/km)	
	Horizontal Polarization	Vertical Polarization
10	3.24	2.69
20	9.72	7.50
30	15.87	12.61
40	19.34	16.23
50	20.62	18.04

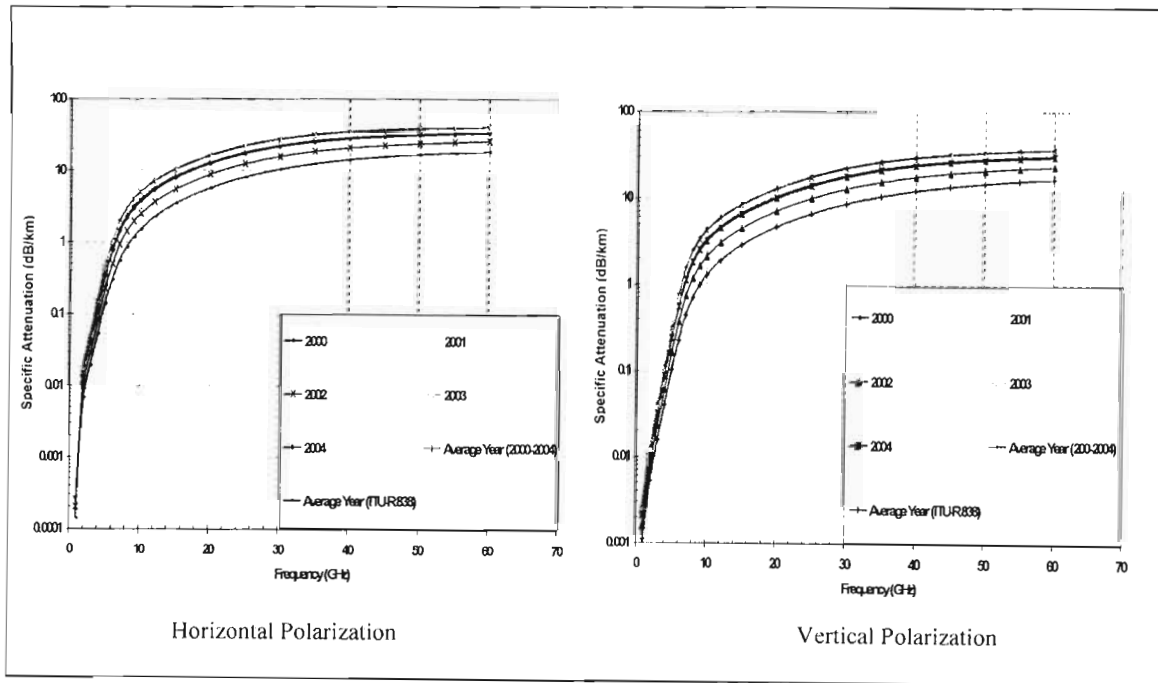


Fig. A1.7 Specific rain attenuation for horizontal and vertical polarization in Bloemfontein; taking rain rate exceeded for 0.01% of the time

Table A1.7 Values by which the ITU-R under-estimate the specific rain attenuation for Bloemfontein

Frequency (GHz)	ITU-R Under-estimate Values (dB/km)	
	Horizontal Polarization	Vertical Polarization
10	2.38	1.98
20	7.13	5.51
30	11.66	9.27
40	14.23	9.40
50	15.16	13.27

Appendix B: Estimation of Path Attenuation Using Different Existing Models on the Available Local Rain Data

The plots of the three existing models using the actual local measurements recorded for each geographical location situated at different frequencies for the estimation of the path attenuation exceeded at 0.01% of time not shown in chapter five of this work are shown in the figures below.

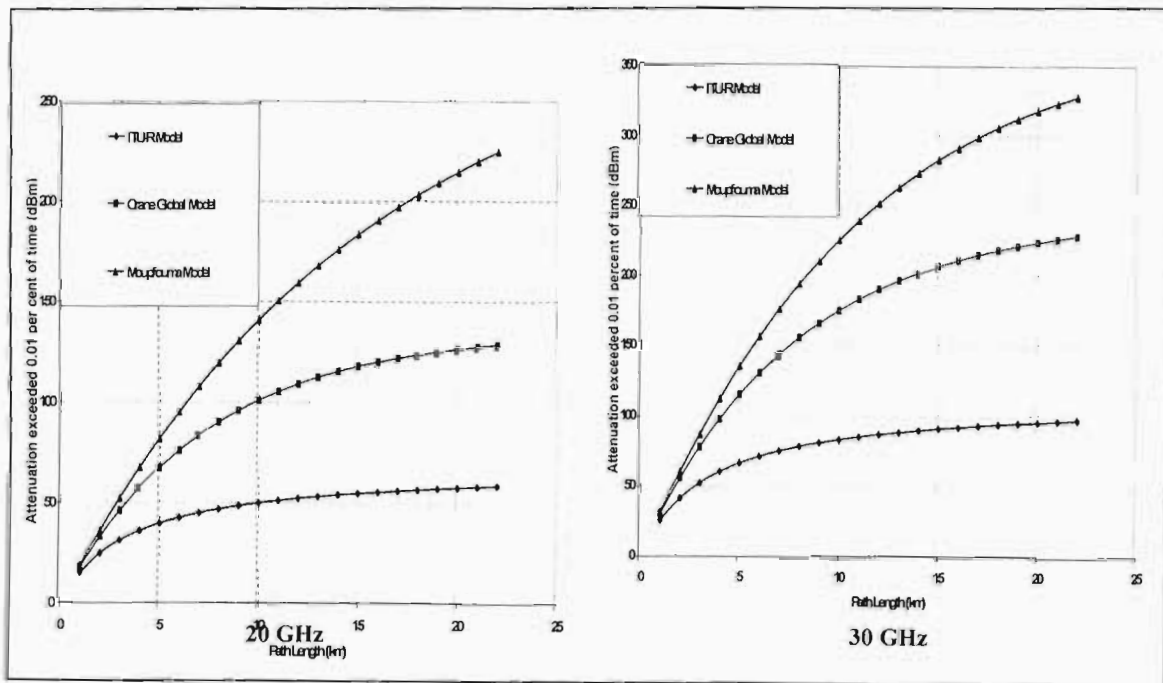


Fig B2.1 Rain attenuation prediction models for terrestrial line-of-sight links for Richards Bay for frequencies 20 GHz and 30 GHz

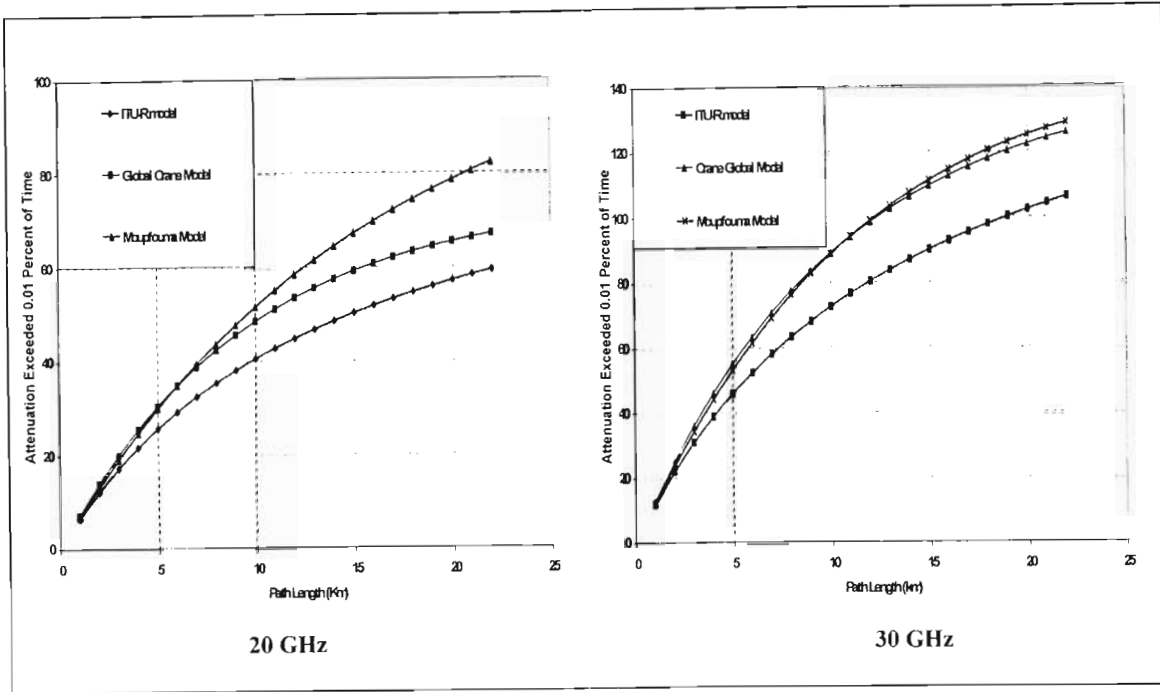


Fig. B2.2 Rain attenuation prediction models for terrestrial line-of-sight links for Cape Town for frequencies 20 GHz and 30 GHz

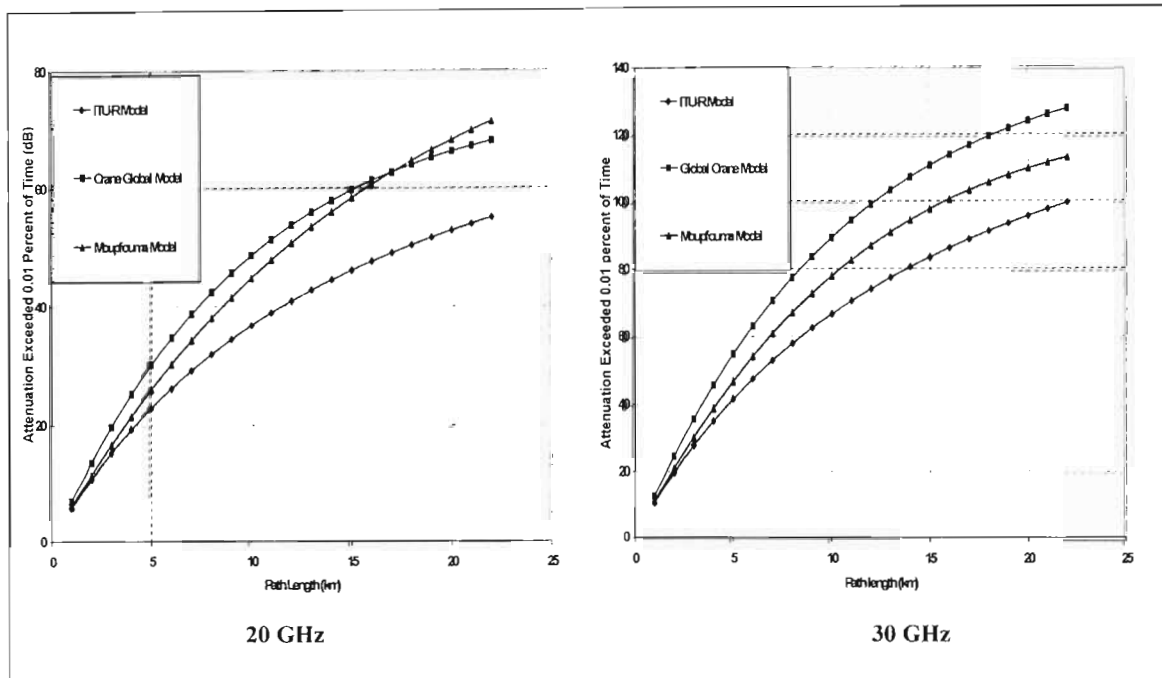


Fig. B2.3 Rain attenuation prediction models for terrestrial line-of-sight links for Brandvlei for frequencies 20 GHz and 30 GHz

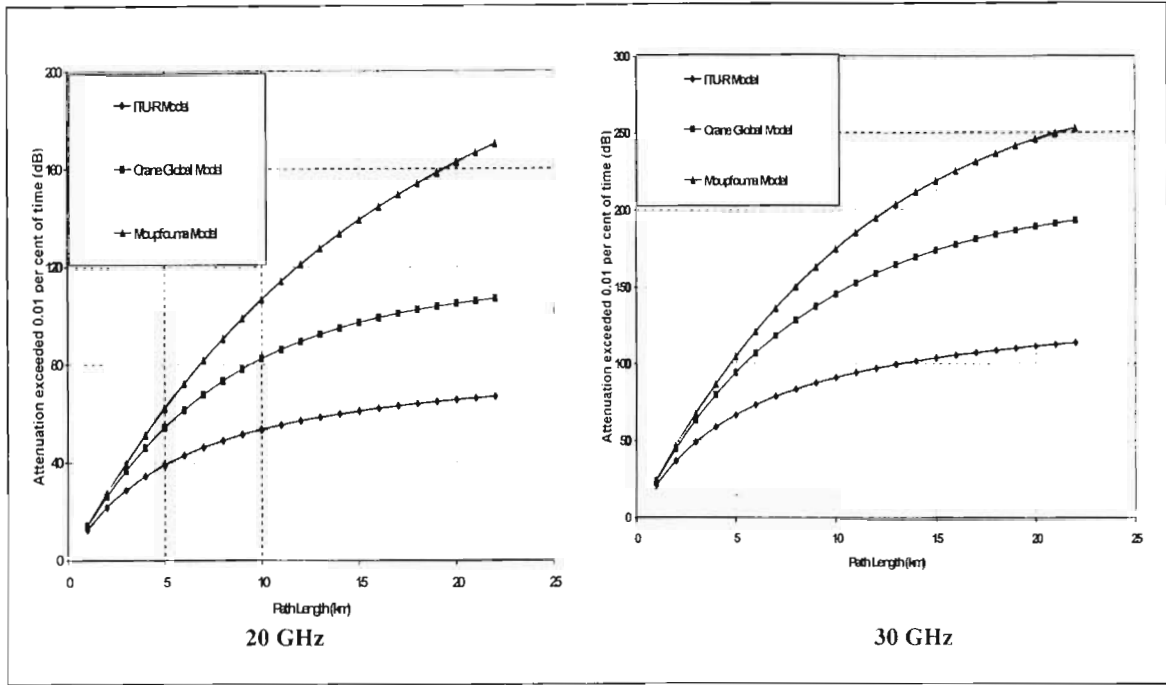


Fig. B2.4 Rain attenuation prediction models for terrestrial line-of-sight links for Pretoria for frequencies 20 GHz and 30 GHz

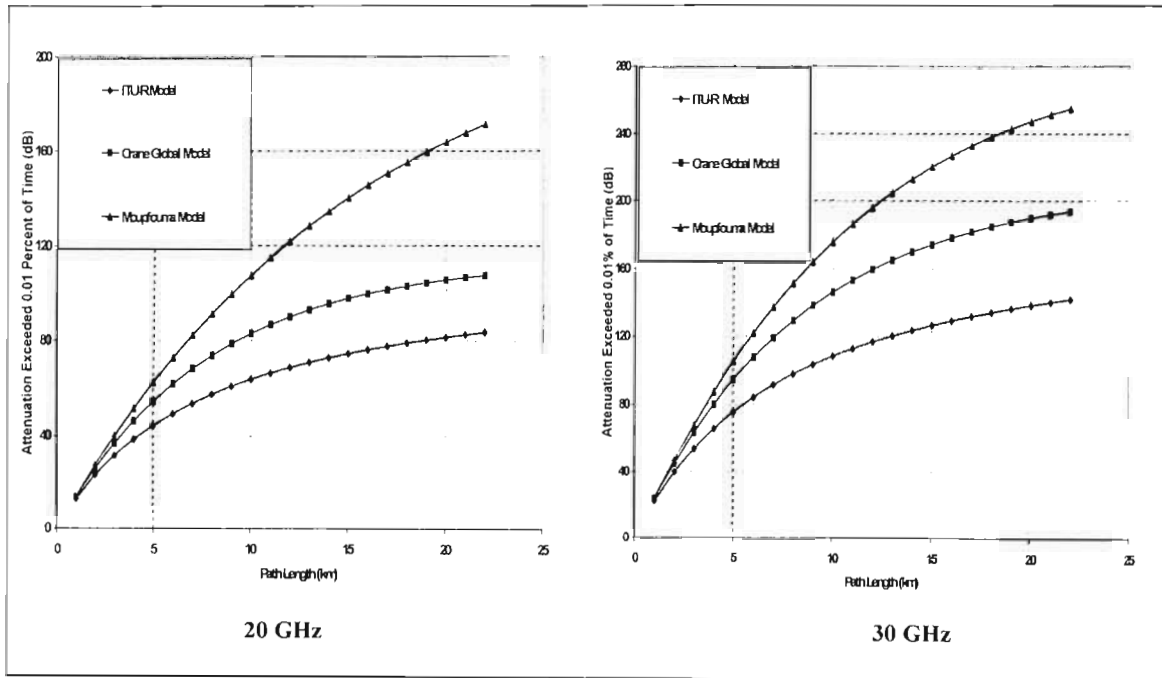


Fig. B2.5 Rain attenuation prediction models for terrestrial line-of-sight links for Durban for frequencies 20 GHz and 30 GHz

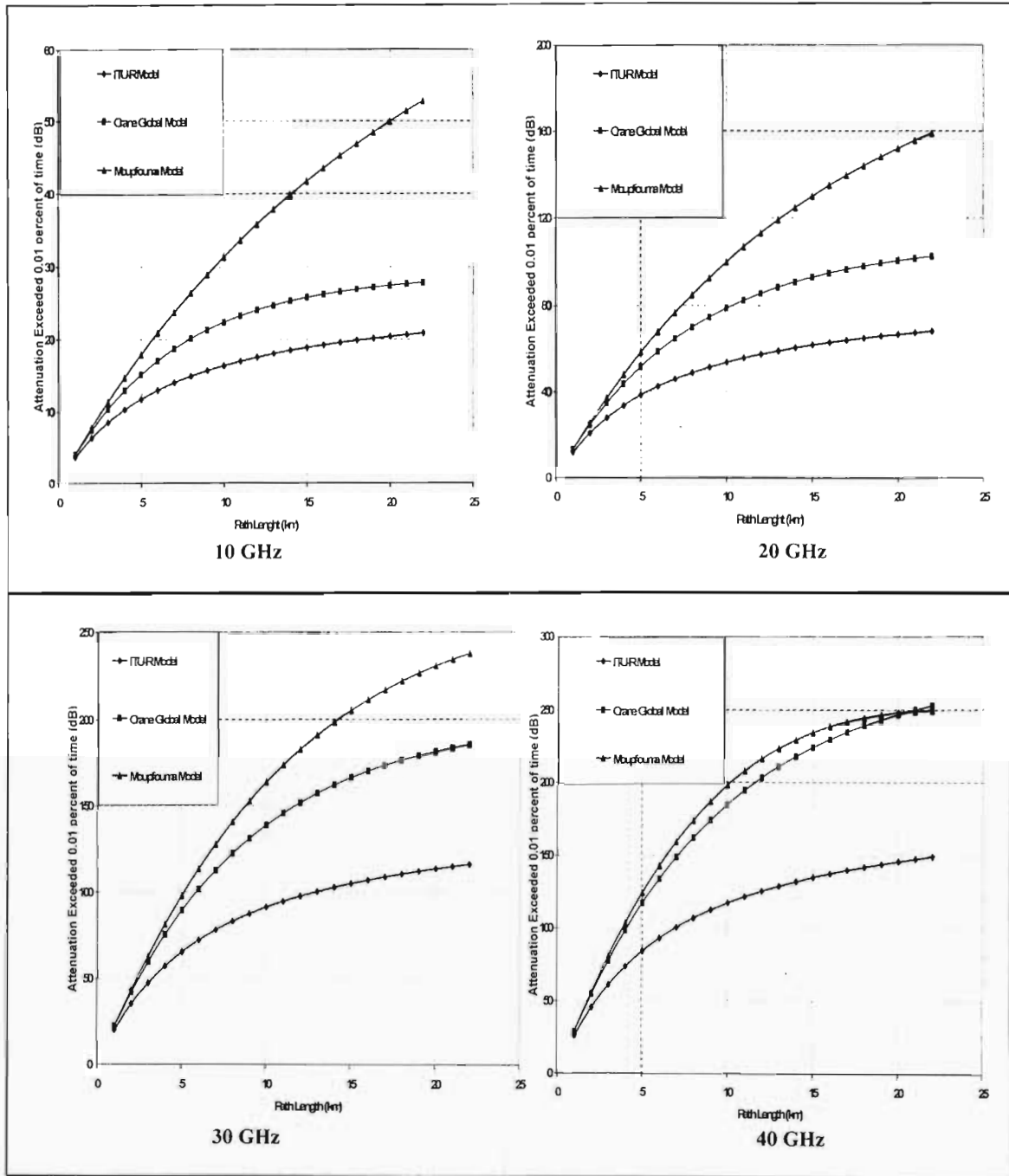


Fig. B2.6 Rain attenuation prediction models for terrestrial line-of-sight links for Ladysmith for frequencies 10 GHz, 20 GHz, 30 GHz and 40 GHz

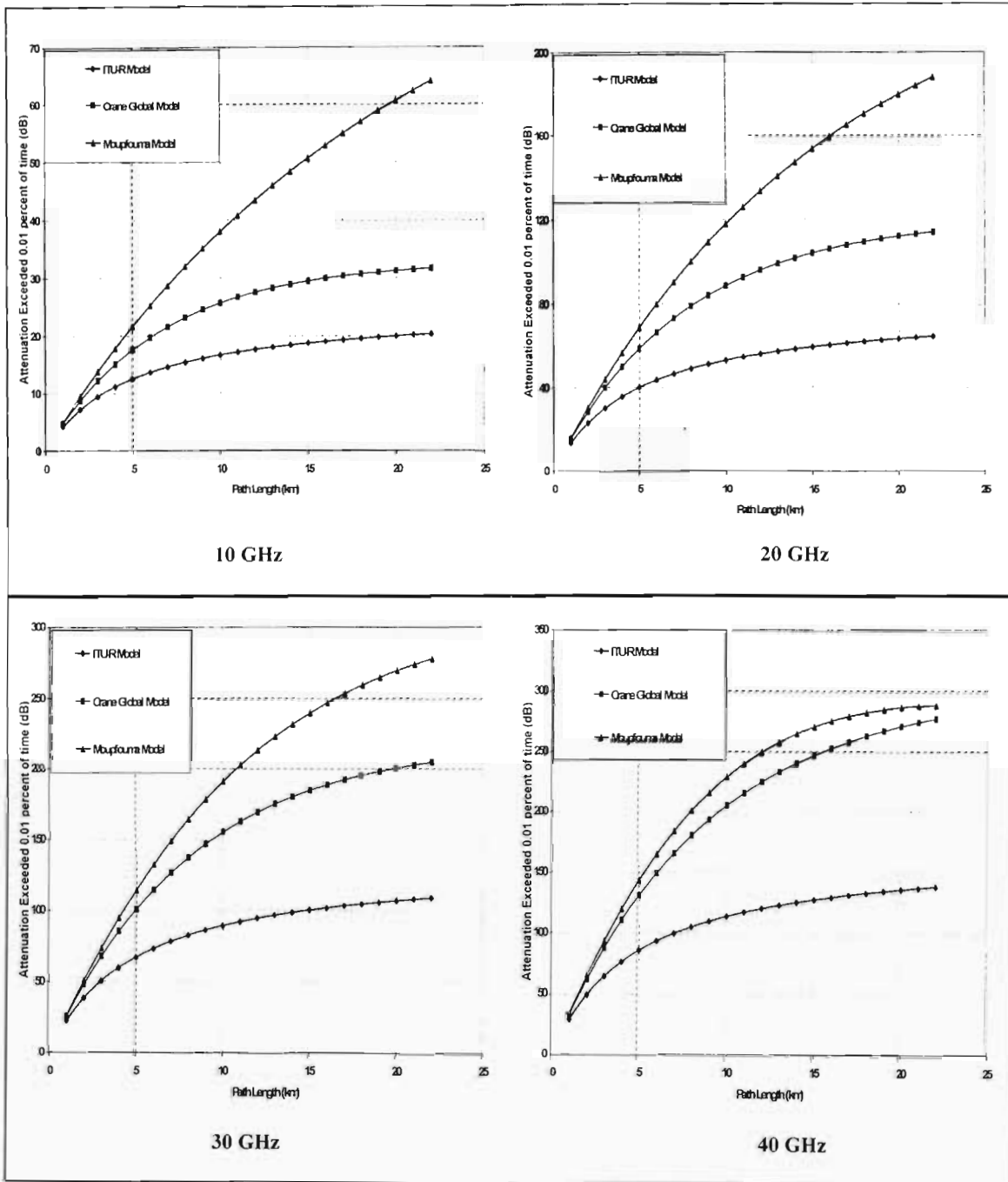


Fig. B2.7 Rain attenuation prediction models for terrestrial line-of-sight links for Newcastle for frequencies 10 GHz, 20 GHz, 30 GHz and 40 GHz

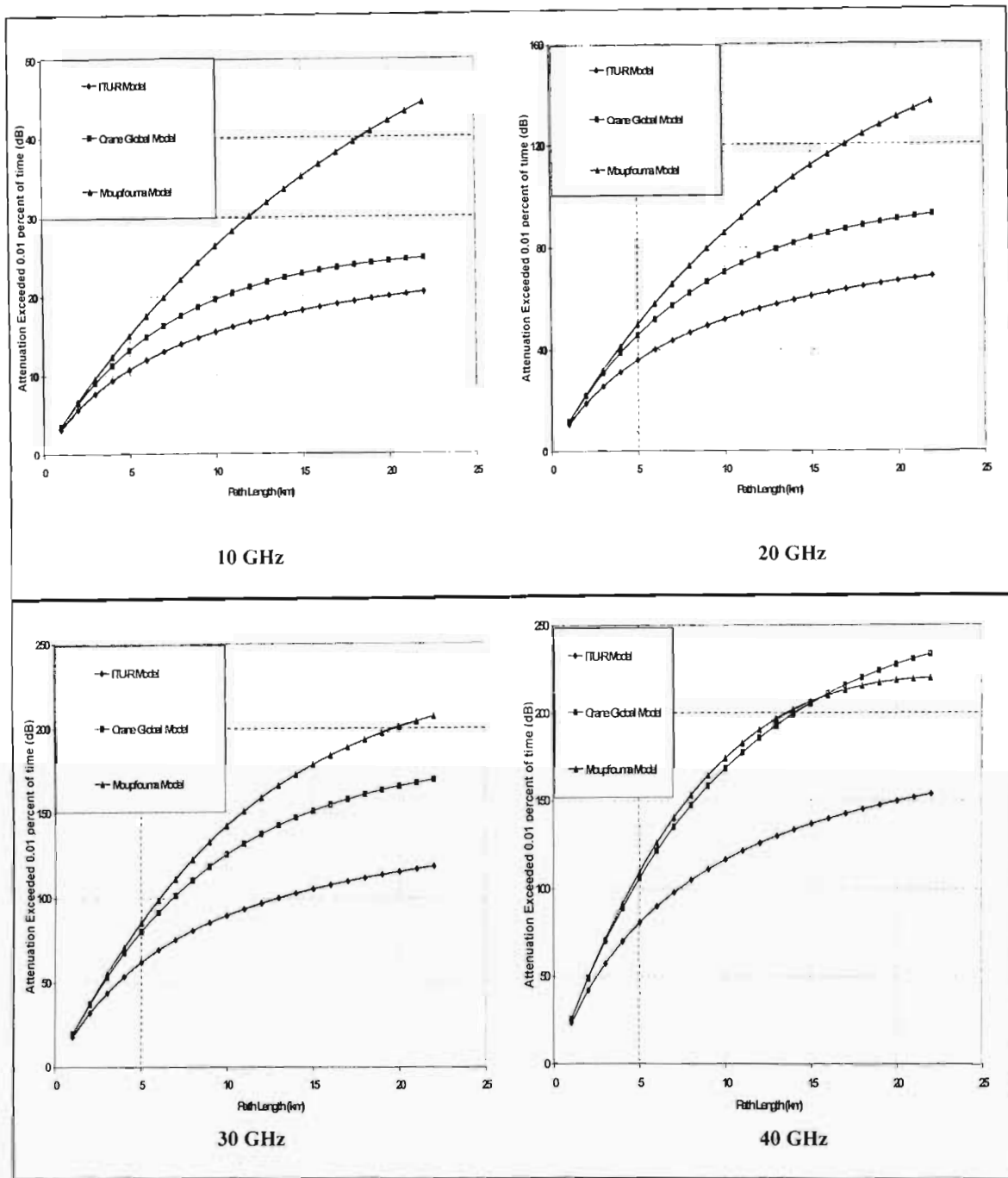


Fig. B2.8 Rain attenuation prediction models for terrestrial line-of-sight links for Vryheid for frequencies 10 GHz, 20 GHz, 30 GHz and 40 GHz

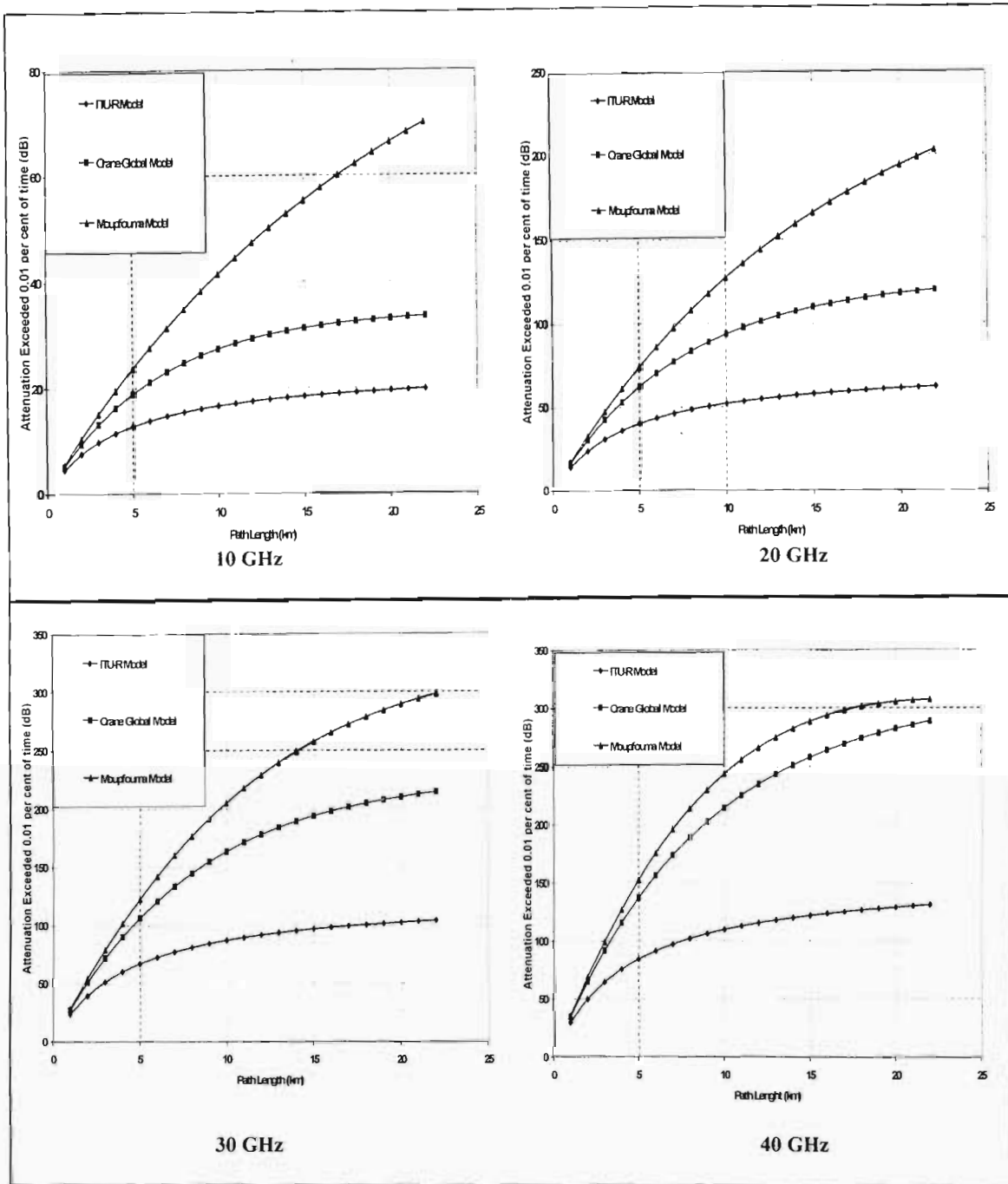


Fig. B2.9 Rain attenuation prediction models for terrestrial line-of-sight links for Pietermaritzburg for frequencies 10 GHz, 20 GHz, 30 GHz and 40 GHz

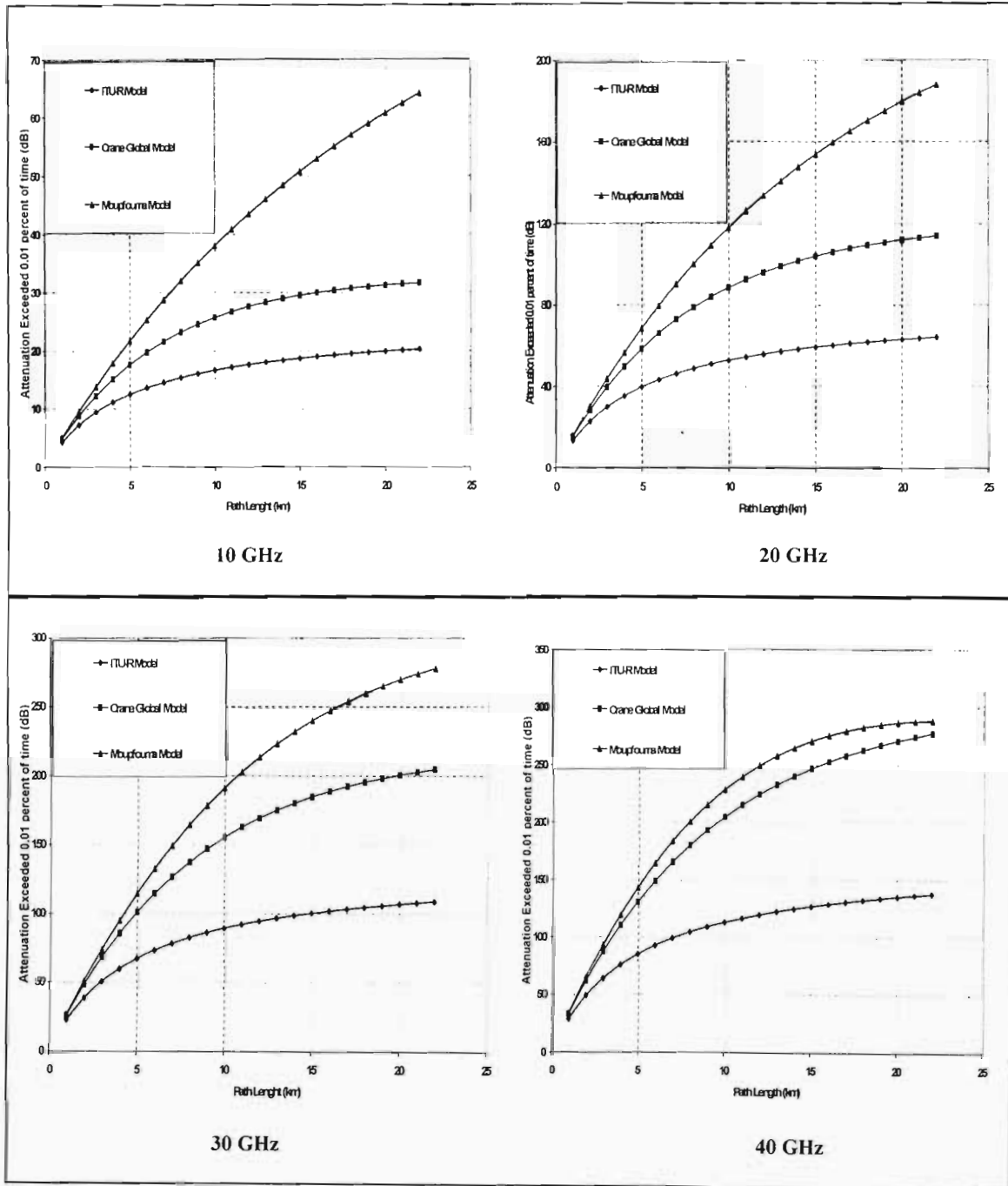


Fig. B2.10 Rain attenuation prediction models for terrestrial line-of-sight links for Ulundi for frequencies 10 GHz, 20 GHz, 30 GHz and 40 GHz

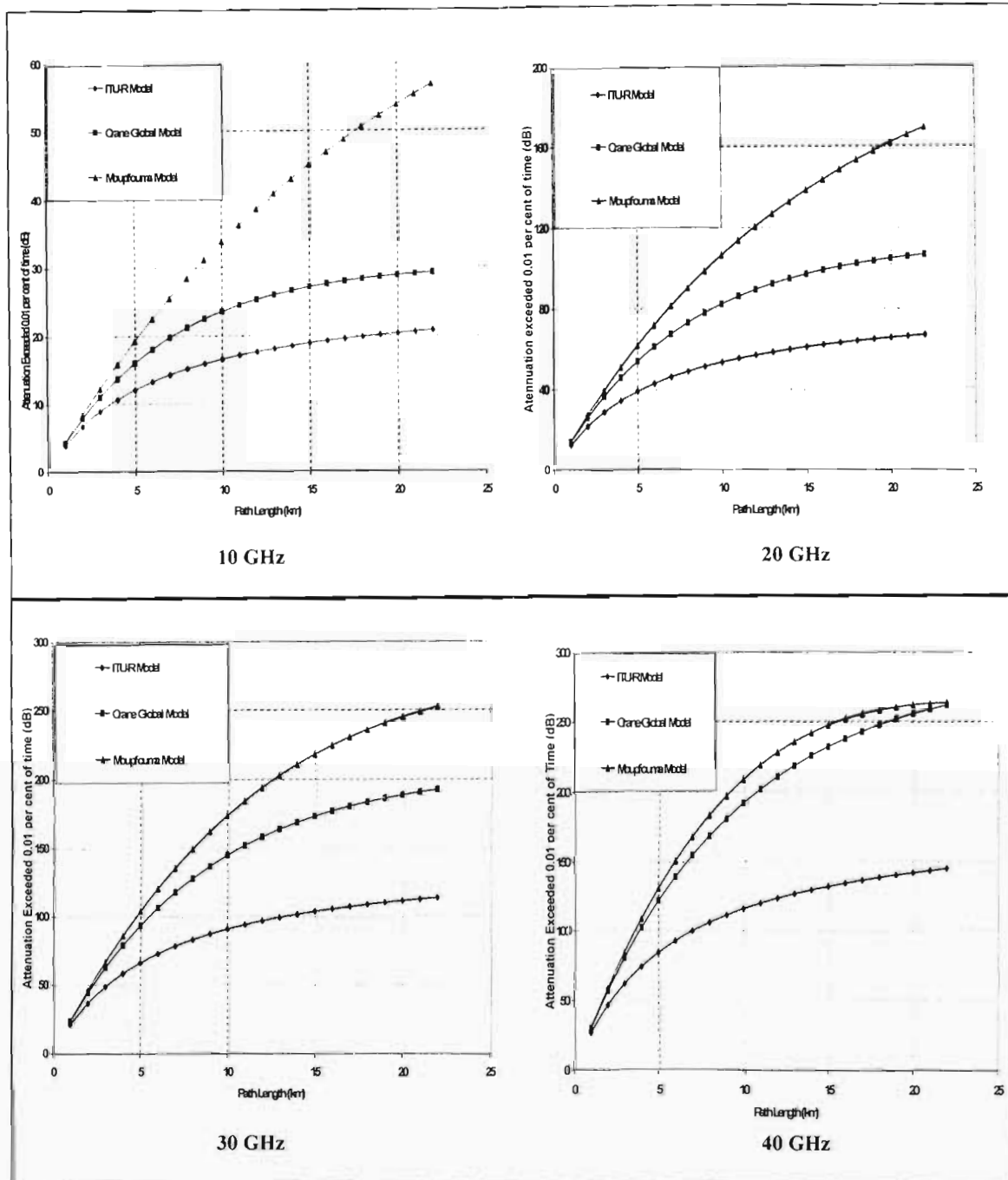


Fig. B2.11 Rain attenuation prediction models for terrestrial line-of-sight links for East London for frequencies 10 GHz, 20 GHz, 30 GHz and 40 GHz

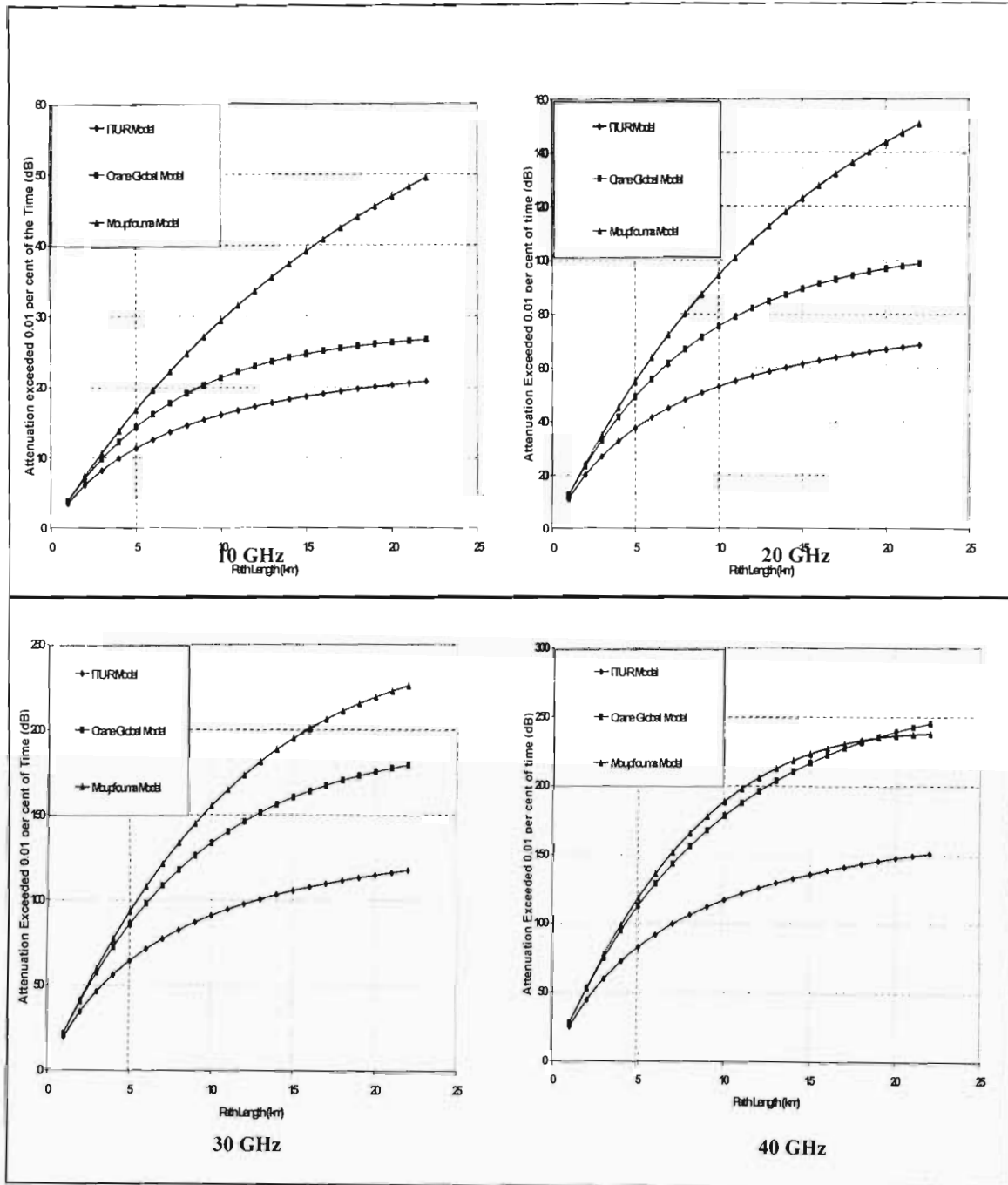


Fig. B2.12 Rain attenuation prediction models for terrestrial line-of-sight links for Bloemfontein for frequencies 10 GHz, 20 GHz, 30 GHz and 40 GHz

Appendix C: The Threshold values of the Chi-Square Test

Degrees of Freedom	Threshold at $\alpha = 1\%$	Threshold at $\alpha = 5\%$	Degrees of Freedom	Threshold at $\alpha = 1\%$	Threshold at $\alpha = 5\%$
1	6.6349	3.8415	18	34.8053	28.8693
2	9.2103	5.9915	20	37.5662	31.4104
3	11.3449	7.8147	25	44.3141	37.6525
4	13.2767	9.4877	30	50.8922	43.7730
5	15.0863	11.0705	35	56.0609	49.8018
6	16.8119	12.5916	40	63.6907	55.7585
7	18.4753	14.0671	50	76.1539	67.5048
8	20.0902	15.5073	60	88.3794	79.0819
9	21.6660	16.9190	70	100.4252	90.5312
10	23.2092	18.3070	80	112.3288	101.8795
12	26.2170	21.0261	90	124.1163	113.1453
14	29.1412	23.6848	100	135.8067	124.3421
16	31.9999	26.2962	1000	1106.9690	1074.6794